# Master's Thesis

## Magnetic Microfluidic System for Isolation and Detection of Rare Circulating Tumor Cells

Project Leader:      Univ.Ass. Dr.techn. Ioanna Giouroudi

Supervisor:          Ao.Univ.Prof. Dipl.-Ing. Dr.techn. Franz Keplinger

Advisors:            Georgios Kokkinis, MSc.
                     Theocharis Berris, MSc.


Master Student:      Richard Mitterböck, BSc.
                     Matriculation no.: 0526477
                     Schönbauergasse 4
                     3180 Lilienfeld
                     richard.mitterboeck@outlook.at

10th of November, 2014                    .......................................................

# Project Summary

**FWF - Project P24372-N19 - "On-Chip Biosensing utilizing the Motion of Magnetic Particles"**

This project concerns the design and realization of a compact, portable and cost-effective microfluidic system for isolation and detection of rare circulating tumor cells (CTCs) in suspension. The system consists of microfluidic channels with microtraps. The liquid sample is mixed with magnetic particles (MPs) coated with ligands of specific affinity to the CTCs, prior to injection into the device. Afterwards, as the magnetically labeled CTCs travel inside the channel they are selectively isolated in the microtraps by current carrying microstructures (microconductors) which are positioned underneath the microtraps during fabrication.

The channel and trap dimensions are optimized to protect the cells from shear stress and achieve high trapping efficiency. These intact CTCs can then be used for additional analysis, testing and patient specific drug screening. A sensing device, e.g. a magnetic microsensor underneath the microtraps, is used to detect the magnetically labeled CTCs.

# Abstract

The innovative aspect of the proposed isolation and detection method is that it utilizes magnetic particles (MPs) to label CTCs and then isolate those using microtraps with integrated current carrying microconductors. The magnetically labeled and trapped CTCs can then be detected by integrated magnetic microsensors e.g. giant magnetoresistive (GMR) or giant magnetoimpedance (GMI) sensors.

Specifically, the proposed magnetic microfluidic system consists of microfluidic channels and trapping microchambers (microtraps) fabricated using a dry photoresist thin film (Ordyl) and a standard photolithography process.

Commercially available functionalized MPs with selective affinity to CTCs are used to label the CTCs in the sample under investigation. The isolation and capturing of the magnetically labeled CTCs is achieved through current carrying microstructures. These microconductors are fabricated underneath the microtraps using evaporation deposition technique and photolithography.

The sample containing the CTCs which is prior mixed with the functionalized MPs to ensure labeling of the CTCs flows through the microfluidic channel. Current is applied sequentially at the microconductors. This causes a magnetic force to act on the magnetically labeled CTCs which flow through the microchannel along the x-axis. This lateral magnetic force attracts them, separates them from the other cells in the sample and captures them inside the microtraps. By placing a magnetic microsensor underneath the microtrap during fabrication the proposed method can additionally be used to detect the presence of CTCs in the future.

The thesis includes the design, fabrication and testing of the proposed microfluidic system with the integrated current carrying microconductors. The testing is carried out with magnetically labeled Jurkat cells (human T-lymphocyte cells).

# Kurzfassung

Der innovative Aspekt der vorgeschlagenen Isolations- und Detektierungsmethode besteht in der Verwendung von magnetischen Partikeln zum Markieren der zirkulierenden Tumorzellen (CTCs). Es erfolgt eine Isolierung und Detektion durch Mikrofallen mit integrierten stromdurchflossenen Mikroleiterstrukturen. Die magnetisch markierten CTCs können danach durch integrierte, magnetische Mikrosensoren z.B. Giant Magnetoresistive- (GMR) oder Giant Magnetoimpedance- (GMI) Sensoren detektiert werden.

Das vorgeschlagene magnetische Mikrofluidiksystem besteht aus Mikrofluidikkanälen und Mikrofangkammern (Mikrofallen), welche aus einem Trocken-Fotolack-Dünnfilm (Ordyl) mit Standard Fotolithografieprozessen hergestellt werden.

Kommerziell verfügbare MPs mit funktionaler Oberfläche mit spezieller Affinität zu CTCs werden für die Markierung dergleichen in der Probe verwendet. Isolation und Einfangen der magnetisch markierten CTCs wird durch stromdurchflossene Mikrostrukturen erreicht. Diese Mikrostrukturen werden mittels Aufdampfen und Fotolithografie erzeugt und unter den Mikrofallen positioniert.

Die Probe mit den CTCs wird im Vorfeld mit den funktionalen magnetischen Partikeln gemischt, um sicherzustellen, dass markierte Zellen durch das Mikrofluidiksystem fließen. Durch das sequenzielle Anschalten von Strömen in den Mikrostrukturen wirkt eine laterale Kraft auf die vorher in x-Richtung fließenden CTCs. Diese Kraft zieht Zellen mit MPs an und hält diese in den Mikrofallen fest. Durch die Positionierung eines magnetischen Sensors unter der Mikrofalle kann das vorgeschlagene Mikrofluidiksystem in Zukunft auch dazu verwendet werden die Anwesenheit der CTCs zu detektieren.

Diese Arbeit umfasst Planung, Produktion und Test des vorgestellten Mikrofluidiksystems mit stromführenden Mikrostrukturen. Die Tests werden mit magnetisch markierten Jurkat-Zellen (Menschliche T-Lymphozyt-Zellen) durchgeführt.

# Acknowledgements

First and foremost, I would like to thank Franz Mitterböck Senior, Inge Zeilerbauer, Edith Mitterböck and my family for their help throughout my studies and during the preparation of this thesis.

I would like to express my appreciation to Dr. Ioanna Giouroudi for the continuous support and guidance throughout my work.

I also would like to express my gratitude to Ao.Univ.Prof. Dipl.-Ing. Dr.techn. Franz Keplinger for the opportunity to work in such an interesting and paradigm changing field of research.

I am especially grateful to Georgios Kokkinis, MSc. who helped with the development of the device and gave necessary insight into the ongoing project works.

I also want to thank Theocharis Berris, MSc. for useful tips regarding simulations.

I also would like to thank the other colleagues at the "Institute of Sensor and Actuator Systems" for creating such a pleasant working atmosphere.

Finally I want to thank everybody who contributed to the success of this master thesis with their technical and / or personal support and was not mentioned by name.

# Table of Contents

# 1    Theory

In this chapter the theory related to the methods and materials used in this thesis will be presented. Information will be given regarding "Circulating Tumor Cells" (CTCs), techniques for cancer cell diagnostics and principles of microfluidics. Furthermore, fundamental magnetic phenomena associated with this thesis, like superparamagnetism and the magnetophoretic force will be outlined.

## 1.1    Rare Circulating Tumor Cells

Circulating tumor cells (CTCs) are cancer cells, which are circulating in the blood stream. They were first observed in the mid of the 19th century during an autopsy. From this time on it was clear that cancer cells can spread through the bloodstream [1].

Malignant tumors tend to grow new vasculature for supply of the growing tissue. This vessels provide an entry gate for cancerous cells into the bloodstream. After reaching this point they are free to move in the vessels and thus able to attach at new locations in the body and form metastatic tumors. The way of CTCs from the primary tumor through the body can be seen in Fig. 1 [2].

In fact, it took another one and half centuries before the spreading of malign tumor cells over lymphatic vessels was also confirmed at the beginning of the 21st century. It was not possible to prove this concept earlier without modern imaging like MRI [3].
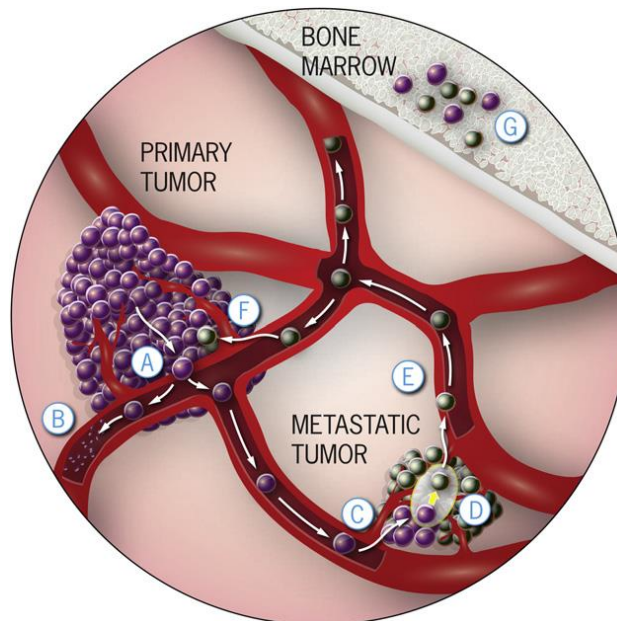


*Figure 1:     Way of CTCs through blood vessels [4]*

> A)    *Release of cancer cells into the bloodstream*
> B)    *Some CTCs get destroyed*
> C)    *Some may leave the stream and form new tumors (called metastasis)*
> D)    *Metastatic cells can evolve and show different characteristics than the primary tumor*
> E)    *Also the metastatic tumor can dispatch new CTCs into the blood*
> F)    *Maybe some of the new CTCs attach at the primary tumor and alter its behavior*
> G)    *CTCs can be stored in different locations in the human body*

Usually, it takes some time for primary tumors to grow to such an extent that CTCs are released into the body. At this early stage maybe only 1 out of $10*10^9$ cells in the blood is a CTC. That means that there is a possibility to find only 1 CTC in 1ml of blood, which is very rare and hard to measure [5]. Nevertheless, it is crucial to detect CTCs in this early stage, because after forming metastasis the mortality rate increases rapidly. For instance in breast cancer the survival rate is about 98.6%. After first metastasis in regional lymph nodes the survival rate drops to 83.8% but when the metastasis affects distant organs only 23.4% of the patients will survive [6].

Another problem is (besides the quantity), that different cancer types often have different characteristics and thus also the CTCs show different behavior. So theoretically for many tumor types distinct protocols for capturing and analysis have to be established. What appears as a big drawback of CTC analysis could in fact open possibilities to determine special tumor types from a blood sample and get the right treatment for the patient.

Today the enrichment and detection of CTCs is mostly based on the epithelial cell adhesion molecule (EpCAM). EpCAM is a protein marker and thus a biological property of some CTCs but not all; these techniques maybe miss EpCAM negative cancer cells, which do not show this biological property [4].

Maybe in the future the detection and examination of CTCs will provide better insight on tumor biology and will promote the use of patient specialized therapeutic treatment. That would not only mean a minimal invasive withdrawal of samples but also a possibility to track patient status after cancer treatment and prevent relapse [2].

These are very promising outlooks, but it is very difficult to detect rare circulating tumor cells, due to their low quantity. That is why so far there is only one from the "Food and Drug Administration (FDA)" approved technique, called "CellSearch". There are other techniques available but not allowed for clinical use in the USA [2].

## 1.2  Cancer Cell Diagnostics

Modern techniques developed for cancer diagnostics normally use a 3 step procedure.

First the sample has to be taken from the patient. The most promising way for the future is a minimal invasive blood sample from a vein, which will maybe supersede invasive biopsies in some areas.

The second part is the enrichment of the sample. For instance in a blood sample there are only very few CTCs as mentioned in the chapter 1.1. So at some point it is useful and/or necessary to yield a higher density of cancer cells to simplify detection and further research.

Afterwards the detection is performed. In nature it is nearly impossible to take a sample with only one cell type, thus the CTCs have to be highlighted in some way [2, 4].

## 1.2.1 Enrichment techniques for CTCs

In the past decade many different techniques for isolation and enrichment of CTCs were established and tested. Some examples are given for research based on prostate cancer. For a quick overview Table 1 provides the most important data.

| Method | Mechanism | Blood used [ml] | Capture rate |
|---|---|---|---|
| **Density gradient centrifugation** | Differential migration of CTCs during centrifugation | Variable | 70% |
| **Size-dependent selection** | Separation based on cell diameter | 6–7.5 | 90% |
| **Magnetic negative selection** | Antibody-based depletion of normal blood cells using CD-45 coated magnetic particles | 2.5 | 52% to 88.4% |
| **Magnetic positive selection (CellSearch)** | Immuno-magnetic selection using EpCAM coated magnetic particles | 7.5 | 85% |
| **Flow cytometry** | Cell sorting using fluorescently labeled epithelial antigens | NA | NA |
| **Microfluidic device** | Positive selection of CTCs using antibodies attached to microfluidic device | 1 to 5.1 | 60% to 91.8% |

*Table 1:        Different techniques used to isolate prostatic CTCs in past research. [2]*

**Density dependent** enrichment methods like gradient centrifugation utilize the different densities of the sample parts. Normally a gradient solution is used to separate the sample according to the density and split into distinct layers during centrifugation. CTCs accumulate in one layer and can be extracted for further enrichment or detection.
Due to the possible mixing of the separated layers, this technique is often used as precursor for other methods [2].

Another promising approach is the **size-dependent** selection of cancer cells mostly through filtration of the sample. For this a porous array with distinct pore diameter is used (usually about 8μm) to hold back the CTCs which are usually bigger than other cells found in human blood or other liquids. Retained cells can then be stained to estimate the amount of the captured CTCs.
One big drawback of this system is that malign cell are not captured when they are smaller than the pore diameter. Sometimes due to the unpredictable shape and volume it is possible that they are actually smaller than the usual cancer cells and slip through the holes [2, 7].

Other laboratory techniques utilize a **magnetic field** and immune-magnetic particles for enrichment of malign cancer cells out of a blood sample. There are two different (simplified) ways to do this:
Positive selection:          Directly tag and extract the CTCs
Negative selection:          Label everything else and discard it. CTCs should remain.

When using the **negative selection** it is recommended to first use density centrifugation to enrich the cells. Then a special marker is used which is not existent on epithelial cells, called CD45 (Cluster of Differentiation 45). The particles are coated with anti-CD45 and thus are binding to the red blood cells and other CD45 exhibiting cells. These cells are then extracted with a magnet and discarded. Only cells without the CD45 marker, like the CTCs should remain. The cells do not get destroyed and are available for further investigation.

The disadvantage of this technique is, that it also lacks sensitivity, because of the loss of CTCs in other layers during centrifugation. Also the purity is sometimes not so high due to the remaining CD45 cells, which may not have been extracted completely [2, 8].

The most common method is the **positive selection** thanks to the only FDA approved device called "CellSearch Circulating Tumor Cell Test". This approach normally uses epithelial cell-surface antigens like EpCAM (epithelial cell adhesion molecule) and CK (Cytokeratin). The particles are labeled with anti-EpCAM or anti-CK. Before mixing the cells with the particles also a density gradient centrifugation should be made to separate the cells from the sample. Then the particles are mixed with the remaining cells. But opposite to the previous mentioned negative selection, here the CTCs are directly binding to the particles and then extracted with a magnetic field.

The downsides are that it is extremely time consuming and expensive. Furthermore it is also not very sensitive, because it relies only on surface antigens and thus maybe misses many CTCs. Researches have shown that cancerous cells can undergo a transformation from epithelial to mesenchymal cells and so they are not found with this technique [2, 8].

All the above mentioned techniques require expensive laboratory infrastructure and/or trained personnel, hence there is a need for new cost effective techniques with simple handling like the method proposed in this thesis.

### 1.2.2   Enrichment of CTCs with microfluidics

The most promising way for the future to enrich and detect CTCs is the use of **microfluidic devices**. It is the best approach to combine all steps into a single device and tailor it to special needs and cancer types. With microfluidic devices it is possible to combine the enrichment with physiological (e.g. size) and biological properties (e.g. antigens) and thus get a higher purification by avoiding the capture of background cells. Moreover the cells are viable after capturing and can be used for further analysis [4].

There are two main properties and their combination to be considered, when it comes to designing a microfluidic enrichment device:

1. Physical properties of the cells (size, charge, density)
2. Biological properties of the cells (antigens – surface marker)
3. A combination of physiological and biological properties

## 1.2.2.1  Microfluidic device utilizing physical properties

The easiest way to use physical properties of CTCs to capture them is probably the size. That means that the device has some sort of bottlenecks where the cells get squeezed and cannot move further. This approach has many drawbacks; in case of clogging the particle flow gets hindered and maybe also other particles get captured at these bottlenecks. This is why many researchers try to find better solutions to exploit the physical properties from cells.

One new approach for capturing and even separating different CTCs uses the effect of particle polarizability. An alternating electric field generates a dipole moment in the cells. In combination with the surrounding electric field an electrical net force occurs which induces a movement. This effect is called dielectrophoresis (DEP). The magnitude of this effect depends on the cells (size and polarizability – dielectric characteristics), the frequency, the electrical field and the fluid properties [9].
Roughly there are two possibilities for using DEP. Migration and retention. With migration the movement to different regions, because of polarizability, is used. With retention only the strongly polarizable particles stick to an electrode and are not washed away by fluid flow [4].

When using a frequency roughly lower than 10MHz two effects can be observed that rely on the conductivity difference. When the conductivity of the cell is bigger than that of the surrounding media it is called positive DEP (pDEP). That means the polarizability of the particle is bigger and therefore it is moving to the region of higher field densities. When the conductivity is lower it is called negative DEP (nDEP), which means that the cells are moving towards a region where the effective field is smaller. This nDEP effect is now used to separate different cells, because every cell type shows DEP properties at different frequencies. By choosing the right frequency the CTCs of interest undergo nDEP and thus get separated, otherwise the uninteresting cells or CTCs show nearly no DEP force. Fig. 2 shows the fundamental approach, which was used for nDEP separation [10].
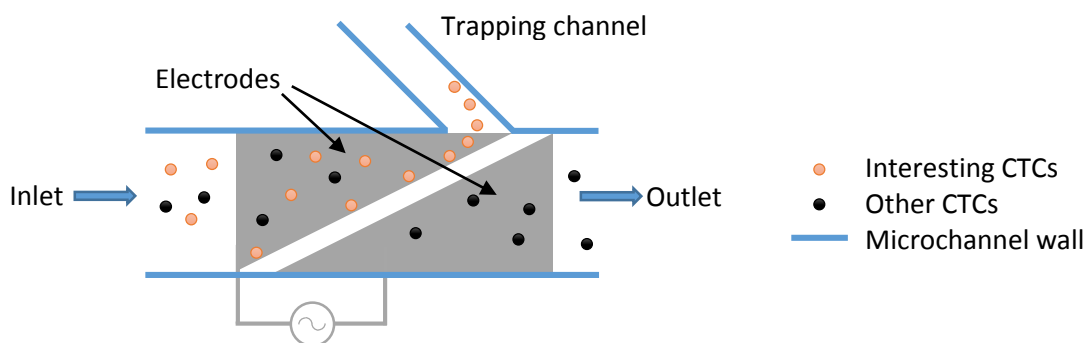


*Figure 2:        Schematic of DEP-based particle separation system [10]*

The advantages of this method are that no CTCs specific markers are needed. A direct separation is possible. Also different CTCs can be separated, but all that is only possible after previous investigation of DEP frequencies for different cells in varying media. Otherwise, finding the right frequency can be rather difficult and it is maybe necessary to change the medium to get different conductivities and, therefore, a better separation of the particles.
This approach can be easily combined with other techniques which exploit biological properties. One is described in the next chapter. Also a combination is given in chapter 1.2.2.3.

## 1.2.2.2 Microfluidic devise utilizing biological properties

The use of biological properties is very prominent, which normally requires antigens and specific surface markers to capture or separate different cells. This can be achieved by two different ways:

1. Antibodies are mixed with the cells suspension and the cells have to be separated from the fluid in a specific manner after antigen-antibody binding.
2. Antibodies are bound to a surface and bonding happens when cells with antigens are passing by and get captured [11].

The second method has some disadvantages such as aging and contamination of the coated surface. Long-term stability (time dependent changes) is an issue and therefore the first option is used for the device proposed in this thesis. For this purpose the special abilities of super-paramagnetic particles in combination with antibodies are used. A detailed description for this is given in chapter 1.4.2.

Nevertheless the second method can also be combined with the first one. For instance it is possible to bind biotin-labeled (biotin is a vitamin) antibodies to previously enriched fluids with CTCs and then insert the mixture into a microfluidic device with walls and obstacles, which are coated with streptavidin (protein). The biotin – streptavidin bonding which will occur is one of the strongest non covalent binding mechanisms in biology and, therefore, often used in molecular biology or biochemistry [11].

The design of the flow channel and the obstacles have a big impact on the efficiency of devices with capturing agents fixed on the walls. It is crucial that the CTCs hit the walls so that they can be captured. Many different designs were tested in recent years by many different authors [11, 12].

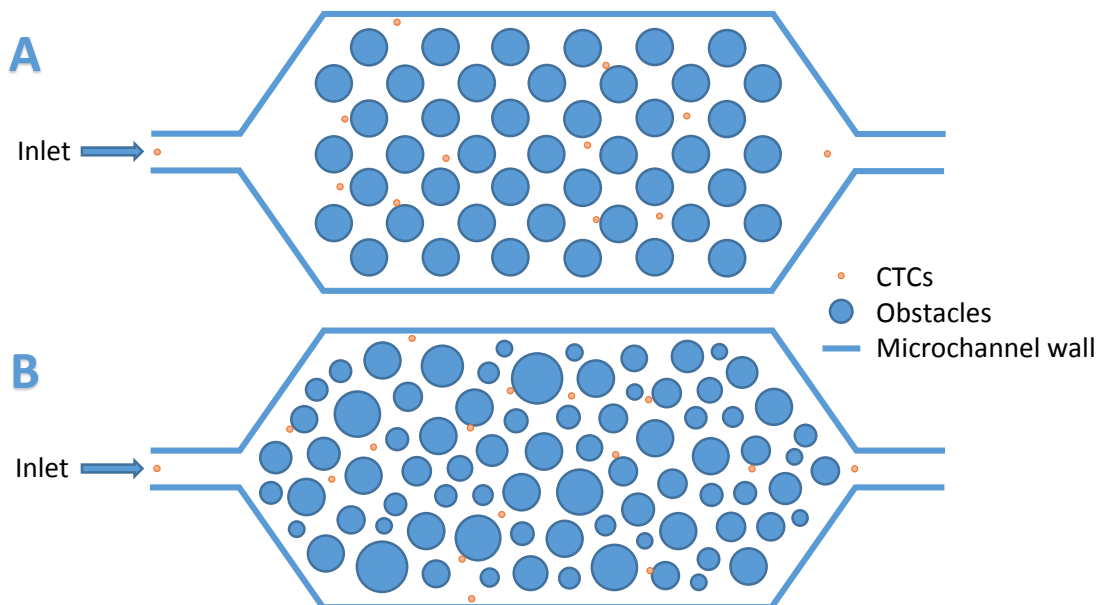Fig. 3 shows two different previously used obstacle distributions.



*Figure 3:*      *Different previously used obstacle distributions in microfluidic devices*
                *A) Symmetrically distributed micro-posts [12]*
                *B) Randomly distributed micro-posts [11]*

It is known that cells follow streamlines when the Stokes number is much smaller than one. When a CTC is not hitting the obstacle directly or directly flowing over the surface it will be shifted away according to the streamlines. Therefore, the obstacle designs are always arranged in such a manner that cells, which pass by one post will maybe hit the next one. This can be done with a previously calculated arrangement or with a randomly generated distribution of about 100.000 pillars.

The capture efficiency sometimes reaches 99%. Which shows one of the big advantages of such devices. Another benefit is the high survival rate of the captured CTCs [11, 12].

The obstacle arrangement can be adjusted to achieve higher capture rates but the streamline shift which arises from obstacles in the channel is still a problem when using this capture technique [11].

One major drawback of this technique is that these special microfluidic devices are quite difficult to manufacture and to prepare, because of the many obstacles and their complicated arrangement. It is also not possible (or highly complicated) to clean these devices, due to the residues on the walls and obstacles.

### 1.2.2.3   Microfluidic device utilizing a combination of physiological and biological properties

As mentioned before it is possible to use more than one cell property to separate or trap them, because the more specific characteristics are being addressed the better the outcome of the enrichment and the higher the achieved purification [4].

**The first example** is a combination of dielectrophoretic (DEP), gravitational and hydrodynamic lift forces; more than one physiological property is used to separate and enrich CTCs.

This technique utilizes the different velocity regions due to laminar flow in the microfluidic channel. Cells near the wall move slower than the ones in the center of the channel. The electrodes on bottom of the device are operated with a frequency and strength that pulls the CTCs to the bottom of the channel but has nearly no affect onto other cells like Red Blood Cells. As a result of this the CTCs on the bottom of the chip travel much slower and tend to stay in the device when other cells are already washed out by normal fluid flow in the center. This issue is shown in Fig. 4 [4, 9].
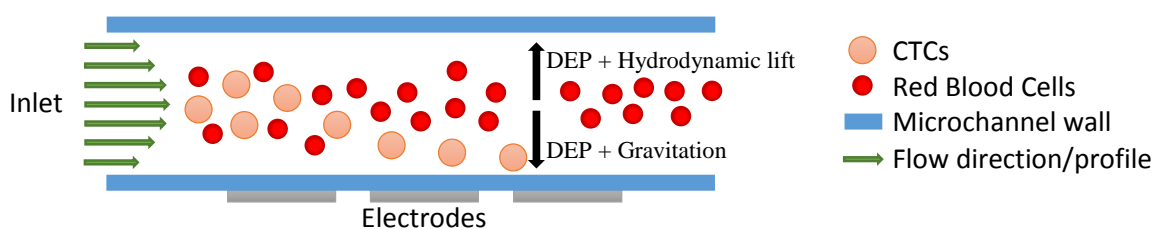


*Figure 4:        Utilizing different physical properties in one microfluidic device. [9]*

This device could be compared to a chromatograph. The particles (cells) are eluted at different times and therefore it is possible to separate them.

Research has shown that high loads have a negative effect on recovery of CTCs, but it is possible to make the device bigger for applications were high throughput is needed. One major drawback of this technique is, that it is very time consuming. One single application can take 20 to 60 minutes [9].

**The second example** is a simple combination of size (physiological) and immunological (biological) capture. As shown before it is possible to use each of these enrichment/capture methods as a standalone device, but it is much more promising to combine them and get a higher capture rate and/or purification of CTCs [4, 13].
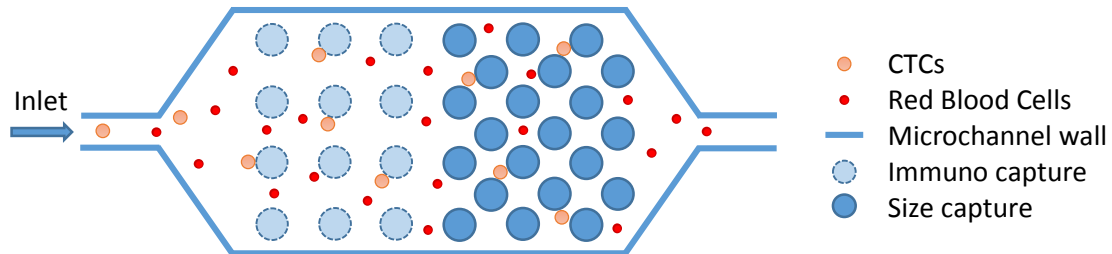


*Figure 5:    Combining physiological and biological capturing techniques. [13]*
*First obstacles are coated with antibodies specific to the CTCs and the later ones*
*are size specific for CTCs (only smaller cells can pass)*

The device shown in Fig. 5 is very promising, because it combines the advantages of two well researched capture techniques. Unfortunately it also combines the disadvantages. Cells can clog in the second part of the device and also streamline shift occurs due to the obstacles used to capture the cells [13].

In order to prevent these disadvantages the device proposed in this thesis uses trapping chambers (microtraps) which do not alter the streamlines in the channel. There are also no obstacles which can generate bottlenecks and hinder the flow.

## 1.2.3    Detection of CTCs

The methods mentioned in section 1.2.1 and 1.2.2 are not always a necessary prerequisite for the detection of CTCs, but normally very useful to get a better outcome.

One detection procedure is the **RT-PCR** (reverse transcription - polymerase chain reaction). It can be used to detect cancer specific RNA transcripts (e.g. PSA – prostate antigens) from whole blood samples, even when the CTCs are not intact. So it is possible to even detect the remains of cancer cells in blood. The more RNA markers are used the more specific the approach, but it is always limited.
Low numbers of target RNA can lead to false negative results and also it is not possible to distinguish between viable or dead CTCs which can be of great interest for correct patient treatment [2, 14].

More widely used are **surface markers**. By addressing antigens or molecules it is possible to attach stains or particles to the surface and make them visible for the measurement devices.

One type of surface marking is **Immuno-fluorescent staining**. It can be directly seen with fluorescent microscopes and is therefore often used. Also the "CellSearch" device relies on such kind of staining to visualize the outcome [15]. To differentiate different cells normally more than one marker is applied. Typical markers are summarized in Table 2.

| Abbreviation | Name | What is it? |
|---|---|---|
| **DAPI** | 4',6-diamidino-2-phenylindole | Molecule that binds directly to DNA and highlights it |
| **CK** | Cytokeratin | Antigen on epithelial cells |
| **EpCAM** | Epithelial cell adhesion molecule | Antigen on epithelial cells |
| **PSMA** | Prostate-specific membrane antigen | Antigen on prostate cells |
| **CD45** | Cluster of differentiation 45 | Antigen on leucocytes which is used to distinguish them from epithelial cells |
| **CD3** | Cluster of differentiation 3 | Antigen on T-Cells (T-Cell Receptor) |

*Table 2:*    *Molecules or antigens used for typical fluorescent staining [2]*
*Note that DAPI is directly the stain and all other mentioned are antigens, which are addressed with an antibody coupled with stain or particles*

When someone is looking for prostate cancer DAPI would be used for staining the cell-cores, PSMA for marking the prostate cells, Cytokeratin for marking all epithelial cells and CD45 for highlighting leucocytes. The cells are now being looked for are PSMA, CK and DAPI positive and CD45 negative. A real picture of such a measurement for prostate cancer is shown in Fig. 6.
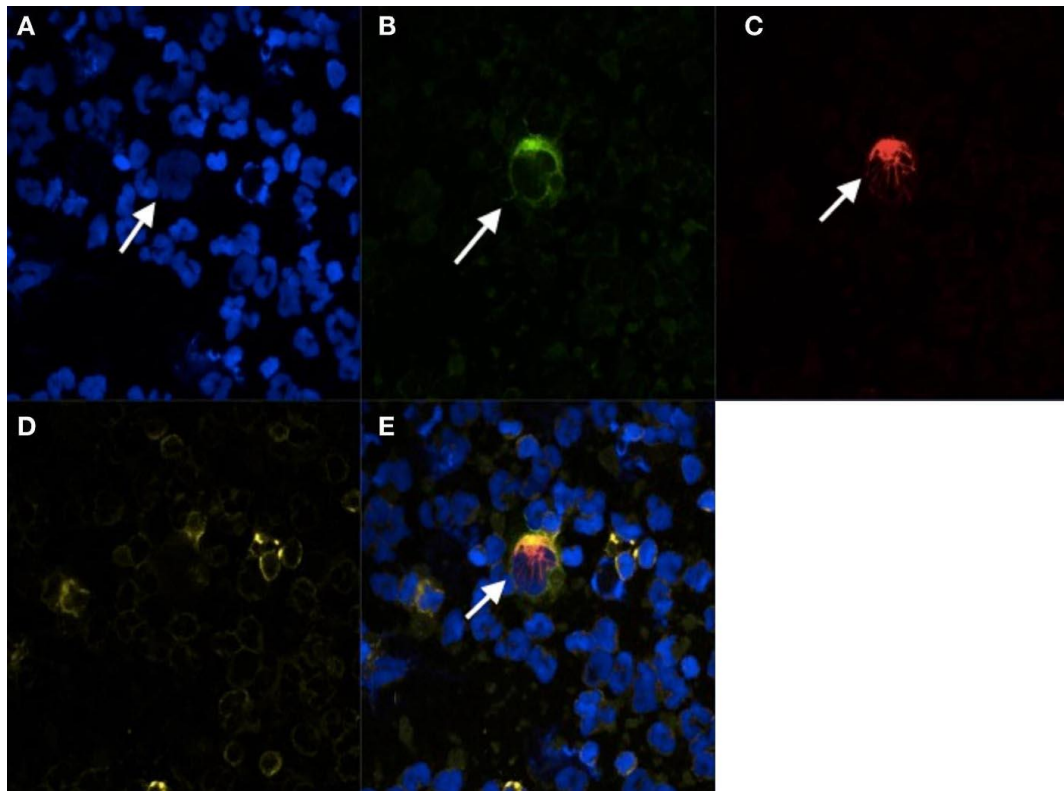


*Figure 6:*    *Stains used to mark antigens and DNA in a prostate cancer blood sample [2]*
*A: DAPI        B: PSMA        C: CK        D: CD-45        E: Composite Image*

Fluorescent staining is a very prominent detection method nowadays. It is easy to use and a big variety of stains for all purposes are available. There are also many standardized devices and procedures available.

Nevertheless there are also many drawbacks, like narrow excitation range and broad emission range of some stains, which makes it very difficult, time consuming and expensive to observe the desired objects. Also the long-term photo stability of the fluorescent dyes is often a problem. That means that it is not possible to treat cells with a stain and then store them for later usage. It is also not possible to show different features with one stain. So, there is a need for different stains, which also includes the requirement of different wavelengths of the excitation light. Furthermore, it is only a detection method and enrichment is a prerequisite.

A more stable type of surface markers are **magnetic particles**. Nowadays, they are often used for enrichment, but not for detection of cells (Fig. 7). This thesis is a part of a project, which aims to make use of the particles in both ways. With highly sensitive sensors it is possible to detect the presence of one particle and in the future it may even be possible to detect certain characteristics of the bounded cell by special movement of the particle in relation to the sensor [16].

It is clear that it is cheaper and timesaving to use the same marker for enrichment and detection. Also the storage of magnetically labeled cells is not a problem under proper conditions. That means that the same cells can be examined more than one time (also with days between). In combination with microfluidics it could be possible to build µTAS (Micro total analysis system) for detection of CTCs without using a lab or a microscope.



*Figure 7:      Jurkat-Cell labeled with a superparamagnetic particle on the surface*

## 1.3 Microfluidics

In the last decades the miniaturization of systems progressed in nearly every field. This introduced a new area called MEMS (micro-electro-mechanical-systems). More and more of these devices are being used for biological, chemical and medical applications often with a scope on fluid flow. This new fluid driven approaches are now termed "microfluidics" [17].

### 1.3.1 The need for miniaturization

There are many reasons, why microfluidics is very important for present and future applications. The main one is the need for affordable quick test devices for "Point of Care Diagnostics" use and new possibilities for detecting rare cells and liquids, which would not be possible in macro scale.
What are the benefits of scaling down and integrating?

- Outstanding performance in
    - speed – More reactions and smaller diffusion length
    - efficiency – Lesser volume and nearly no consumption of resources
    - control – Integrated systems are easy to handle and often independent from other devices and calibration

- Combination

    It is possible to combine various different steps into one device. For instance the enrichment, detection of CTCs can be made on a single chip

- Simple integration

    Electrical and mechanical sensors and actuators can be integrated very easily, which reduces the need for additional equipment (cost and space reducing)

- Reduced consumption

    Very small volumes of sample and reagent are needed

- Portability

    Small integrated systems are very portable and are easy to use for "Point of Care" and Field detection

The main reason why microfluidics are used for CTC detection is the rare occurrence of these special cells. Maybe only every billionth cell or less is a CTC and without microfluidics it is nearly impossible to generate repeatable protocols to find, catch and characterize them for further patient treatment.
One big advantage used in cancer diagnostics is that the surface to volume (S/V) ratio is getting bigger by scaling down the system. This is important when using immunological techniques for capturing CTCs on walls and other obstacles, because when the reaction surface gets bigger it is much more likely that the cells will stick to the surface inside the channel.

## 1.3.2 Fluid mechanics in micro channels

In microfluidics the flow is normally laminar, which means that no turbulences occur and mixing is mainly made by diffusion. For confirming this type of flow the "Reynolds Number $R_e$" defined in Eq. 1 is used.

$$R_e = \frac{inertial\ force}{viscous\ force} = \frac{\varrho\ u\ l}{\eta} = \frac{u\ l}{\nu}$$

*Equation 1: Reynolds Number [18]*

$\varrho$ ........................ *Density of the fluid*                  *(kg/m³)*
*u or v* ................ *Velocity of the flowing fluid*       *(m/s)*
*l* ........................ *Characteristic length*               *(m)*
*η or μ* ............... *Dynamic viscosity of the fluid*    *(Ns/m² = kg/ms)*
*ν* ........................ *Kinematic viscosity of the fluid*   *(m²/s)*

Usually, the dynamic viscosity is used to calculate the Reynolds number, but sometimes also kinematic viscosity is used. Therefore in Eq. 2 the relation between these two parameters is given.

$$\eta = \nu\ \varrho = \frac{1}{\varphi}$$

*Equation 2: Relation between dynamic and kinematic viscosity as used in Eq. 1*

*φ* ........................ *Fluidity: Reciprocal of dynamic viscosity*     *(ms/kg)*

The Reynolds number is a dimensionless entity to estimate the flow type. When a critical value is reached, small objects can generate turbulences in a laminar flow, even though the flow was laminar previously. Researchers have shown that there is a rough pattern, which can be used to distinguish between laminar and turbulent flow. Normally, the critical value of the Reynolds number is between 2000 and 3000. It can be assumed that numbers under 10 are always laminar and numbers between 10 and 2000 are very likely laminar [18].

Fluids flowing inside a microfluidic channel have a very small velocity what normally generates low Reynolds numbers (usually smaller than 1) and thus a laminar flow [17].

A comparison between laminar and turbulent flow can be seen in Fig. 8.

Laminar flow ($R_e$ < 10)    Turbulent flow ($R_e$ > 1000)

Microchannel wall
Flow direction/profile
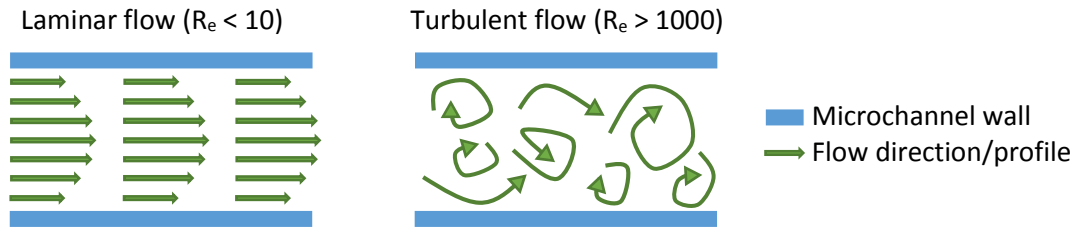
*Figure 8:    Schematic of laminar and turbulent flow in a microfluidic channel*
*Laminar flow comes with a laminar flow profile, but a laminar flow profile does not*
*necessarily need a laminar flow to occur*

It is clear that in a microfluidic system normally no mixing of fluids occurs without diffusion and this takes time. Therefore, cells and particles move along streamlines through the channel, which they are only leaving when obstacles are on their way. Some of the approaches used in CTC diagnostic rely upon this feature as described in chapter 1.2.2.2.

The characteristic length, which is used in Eq. 1 takes into account that different channel shapes and filling heights can appear. When cylindrical channels are used the characteristic length is the same as the diameter. For all other shapes Eq. 3 can be used to calculate the hydraulic diameter, which can be used as characteristic length. The Reynolds numbers is normally very small in microfluidics, which makes it not critical to calculate a really exact number, because the difference between cylindrical and rectangular hydraulic diameters is smaller than factor 2 [18].

$$l = D_h = \frac{4 \; times \; "Cross \; Section \; of \; the \; Area"}{"Wetted \; Perimeter"} = \frac{4 \, A}{P_{wet}}$$

*Equation 3:    Hydraulic diameter as characteristic length for the Reynolds number [18]*

$l$ ......................... *Characteristic length*                          *(m)*
$D_h$ ..................... *Hydraulic diameter*                          *(m)*
$P_{wet}$ ................... *Perimeter which is in contact with fluid*    *(m)*
$A$ ....................... *Cross Section of the channel*                *(m²)*

One could expect that laminar flow is only possible with very small dimensions (low characteristic length – range of µm) and with bigger dimensions (characteristic length of about 1m and above) there is always turbulent flow; however there are some extremes. For instance glaciers are flowing very slowly so that the Reynolds number is very small even on a macroscopic scale.

## 1.4 Magnetic Methods

### 1.4.1 Magnetic materials

Some materials get magnetized when a magnetic field is applied on them. Eq. 4 gives the macroscopic relationship between magnetic materials and a magnetic field [19].

$$\vec{B} = \mu\,\vec{H} = \mu_0\,\mu_r\,\vec{H} = \mu_0\,(\vec{H} + \vec{M}) = \mu_0\,(1 + \chi)\,\vec{H}$$

$$\vec{M} = \chi\,\vec{H}$$

*Equation 4:    Macroscopic relation between magnetic field and materials [19]*

| | | |
|---|---|---|
| $B$ ...................... | Magnetic flux density | $(Vs/m^2 = T)$ |
| $H$ ...................... | Magnetic field | $(A/m)$ |
| $\mu$ ...................... | Permeability | $(Vs/Am)$ |
| $\mu_0$ ..................... | Permeability of the free space (constant) | $(4\mu*10^{-7}\ Vs/Am)$ |
| $\mu_r$ ..................... | Relative Permeability | $(1)$ |
| $M$ ..................... | Magnetization | $(A/m)$ |
| $\chi$ or $\chi_m$ ............. | Magnetic susceptibility | $(1)$ |

Ferromagnetic materials exhibit high susceptibilities and a hysteresis loop (Fig. 9) which means that susceptibility is neither constant nor a function of the magnet field [20].
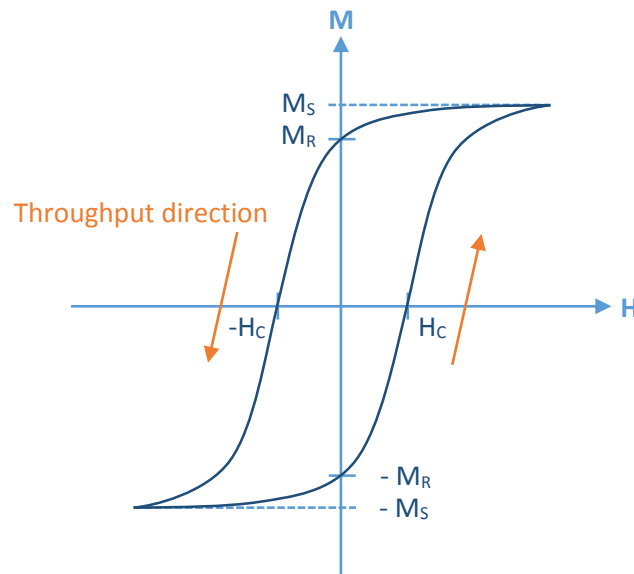


*Figure 9:        Typical magnetization curve of ferromagnetic materials (hysteresis loop) [20]*

| | | |
|---|---|---|
| $H_C$ ..................... | Coercivity | $(A/m)$ |
| $M_R$ ................... | Remanent magnetization (Remanence) | $(A/m)$ |
| $M_S$ .................... | Saturation magnetization | $(A/m)$ |

The hysteresis loop results from the domain structure of magnetic materials. A domain is a part of the material where the magnetic moments are in the same direction and therefore act cooperatively. They are separated by walls and the movement of these walls is a primary reason for magnetic loss and the existence of the hysteresis loop (Fig. 10). The shape of this loop is to some part determined by the structure geometry. In the range of micrometers (and bigger) a particle usually has a magnetic multi-domain structure. Loops of such small particles are usually narrow, because it is easy to move the orientation [21].
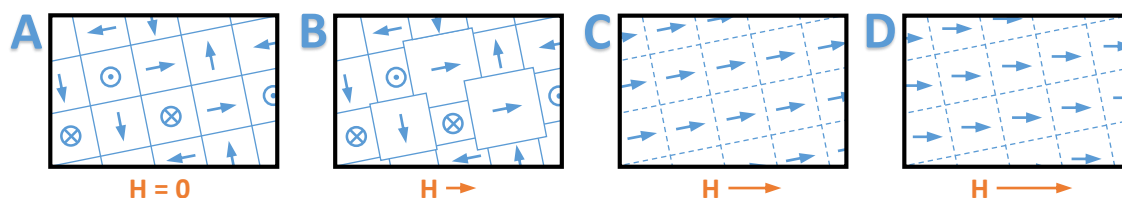


Figure 10:     Domain processes and change of magnetization [20]

A) Demagnetized state (no field)
B) Partial magnetization by domain wall movement (weak field)
C) Irreversible rotation of domain magnetization into the direction of a crystallographic easy axis (moderate field)
D) Reversible rotation of the field until saturation (high field)

The high magnetization of ferromagnetic materials (and particles) is favorable, but it comes with the described loop characteristic. The problem for many applications is that these materials preserve their magnetization (remanent magnetization) when the field is removed, but for many biomedical applications this is of high importance. For instance magnetic particles would be sticking to each other and form big agglomerates [21].

This is the reason why there is a need for materials with no remanent magnetization. Many materials have this characteristic like paramagnets and diamagnets. The disadvantage of paramagnets/diamagnets is that they only have a very small susceptibility. This is the reason why the proposed device uses superparamagnetic materials. They exhibit no remanent magnetization nevertheless they have a very high susceptibility (like ferromagnets).
Fig. 11 shows a comparison of the discussed types of magnetism, which have a zero remanent magnetization in common.
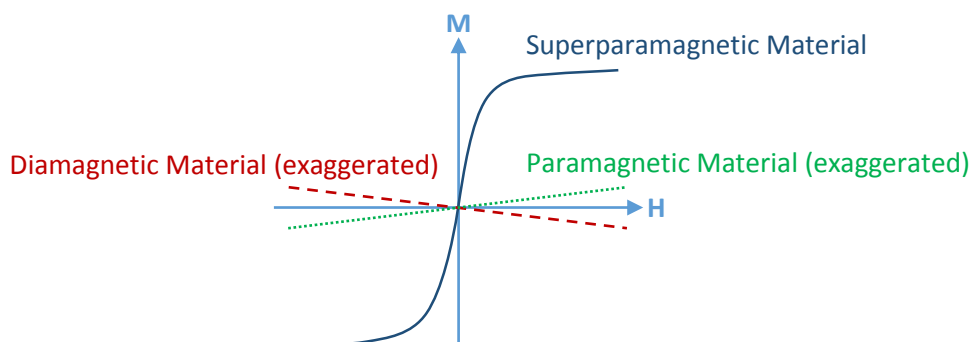


Figure 11:     Magnetization curve of para-, dia- and superpara-magnetic materials [19]

## 1.4.2   Superparamagnetic particles

The coercivity of a magnetic material depends on the grain size (Fig. 12). Large grains tend to generate multi-domain structures (Fig. 12.D) [22].
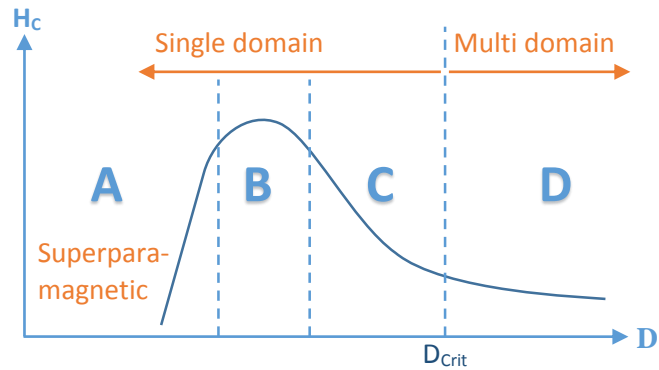


*Figure 12:*      *Schematic illustration of the coercivity as a function of the particle diameter [22]*

A)      *Superparamagnetic behavior due to thermally activated rotation processes*
B)      *Reversion of magnetization by a homogeneous rotation process*
C)      *Reversion of magnetization by inhomogeneous rotation processes*
D)      *Reversion of magnetization by domain wall displacements*

$H_C$ .....................*Coercivity*                                   *(A/m)*
$D_{Crit}$ ..................*Critical particle diameter*                      *(nm)*

When the grain size decreases until a critical value is reached (listed in Table 3 for some spherical materials), the formation of walls is no longer favorable and, therefore, they become single domain (Fig. 12.A-C) [23].

| Material | $D_{crit}$ (nm) |
|---|---|
| Fe | 14 |
| Ni | 55 |
| Co | 70 |
| $Fe_3O_4$ | 128 |
| $\gamma$-$Fe_2O_3$ | 166 |

*Table 3:*      *Estimated single domain sizes for spherical particles with no shape anisotropy [23]*

The basic mechanism of superparamagnetism is the relaxation of the net magnetism through the temperature. Particles get so small that the energy barrier of moment reversal (ΔE) gets also very small and thus the relaxation time gets independent from the temperature (Fig. 12.A). This behavior is shown in Eq. 5 [21].

$$\tau = \tau_0 \, e^{\frac{\Delta E}{k_B \, T}}$$

*Equation 5:    Relaxation time of the net magnetization of a magnetic particle [21]*

| | | |
|---|---|---|
| $\tau$........................ | *Relaxation time* | $(s^{-1})$ |
| $\tau_0$...................... | *Used as constant* | $(s^{-1})$ |
| $\Delta E$..................... | *Energy barrier to moment reversal* | $(kgm^2/s^2 \text{ or } J)$ |
| $k_B$...................... | *Boltzman constant* | $(1.38*10^{-23} \, kgm^2/s^2K)(J/K)$ |
| $T$....................... | *Temperature* | $(K)$ |
| $k_B*T$................. | *Thermal energy* | $(kgm^2/s^2 \text{ or } J)$ |

To summarize it is superparamagnetism when two criteria are fulfilled [23]:

1. The magnetization curve exhibits no hysteresis
2. Magnetization curves at different temperatures superpose (M over H/T)

For research and treatment there is a need for superparamagnetic particles in the size of hundreds of nanometers to some micrometers. Bulk materials do not show superparamagnetic behavior in this size. Hence it is necessary to combine nanoparticles in a sort of matrix to get bigger particles with the same behavior as the nanoparticles; they have bigger overall magnetization and therefore a bigger force onto the particles can be exerted (which for instance necessary to move cells). Such a composite of nanoparticles is shown in Fig. 13 [21].
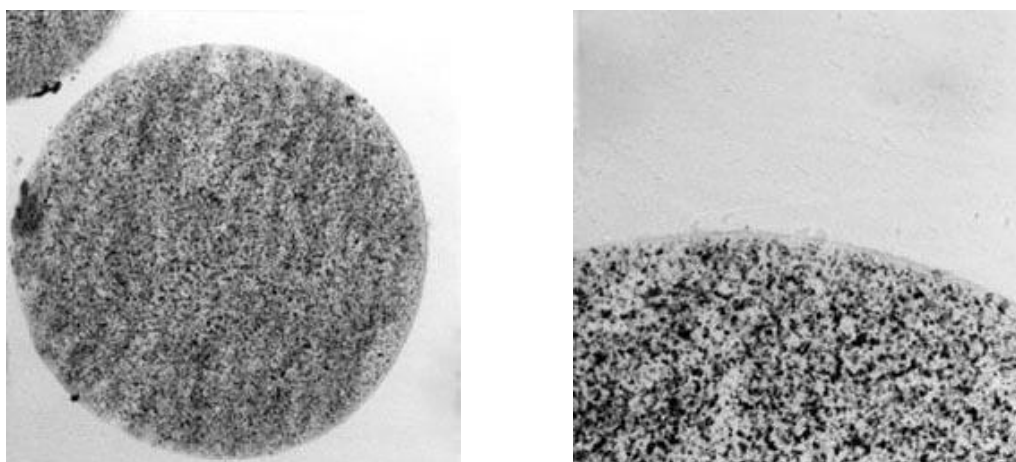


*Figure 13:     Magnetic particles (app. 5µm) build up by nanoparticles in polystyrene [24]*

For biological application this composite materials are usually modified at the surface to be useful for different tasks. This treatment for instance hinders aggregation, raises biocompatibility and prepares the particle for coupling to biological entities as antibodies or antigens.

### 1.4.3 Forces on superparamagnetic particles in microfluidic channels

#### 1.4.3.1 Magnetic force

Superparamagnetic particles or nanoparticles in a magnetic field can be approximated by a point like magnetic dipole (with the moment m) hence also the same equations can be used. So we can use the gradient of the magnetic energy to calculate the force on the particle (Eq. 6) [25].

$$\vec{F_m} = \vec{\nabla} \left( \vec{m} \cdot \vec{B} \right) \approx \left( \vec{m} \cdot \vec{\nabla} \right) \vec{B}$$

*Equation 6:   Magnetic force acting on particle is the gradient of the magnetic energy [25]*

| | | |
|---|---|---|
| $F_m$ .....................Magnetic force on particle | | *(kgm/s² = N)* |
| $m$ .....................Magnetic moment | | *(Am² = J/T)* |
| $B$ .....................Magnetic flux density | | *(Vs/m² = T)* |

Assuming that we use the particle in a liquid environment, the magnetic moment can be calculated like shown in Eq. 7 [25].

$$\vec{m} = V \vec{M} = V \Delta\chi \vec{H} = V \left( \chi_P - \chi_L \right) \vec{H}$$

*Equation 7:   Magnetic moment of a particle in a liquid environment [25]*

| | | |
|---|---|---|
| $V$ .....................Volume of particle | | *(m³)* |
| $M$ .....................Magnetization | | *(A/m)* |
| $H$ .....................Magnetic field | | *(A/m)* |
| $\Delta\chi$ .....................Difference in susceptibility | | *(1)* |
| $\chi_P$ .....................Susceptibility of the particle | | *(1)* |
| $\chi_L$ .....................Susceptibility of the liquid surrounding | | *(1)* |

By combing Eq. 4 (B = $\mu_0$*H), Eq. 6 and Eq. 7 we get Eq. 8 for the magnetic force on a particle [25].

$$\vec{F_m} = \frac{V \Delta\chi}{\mu_0} \left( \vec{B} \cdot \vec{\nabla} \right) \vec{B}$$

*Equation 8:   Magnetic force acting on particle based on its properties [25] [26]*

From Eq. 8 it is clear that the magnetic force on a particle depends on

- the magnetic volume (of the particle)
- the susceptibility (difference between particle and surrounding)
- the strength of the field
- the gradient of the field

Here it is important to recognize that a field gradient is inevitable. In a homogeneous field the particles would only be exposed to a torque and thus they would not move into a desired direction. This circumstance is depicted in Fig. 14 [25, 26].
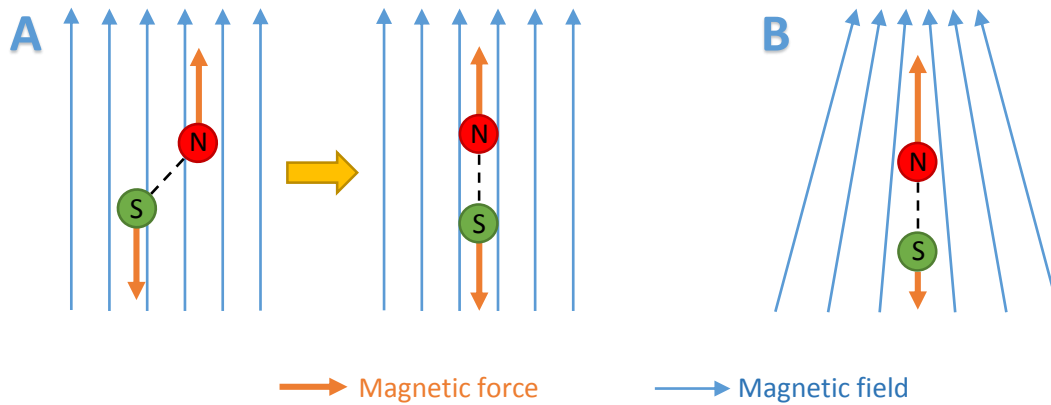


*Figure 14:    Movement of a magnetic dipole in different magnetic fields*
*A)    Torque movement of a dipole in a homogenous field (before and after) – Same force*
*B)    Movement towards higher gradient in inhomogeneous field – Different forces*

To generate an inhomogeneous field there are some possibilities [26]:

- Conventional magnets outside the microfluidic channels [26]
- Micro fabricated magnets directly on the chip
- Electromagnets

Most of them are very convenient but lack the possibility of integration and controlled interaction. For instance it is not easy possible to control the field of a conventional or electro magnet outside the channel to such an extent that manipulation of single particles is possible. This is why the approach of this thesis uses the field of current carrying microstructures to manipulate beads. With this microconductors it is possible to generate very accurate and user controllable fields. The most elementary way is to use the field of a straight conductor, which is very thin and long. The field is then described by Eq. 9.

$$B = \mu_0 H = \mu_0 \frac{I}{2\pi r}$$

*Equation 9:    Flux density of an infinite straight conductor with thin circular perimeter*

*I ........................ Current through conductor                      (A)*
*r ........................ Distance conductor and receiving point      (m)*

### 1.4.3.2 Drag force

Another force acting on particles in suspension is the drag force. It is a consequence of the velocity difference between the particle and the surrounding liquid. Since these particles are always used in a liquid environment, this force is the main one to overcome when moving particles in liquids. The crucial parameter is the velocity difference (Δv) between the liquid and the particle. One or both velocities can get zero when for instance the liquid is static and the particle is moving [25].

$$\vec{F_d} = 6\,\pi\,\eta\,r\,\Delta\vec{v}\,f_D$$

*Equation 10: Drag force acting on particle in liquid environment [25, 27]*

$F_d$ ..................... Drag force       *(kgm/s² = N)*
$\eta$ or $\mu$ .............. Dynamic viscosity of the fluid       *(kg/ms = Ns/m²)*
$r$ ....................... Radius of the particle       *(m)*
$\Delta v$ .................... Velocity difference (fluid – particle)       *(m/s)*
$f_D$ ..................... Drag coefficient (1 to 3)       *(1)*

Eq. 10 shows the calculation of the drag force with the help of a drag coefficient, which takes into account the distance between walls and the particle. In the middle of a channel it is usually one, but it can rise to a factor of three near the walls [25].

### 1.4.3.3 Magnetophoretic mobility

The two biggest forces acting on a particle in a microfluidic channel are the magnetic force and the drag force. To move the particle a velocity difference is needed – as mentioned above. Now assuming that in the horizontal plane only these two forces are of interest we can equal Eq. 8 (Magnetic force) and Eq. 10 (Drag force) and calculate the velocity difference which is generated (Eq. 11.a and b). When we assume that the particle is in the middle of the channel ($f_D = 1$) and the particle is spherical ($V = 4\pi r^3/3$) Eq. 11.c is valid [25]:

a)    $6\,\pi\,\eta\,r\,\Delta\vec{v}\,f_D = \dfrac{V\,\Delta\chi}{\mu_0}\left(\vec{B}\cdot\vec{\nabla}\right)\vec{B}$

b)    $\Delta\vec{v} = \dfrac{V\,\Delta\chi}{6\,\pi\,\eta\,r\,\mu_0}\left(\vec{B}\cdot\vec{\nabla}\right)\vec{B}$

c)    $\Delta\vec{v} = \dfrac{2\,r^2\,\Delta\chi}{9\,\eta}\,\dfrac{1}{\mu_0}\left(\vec{B}\cdot\vec{\nabla}\right)\vec{B}$

*Equation 11: Velocity difference between particle and surrounding liquid [25]*

The first part of Eq. 11.c can now be separated, because it is specific to a particle. It is called "magnetophoretic mobility" and it describes how magnetically manipulable the particle is in the given liquid (Eq. 12) [25].

$$\xi = \frac{2\,r^2\,\Delta\chi}{9\,\eta} = \frac{V\,\Delta\chi}{6\,\pi\,r\,\eta}$$

*Equation 12:  Magnetophoretic mobility of a superparamagnetic particle [25]*

*$\xi$ ....................... Magnetophoretic mobility                        (m³s/kg)*
*r ....................... Radius of the particle                        (m)*
*$\Delta\chi$ .................... Difference in susceptibility                        (1)*
*$\eta$ or $\mu$ .............. Dynamic viscosity of the fluid                        (kg/ms = Ns/m²)*

With the magnetophoretic mobility from Eq. 12 it is now possible to write Eq. 11.c as

$$\Delta\vec{v} = \frac{\xi}{\mu_0}\left(\vec{B}\cdot\vec{\nabla}\right)\vec{B}$$

*Equation 13:  Velocity difference reduced to mobility and flux density [25]*

### 1.4.3.4  Other perpendicular forces

There are additional forces, which are acting onto particles in a microfluidic system, but mostly in a perpendicular direction. It strongly depends on the application if it is necessary to take them into account or not.

One of these forces is the **gravitation $F_g$**. In microfluidics it is a rather small force and for 1µm particles the sinking speed is about 0.5µm/s. In a system with a flow of about 5 to 50µm/s this force is negligible [27].

The **electrostatic force $F_{el}$** is sometimes used to avoid sticking to the surface. It is generated due to the building of an electrostatic double layers in ion-containing solutions. It occurs between the channel wall and the liquid and also between particles and liquid. When the particle moves to the wall this double layers interact and generate an attracting or repulsing force depending on the layer structures of both [25].

**Van der Wasls forces $F_{vdW}$** are short range forces between dipoles and/or induced dipoles. They are acting on a distance of about 100 nm and thus only occur nearby the channel walls. They are in most cases attractive forces [25].

### 1.4.3.5  Example of forces and velocities acting in a microfluidic channel

The velocities and forces which are acting on a particle when it travels through a microfluidic channel are shown in Fig. 15. Like mentioned above the difference in velocity of fluid and particle generates a drag force. This force can also be in flow direction when the magnetic field decreases the velocity in flow direction. This drag force $F_d$ combined with the magnetic force $F_m$ gives the overall force $F_{particle}$ which is moving the particle towards the magnet (or conductor acting as magnet).
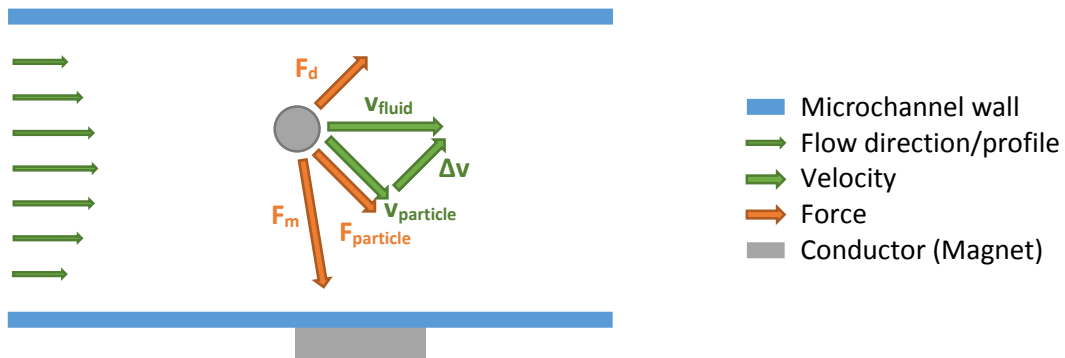


*Figure 15:       Forces and velocities acting on a particle in a microfluidic channel*

# 2  System Design and Implementation

In this chapter the working principle of the proposed device will be explained, followed by theoretical investigations concerning the magnetic flux density and the velocity in the microfluidic channel. Moreover, design requirements and considerations regarding chip design, microfluidic layer structure, microtrap size and position will be illustrated.

## 2.1  Working Principle

The microfluidic device proposed in this work serves the purpose of capturing single (and/or multiple) vital cells in microtraps with integrated current carrying microstructures (microconductors).

The cells are being labeled with superparamagnetic particles in a tube before inserting them into the microfluidic channel. The trapping device itself consists of two main parts; the silicon chip with the integrated microconductors and the microfluidic channels and microtraps which are placed on top of the chip.

The cells are moving through the channel until they reach the trapping holes, which are placed underneath it. Then it depends on the state of the microconductors; if they are activated and the cell is labeled with a magnetic particle then the cell is moving towards the trap due to the magnetic force which is exerted onto the particle. Once captured, the cell stays in the trap even when the conductor is switched off, due to the low fluid velocity in the microtrap. This captured cell can now be used for further analysis (e.g. drug screening). Other cells and parts of the fluid do not get influenced by the trap or the trapped cells and can pass by the section without problems. A schematic drawing of a capture process is shown in Fig. 16.



Legend:

- ▬ Microchannel wall
- → Flow direction/profile
- ▬ Insulation
- ▬ Conductor (Magnet)
- ● CTCs
- ● Other cells (not tagged)
- ● Superparamagnetic particle

- $r_P$ ...... Particle radius
- $r_C$ ...... CTC radius
- $t_W$ ..... Trap width
- $t_H$ ...... Trap height
- $c_W$ ..... Conductor width
- $c_H$ ...... Conductor height
- $FC_H$ ... Fluid channel height
- $I$ ........ Current (in z-plane direction)
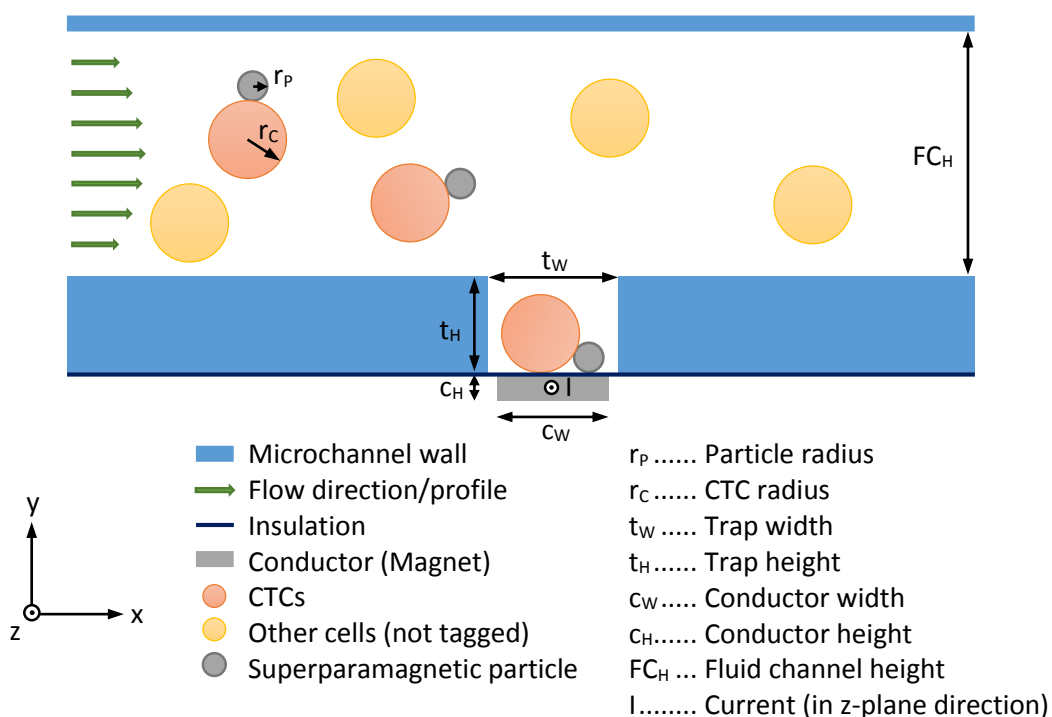
*Figure 16:     Working principle of the cell trapping device (cross section through the x-y plane)*

## 2.2 Theoretical Investigations

In this section simulations of the magnetic flux density, the magnitude of the fluid velocity and the magnetophoretic force are presented. Moreover, a simulation of a complete trapping process will be illustrated.

### 2.2.1 Magnetic flux density calculation

The conductor under the trapping channel is used to generate a force onto particles and cell-particle couples (magnetically labeled cells). To get an estimation of the field's magnitude and to confirm the outcome of the simulation (Chapter 2.2.3) an analytical calculation with "MATLAB R2013b" was carried out.

The equations used for this calculations are based on the Biot-Savart law, which gives the flux density in a specified distance to a current distribution. Eq. 14 gives the Biot-Savart law for a filamentary conductor [28].

$$\vec{B}(P) = \frac{\mu_0}{4\,\pi} \oint \frac{I(Q)\,\vec{e_I}\,ds}{r_{PQ}{}^2} \times \overrightarrow{e_{PQ}}$$

*Equation 14:  Biot-Savart law for a filamentary conductor [28]*

P.....................Receiving Point
Q....................Source
B ....................Flux density in point (P)           (T)
I......................Current at point (Q)               (A)
$r_{PQ}$ ..................Distance between P and Q       (m)
$e_I$....................Direction of the current          (1)
$e_{PQ}$..................Direction between P and Q        (1)

Using Eq. 14 it is possible to combine unlimited filamentary conductors to one big conductor with the shape of a rectangle. The derivation was calculated in previous research and for this work only the results were used [29]. Fig. 17 shows the quantities used for the analytical calculation.
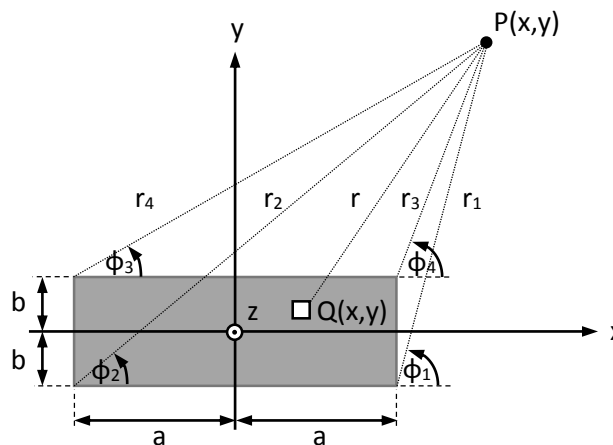


*Figure 17:      Rectangular conductor with out of plane current and labels matching Eq. 15*

Eq. 15 gives the magnitude of a rectangular conductor. The same labels were used as in Fig. 17.

$$r_1 = \sqrt{[(x-a)^2 + (y+b)^2]} \qquad \phi_1 = \frac{y+b}{x-a}$$

$$r_1 = \sqrt{[(x+a)^2 + (y+b)^2]} \qquad \phi_2 = \frac{y+b}{x+a}$$

$$r_1 = \sqrt{[(x+a)^2 + (y-b)^2]} \qquad \phi_3 = \frac{y-b}{x+a}$$

$$r_1 = \sqrt{[(x-a)^2 + (y-b)^2]} \qquad \phi_4 = \frac{y-b}{x-a}$$

$$B_x(x,y) = -\frac{\mu_0\, I}{8\,\pi\, a\, b}\left[(y+b)(\phi_1 - \phi_2) - (y-b)(\phi_4 - \phi_3) + (x+a)\ln\frac{r_2}{r_3} - (x-a)\ln\frac{r_1}{r_4}\right]$$

$$B_y(x,y) = \frac{\mu_0\, I}{8\,\pi\, a\, b}\left[(x+a)(\phi_2 - \phi_3) - (x-a)(\phi_1 - \phi_4) + (y+b)\ln\frac{r_2}{r_1} - (y-b)\ln\frac{r_3}{r_4}\right]$$

$$B(x,y) = \sqrt{B_x^{\,2} + B_y^{\,2}}$$

*Equation 15:  $B_x$, $B_y$, B and distances/angles for Cartesian coordinates [29] [30]*

For the simulation and analytical calculation the plane at x = 0 µm was chosen (Fig. 18) and therefore the diagram shows the flux density over the y-coordinate.
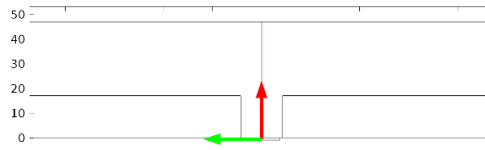


*Figure 18:     Cut-plane for the simulation and the analytical calculation of the flux density*

Fig. 19 shows the diagram with the comparison between simulation and calculation. All values are in the same range and match perfectly for distances bigger than 10 µm, which is important for trapping, because particles in the channel are usually 10 to 40 µm away from the conductor.
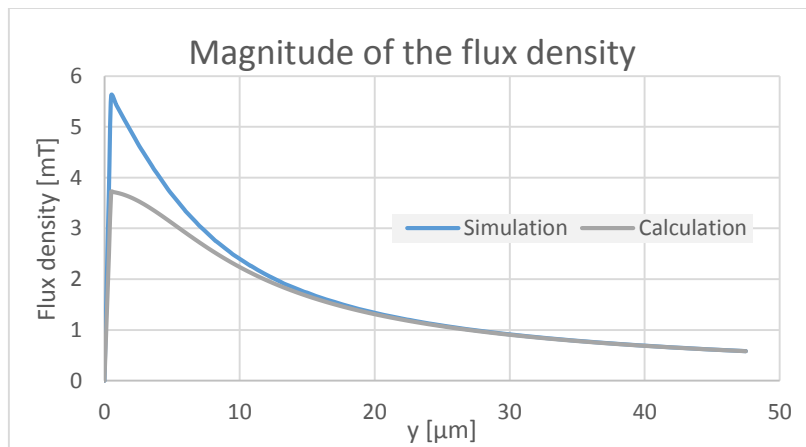


*Figure 19:     Comparison of the simulation and the analytical calculation of the flux density*
*                The border of the conductor is at 0.5µm (peaks)*

### 2.2.2 Simulation basics

All simulations were carried out with "COMSOL Multiphysics Version 4.4".

For that purpose a new model was generated. That includes geometry, physics and parameters. To get a quick overview the model tree is shown in Fig. 20. It depicts the used physics modules as well, which includes "Magnetic Fields (mf)", "Creeping Flow (fpt)" and "Particle Tracing for Fluid Flow (fpt)". That is one of the main benefits of COMSOL; the ability to couple different physical phenomena and get very accurate simulations of complex physical interactions.
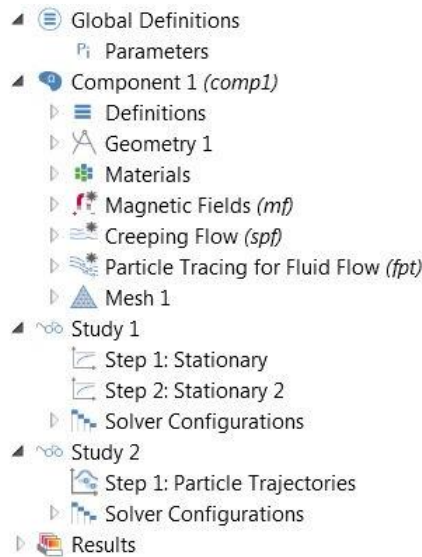


*Figure 20:       Model tree used for the simulation of the cell trap in COMSOL Multiphysics 4.4*

A new simplified geometry was generated based on Fig. 16 (working principle) and can be seen in Fig. 21. It is only a 2D model since a 3D model is much more complicated to generate and needs much more processing power and therefore a longer time to simulate. However it is very accurate, because the cut through the x-y plane contains every important detail about the channel and the trap.
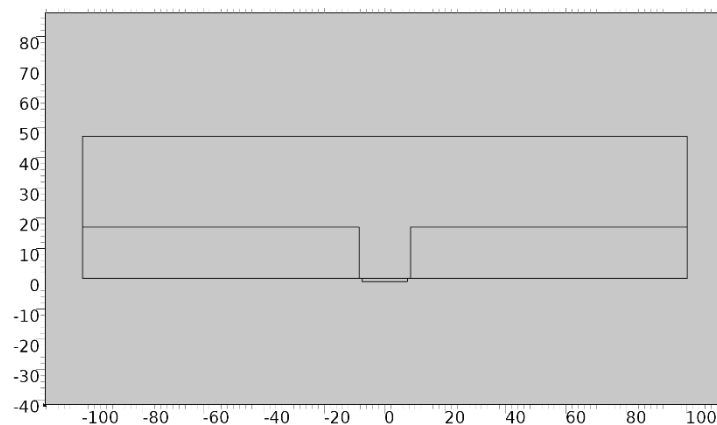


*Figure 21:       Geometry of the cell trap used for simulation in COMSOL (cut through x-y-plane)*

One main aspect of COMSOL is that all variables and magnitudes can be defined in one place and then be changed easily. That means geometries can be drawn without exact measures of the objects by creating variables which are connected to the distinct properties. The following Table 4 shows the variables and magnitudes used for simulating the cell trap.

| Name | Description | Expression |
|------|-------------|------------|
| chan_l | Channel length | 200[µm] |
| chan_h | Channel height | 30[µm] |
| trap_l | Trap length | 17[µm] |
| trap_h | Trap height | 17[µm] |
| con_w | Conductor height | 15[µm] |
| con_h | Conductor length | 1[µm] |
| curr | Current | 0.14[A] |
| je | Current density | curr/(con_w*con_h) |
| par_dia | Particle diameter | 0.0000128 |

*Table 4:  Variables and corresponding magnitudes used for the simulation of the cell trap*

Different parts of the geometry are associated with different materials to get a better simulation. The channel is filled with water, the surrounding is air, the conductor is made of copper and the channel walls are PDMS. Note that these are not exactly the materials used for the real device, but they are incorporated already in the software and are a good approximation.

To prevent inaccurate simulations at the border of the geometry an infinite domain element was used. It is an artificial border of the simulation area, which includes the transition ad infinitum. The infinite element can be seen in Fig. 22.A. The interesting area for simulation is called "Analysis domain" and can be seen in Fig. 22.B. The complete space around the device and in the infinite element domain was assumed to be filled with air for the simulation.
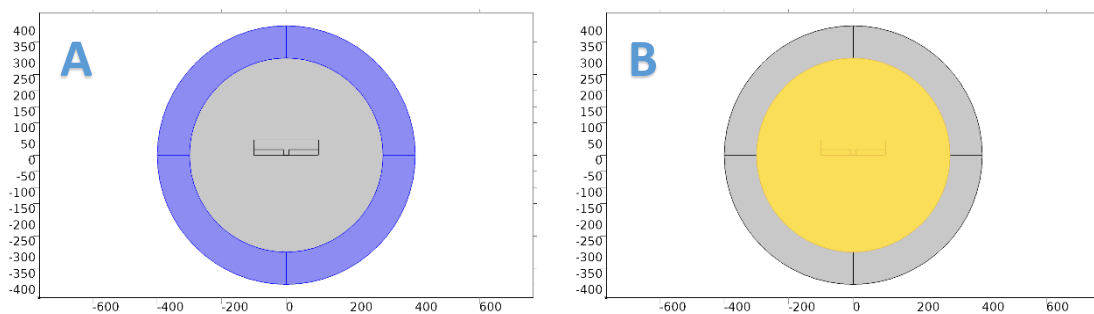


*Figure 22:  A: Infinite element domain (marked blue).  B: Analysis domain (marked yellow)*

The last non-specific part of the simulation is the mesh. Meshing is very important for the simulation, because COMSOL uses finite elements to calculate the values of physical quantities.

COMSOL generates values for every single object of a mesh. That means a very fine mesh results in very long processing time and high CPU load. Therefore it is necessary to find a good tradeoff between simulation time and overall accuracy. For that reason it is useful to manually mesh the geometry and use different meshing densities. The mesh can be seen in Fig. 23.
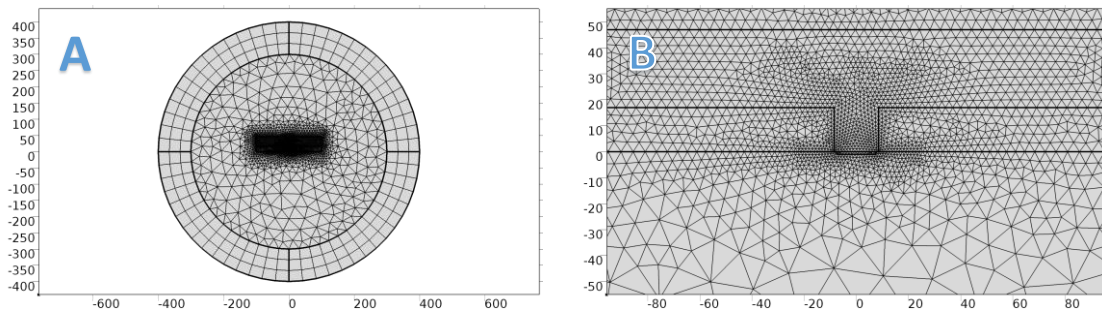


*Figure 23:*     *Mesh used for the simulation of the cell trapping device*

*A: Complete mesh including infinite element domain*
*B: Only the center of the geometry (fluid channel/conductor)*

### 2.2.3    Magnetic flux simulation

For the simulation of the magnetic flux density the "Magnetic Fields (mf)" physics module was used. To get accurate values the field was simulated for the whole geometry including the infinite domain (Fig. 24.A). Important is that the simulation was solved for the full field (including out of plane values), because the current is coming out of plane and so does the vector potential. To start the simulation it was also necessary to define a border, which acts as magnetic insulation (Fig. 24.B).
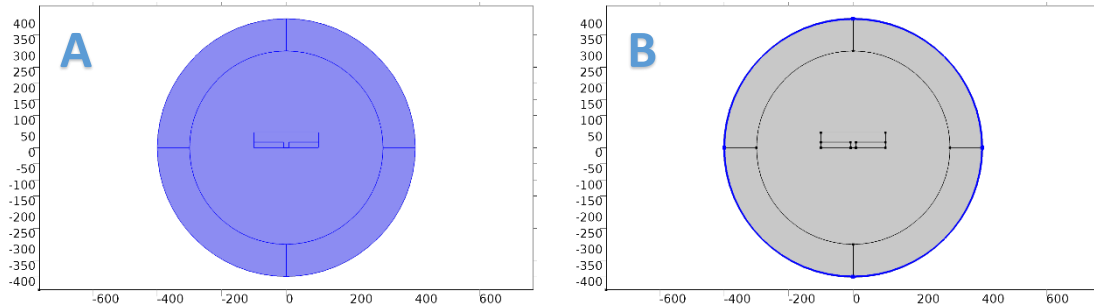


*Figure 24:      A: Simulation area of the magnetic field.   B: Magnetic insulation*

To generate the desired field a conductor was used which is placed under the trap. To simulate this behavior an "External current density" was applied to the conductor. Since the conductor is only a rectangle in the cross section (Fig. 25) the current density was defined to flow into z-direction and therefore out of the simulation plane.
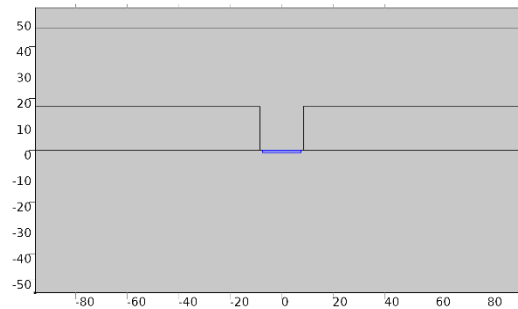


*Figure 25:      Area used as conductor (marked blue). Current is flowing out of plane*

The following figures show the result of the magnetic flux density simulation in a stationary environment (current is not changing over time). Fig. 26 shows the flux density as a surface plot, with high values (in red) near the conductor. The field reaches into the channel for capturing the CTCs with particles on it. Fig. 27 shows the same simulation in a contour plot near the trap. Please note that the field is calculated for the complete area shown in Fig. 24.A, but only visible in the interesting parts of the geometry, like the channel, the trap and the conductor.

## Surface: Magnetic flux density norm (mT)
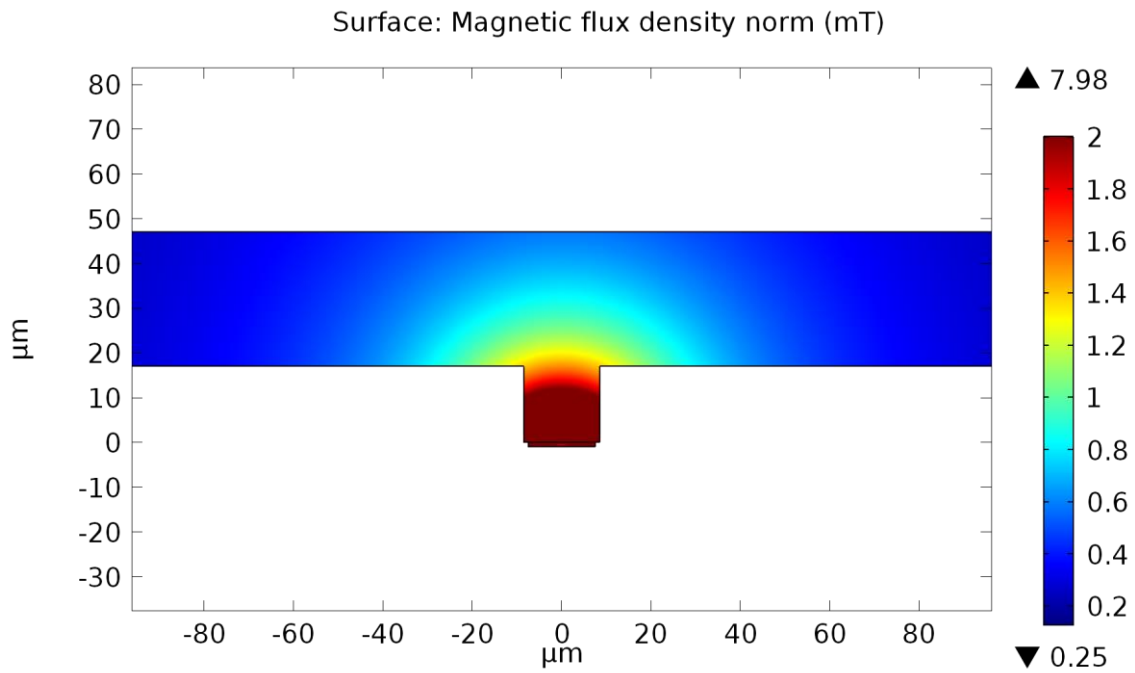


*Figure 26: Magnetic flux density in the microfluidic channel and the trap (surface plot)*
*Current: 140mA*

## Contour: Magnetic flux density norm (mT)
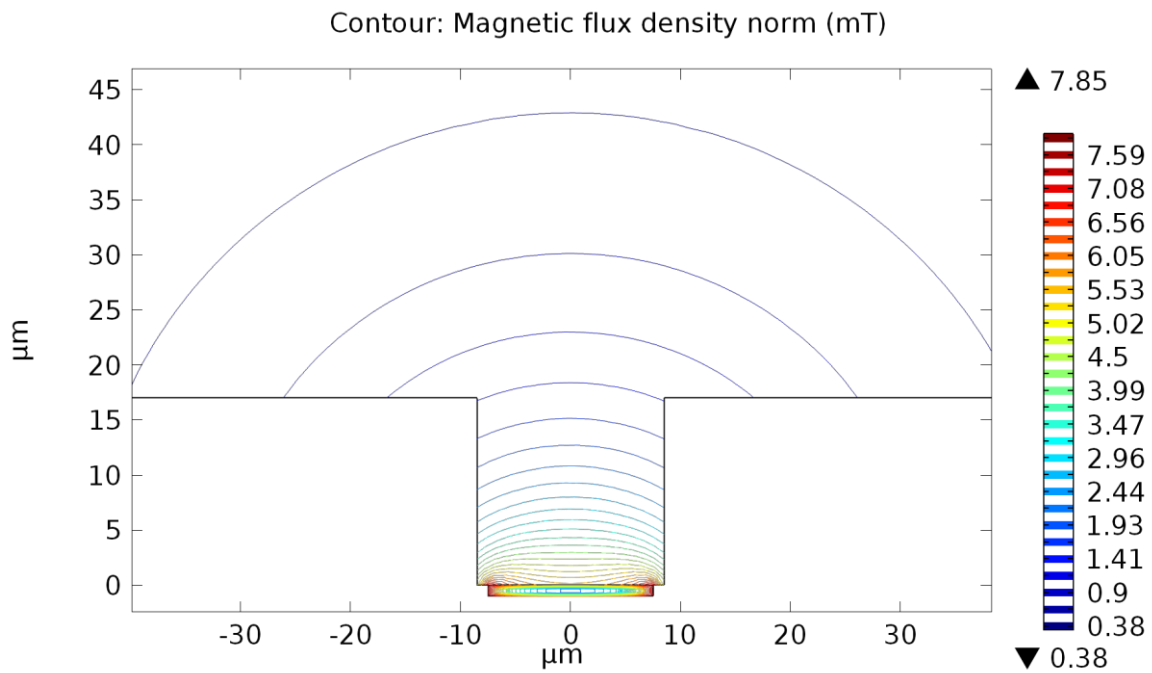


*Figure 27: Magnetic flux density near the trap (contour plot)*
*Current: 140mA*

## 2.2.4   Fluid simulation

For the simulation of the fluid the "Creeping Flow (fpt)" physics module was used. It simulates fluid flows with very low Reynolds numbers (See chapter 1.3.2). The simulation was limited to the channel and the microtrap, because only these areas are filled with fluid (Fig. 28.A).

To get a proper simulation it is very important to define the walls of the channel (Fig. 28.B), an inlet (on the left side of the channel) and an outlet (on the right side of the channel).
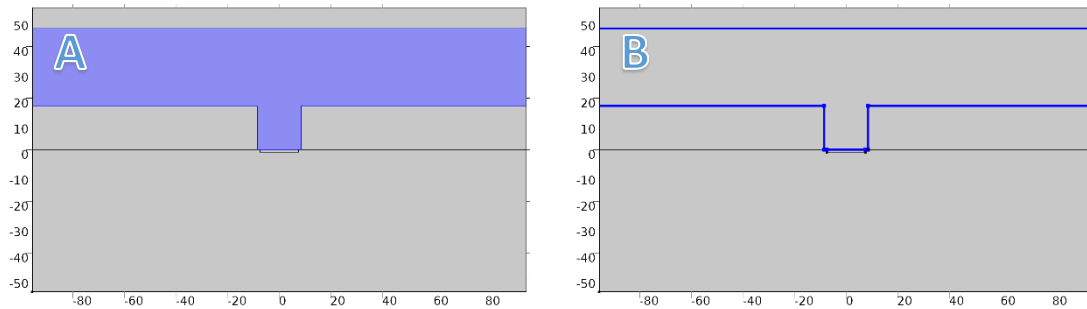


*Figure 28:        A: Simulation area for the fluid flow (marked blue).  B: Walls of the fluid flow*

Similar to the flux density the velocity is not changing and therefore is stationary (not time dependent). For the simulation of the cell trap a velocity of 30 µm/s at the inlet was used. The following Fig. 29 shows a surface plot of the velocity magnitude.
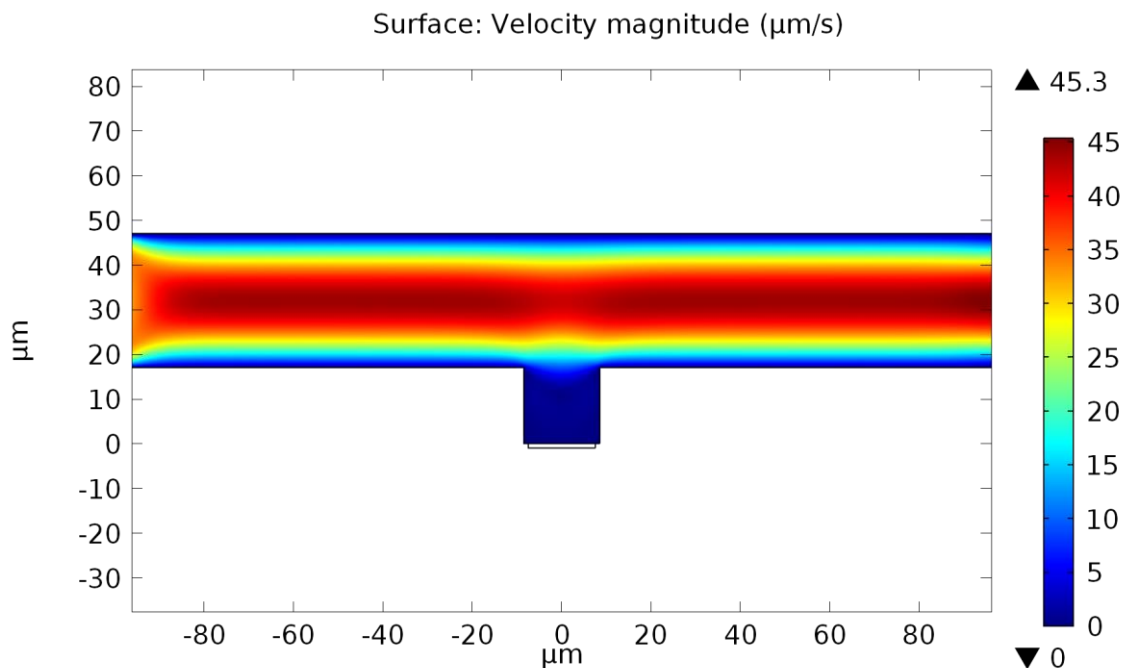


*Figure 29:        Velocity magnitude of the liquid in the microfluidic channel (surface plot)*

Fig. 29 shows that the liquid in the trap is nearly not moving and thus it can be assumed that captured cells will stay in the trapping chamber and also cells and other particles in the channel will not be affected by the trap, which is a desirable effect. These are the main advantages of the proposed method; other available techniques described in Chapter 1.2.2 often do not exhibit these abilities.

## 2.2.5   Cell-Particle movement simulation

One of the most important questions was, if it is possible to move a cell-particle couple. Simulations for particles alone are possible, because COMSOL has a built in module for particle interaction, but however it is not possible to combine two different entities to one.

In order to get an adequate simulation which is trustworthy it was shown that it is best to interpolate the susceptibility of a particle to a complete cell-particle couple (Fig. 30), which is then used for simulation. That means the magnetic behavior of the superparamagnetic particle is mathematically inserted into the cell and thus this new "Magnetic cell" also has a susceptibility different from zero. The radius is the same, because the impact of the particle on the overall volume is negligible and the surface exposed to the drag force will nearly be the same.



$r_P$

$r_C$     $r_C$

$\chi_P$     $\chi_C$

    CTC (not magnetic)      $r_P$ .......Particle radius
    Superparamagnetic particle    $r_C$ .......CTC radius / Magnetic cell radius
    Magnetic cell      $\chi_P$ ......Susceptibility of the particle
     $\chi_C$ ......Susceptibility of the magnetic cell
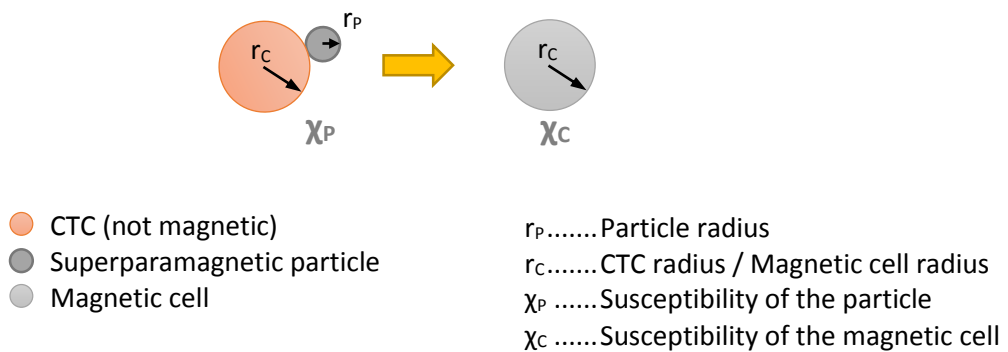
*Figure 30:      Schematic drawing of the transition of a cell-particle couple to a "Magnetic cell"*

The following table shows the data which was used for the interpolation (Table 5). The complete datasheet can be found in the appendix (Chapter 9.1).
The particles differ in diameter and susceptibility to match different applications. Bear in mind that all these particles can be differently modified on the surface for different purposes. In this work the "M-450 Dynabeads" with Anti-CD3-Antibodies on the surface, were used.

| Product | Diameter in µm | Density in g/cm³ | Susceptibility | Iron Content in % |
|---|---|---|---|---|
| **MyOne Dynabeads** | 1.0 | 1.8 | 1.4 | 26 |
| **M-270 Dynabeads** | 2.8 | 1.6 | 1.0 | 14 |
| **M-280 Dynabeads** | 2.8 | 1.4 | 0.7 | 12 |
| **M-450 Dynabeads** | 4.5 | 1.6 | 1.6 | 20 |

*Table 5:      Characteristics of different superparamagnetic particles (Dynabeads ®) [31]*

### 2.2.5.1 Susceptibility calculation

With the information provided in Table 5 the volume (Eq. 16.a), the mass (Eq. 16.b) and the iron content mass (Eq. 16.c) of a 4.5 µm particle were calculated.

a) $V_P = \dfrac{d^3}{6}\pi = \dfrac{(4.5\mu m)^3}{6}\pi = 47.713\ \mu m^3$

b) $m_P = \varrho_P\ V_P = 1.6\dfrac{g}{cm^3}\ 47.714\mu m^3 = 76{,}341 \cdot 10^{-15} kg$

c) $m_{p-iron} = m_P\ 0.2 = 15.268 \cdot 10^{-15} kg$

*Equation 16: Volume, mass and iron content mass of a 4.5µm superparamagnetic particle*

For an accurate interpolation also some information about the cell is needed. For Jurkat-Cells different sources specify a diameter of about 12 µm [32] (varying between 11.5 µm and 13 µm). For a proper calculation the cell water volume from one million Jurkat-Cells (1097 µl/$10^6$ cells) was used and then summed up with the protein content (0.139 mg/$10^6$ cells) of these cells [33]. This is shown in the following Eq. 17:

a) $m_C = \varrho_C\ V_C = 1\dfrac{kg}{dm^3}\ 1097\ \mu m^3 = 1097 \cdot 10^{-15} kg$

b) $m_{C+Protein} = m_C + m_{Protein} = (1097 + 139) \cdot 10^{-15} kg = 1236 \cdot 10^{-15} kg$

*Equation 17: Mass of a single Jurkat-Cell without and with proteins*

With this information it is possible to calculate which amount of the cell-particle couple is made up by iron oxides. Both, without (Eq. 18.b) and with proteins (Eq. 18.a) taken into account:

a) $\dfrac{m_{p-iron}}{m_{C+Protein}} = \dfrac{15.268 \cdot 10^{-15} kg}{1236 \cdot 10^{-15} kg} = 1.24\%$

b) $\dfrac{m_{p-iron}}{m_C} = \dfrac{15.268 \cdot 10^{-15} kg}{1097 \cdot 10^{-15} kg} = 1.4\%$

*Equation 18: Percentage of iron oxide in relation to the complete cell-particle mass*

The calculated information is only useful, when it is known how much susceptibility is exhibited by one percent iron. For this reason Table 5 was used and a mean value of the susceptibility over different iron contents was created. It would be possible to take into account only the information of the 4.5 µm particles but for the simulation the mean value fits the requirements better, because the coupled pair of cell and particle has a new distribution of the iron content. Considering all particle dimension allows to show that the iron content over susceptibility does not vary too much (Fig. 31).
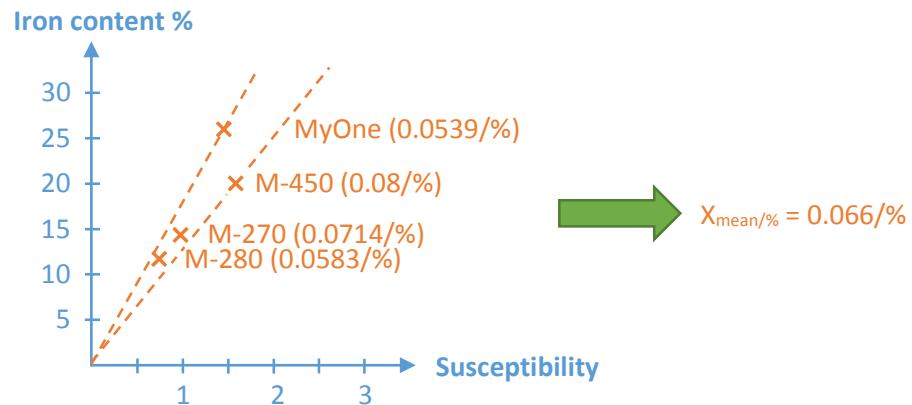


*Figure 31:*      *Iron content over susceptibility of different magnetic particles*

With the data from Fig. 31 it was possible to calculate the susceptibility for a complete cell-particle couple and use this information to generate a magnetic cell for simulation (Eq. 19).

a)   $\chi_C = \chi_{mean/\%} \, 1.24\% = 0.0922$

b)   $\chi_{C+Protein} = \chi_{mean/\%} \, 1.4\% = 0.0818$

*Equation 19:   Susceptibility interpolated for a cell-particle couple (with / without proteins)*

The calculated susceptibility varies between 0.0818 and 0.0922 without proteins. For the simulation a value of 0.085 was used. This value is not the mean value but it represents the value with proteins in real life conditions more accurately.

### 2.2.5.2  Simulation of a cell capture process

As mentioned above it was not possible to simulate a particle-cell couple in COMSOL. This is why a magnetic cell was calculated and used in combination with the "Particle Tracing for Fluid Flow (fpt)" physics module. The simulation area, walls, inlet and outlet are the same as for the fluid simulation, because the cells move with the fluid (compare with Fig. 28).
For the simulation the magnetophoretic force and the drag force is needed. Both are not stationary and not independent from the previous simulations. The magnetophoretic node in COMSOL needs the previously simulated magnetic field (and the calculated substitute susceptibility) and the drag node needs the velocity field as an input. With this information it was possible to simulate the movement of a particle through the channel and the trapping in a microtrap. This simulation is not stationary and therefore the study "Particle Trajectories" was used.

Fig. 32 shows the trace of a magnetic cell moving in the microfluidic channel to the microtrap. From entering the channel until trapping it took 2.37 s with an inlet velocity of 30 µm/s and a current of 140 mA in positive z-direction. The color of the trace is the magnetophoretic force in y-direction which acts on the magnetic cell at every single moment. It can be observed that the cell gets first attracted from the conductor at about -40 µm. The flux density was chosen in a way so that the simulation results in a clear hit of the trap without hitting the walls of the microfluidic channel too early. Sliding along the wall (with a force against the wall active) will maybe impact the cell viability and other surface parameters. So it is essential to adapt the flux density to an optimum value and therefore also the current through the conductor, which produces the field.
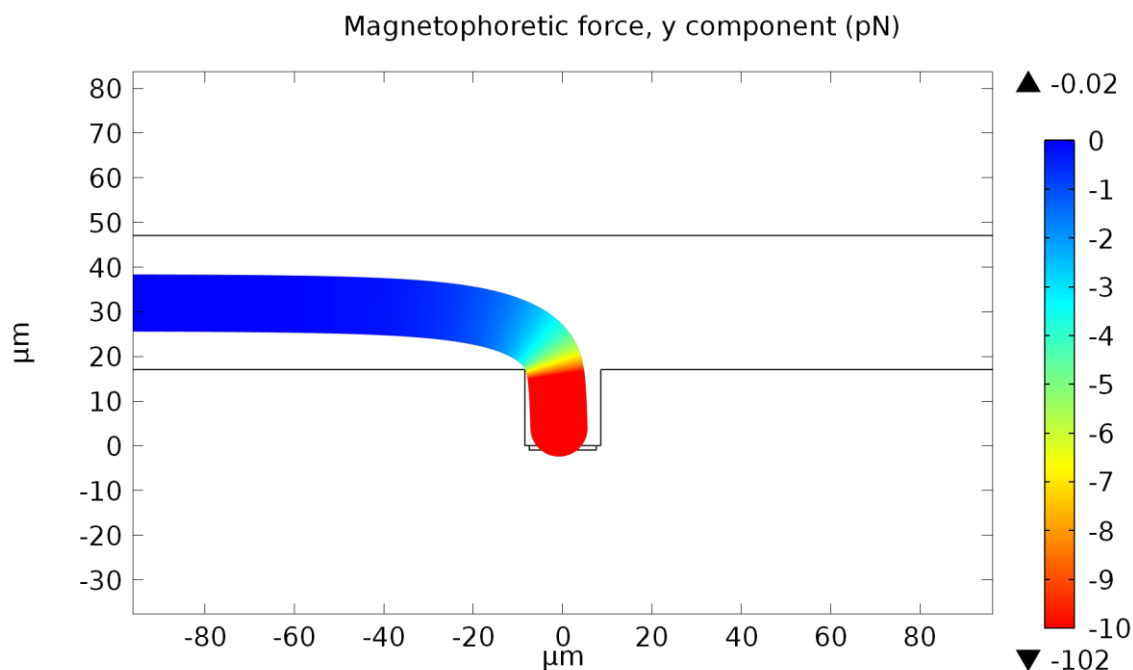


Figure 32:      Simulated trapping of a cell-particle couple (magnetic cell)
                Velocity:        30 µm/s at inlet
                Current:         140 mA
                Time (captured): 2.37 s

Fig. 33 shows the chronology of a single trapping event from the entering of the channel until the capture of the cell-particle couple. The last figure of this set is the aforementioned Fig. 32.
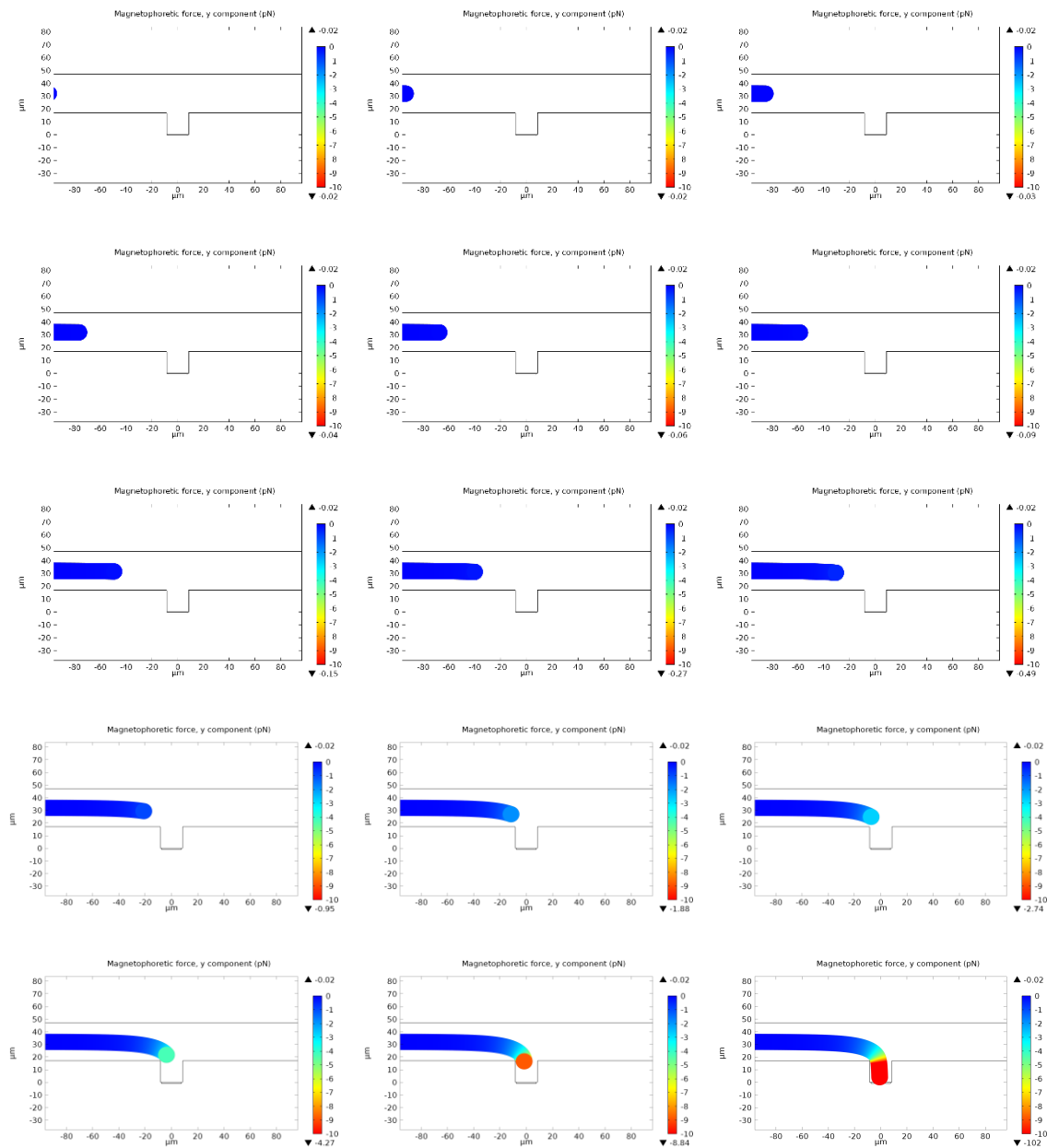


*Figure 33:*     *Simulated chronology of trapping a cell-particle couple (magnetic cell)*

        *The color of the trace shows the y-component of the magnetophoretic force.*
        *The following table gives the time stamps for every single figure above:*

| | | | |
|---|---|---|---|
| *1st Row:* | *0.0 s* | *0.2 s* | *0.4 s* |
| *2nd Row:* | *0.6 s* | *0.8 s* | *1.0 s* |
| *3rd Row:* | *1.2 s* | *1.4 s* | *1.6 s* |
| *4th Row:* | *1.8 s* | *2.0 s* | *2.1 s* |
| *5th Row:* | *2.2 s* | *2.3 s* | *2.37 s* |

## 2.3 Design Requirements and Considerations

In this section the design requirements and considerations are presented. This includes the layered structure of the device, the microconductors and the microtraps.

### 2.3.1 Layered structure

As mentioned before the trapping device consists of a silicon chip and the microfluidic structure on top. The microfluidic structure theoretically can be built up of three parts (microtraps; channel; outlet/inlet). During designing these parts it was concluded that building the microfluidic channel and the microtraps out of two parts was more practical. Although this decision was taken at the beginning and before fabrication, the files consist of three parts for future designs. The separated layers and the structure can be seen in Fig. 34. Thus in principal it is possible to make 3 layers with layer 1b and 2 consisting of Ordyl and layer 1a fabricated of PDMS or glass (only with the inlet and the outlet).
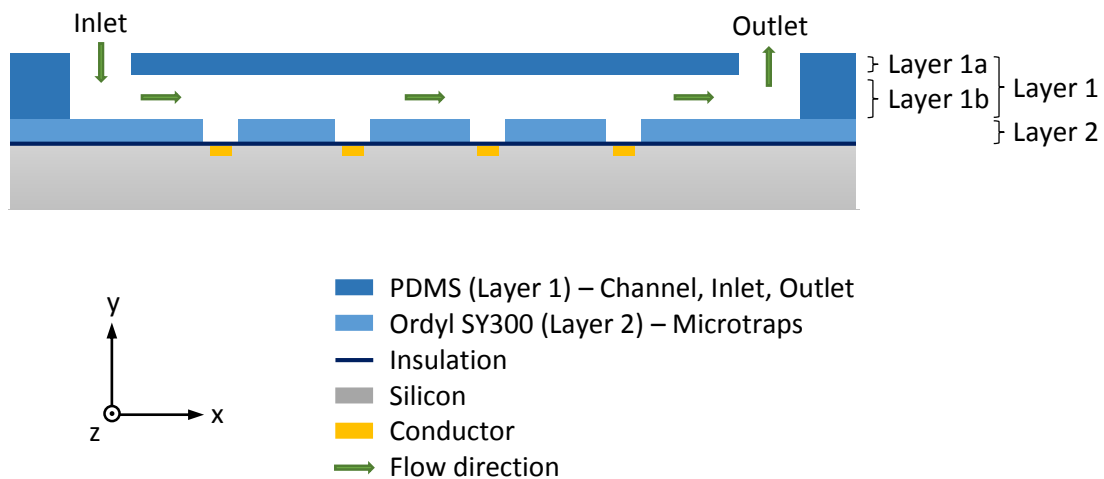


*Figure 34:     Layered structure of the microfluidic channel and the microtraps*

This layered structure permits changing parts of the device without the need to completely redesign all layers. For instance, it is possible to make a new layer 1b to spread the fluid in a different manner (more channels, different dimension, etc.) without making new silicon chips. Even previously prepared and diced chips can be used instantly.

To be fast and cost effective, layer 1 was a PDMS channel which was previously designed and tested in other applications. The big advantage is, that the main fluid channel is always accessible and cheap in production (See Chapter 3.1.3).

### 2.3.2 Microstructures and chip

The simulations showed that a current of about 140 mA is necessary to trap cell-particle couples. In such cases heat dissipation would be a problem, due to the small thickness of the designed conductors (a few µm). In previous work it was proven that a current density of about $20*10^9$ A/m² would not destroy the conductor [16, 30]. Nevertheless the conductor was designed to be 15µm wide and 1µm thick; for continuous use with about 140 mA a current density of $9.3*10^9$ A/m² would be achieved.

The designed wafer consists of 3 different chips (the complete wafer holds 16 chips) with different conductor dimensions (Table 6). The chip labeled "M1" is the standard chip with the simulated/calculated values of the conductor. Each chip has the same dimensions (19.5 mm x 14.6 mm) and layout with sole difference in microconductor dimensions. The complete wafer and the chip positions are given in Fig. 39.

| Label | Conductor width | Conductor height | Quantity |
|-------|-----------------|------------------|----------|
| M0 | 10µm | 1µm | 2 |
| M1 | 15µm | 1µm | 8 |
| M2 | 20µm | 1µm | 6 |

Table 6:   *Conductor width and height of the different silicon chips (on one wafer)*

More than one conductor was used on every chip to be able to capture more cells and test different microtraps dimensions (Fig. 35). On this design there are 9 parallel conductors with 360 µm distance between them to ensure that there is no influence from one conductor to the next one. They can be controlled independently from each other, which means they can be used alone (each one) or at the same time.
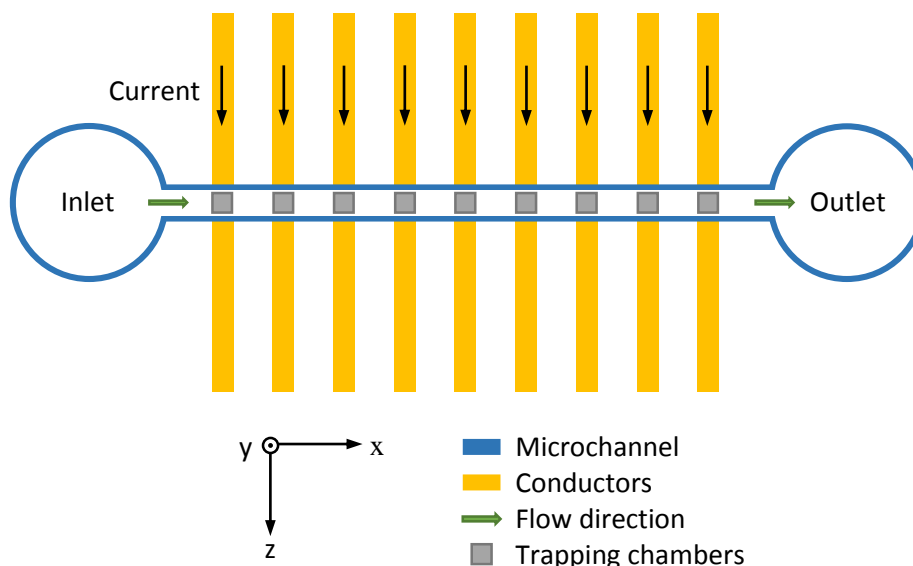


Figure 35:   *Top down view shows the conductors and the traps placed over them*
*Proportions are not correct. Conductors are about 15 µm wide and their distance from each other is about 360 µm.*

To measure the heat influences, the chips have two heat sensing conductors, which are positioned near the first and last conductor. They are meant for future usage and were not connected during the measurements for this thesis.

To be cost effective a previously fabricated passivation mask was used and therefore it was necessary to position the bonding pads to match the passivation mask. That includes 10 conductor pads (9 individual and one common pad) and the 4 temperature sensing pads. A complete overview of positions and pad assignment is shown in Fig. 36 (or Appendix 9.5).
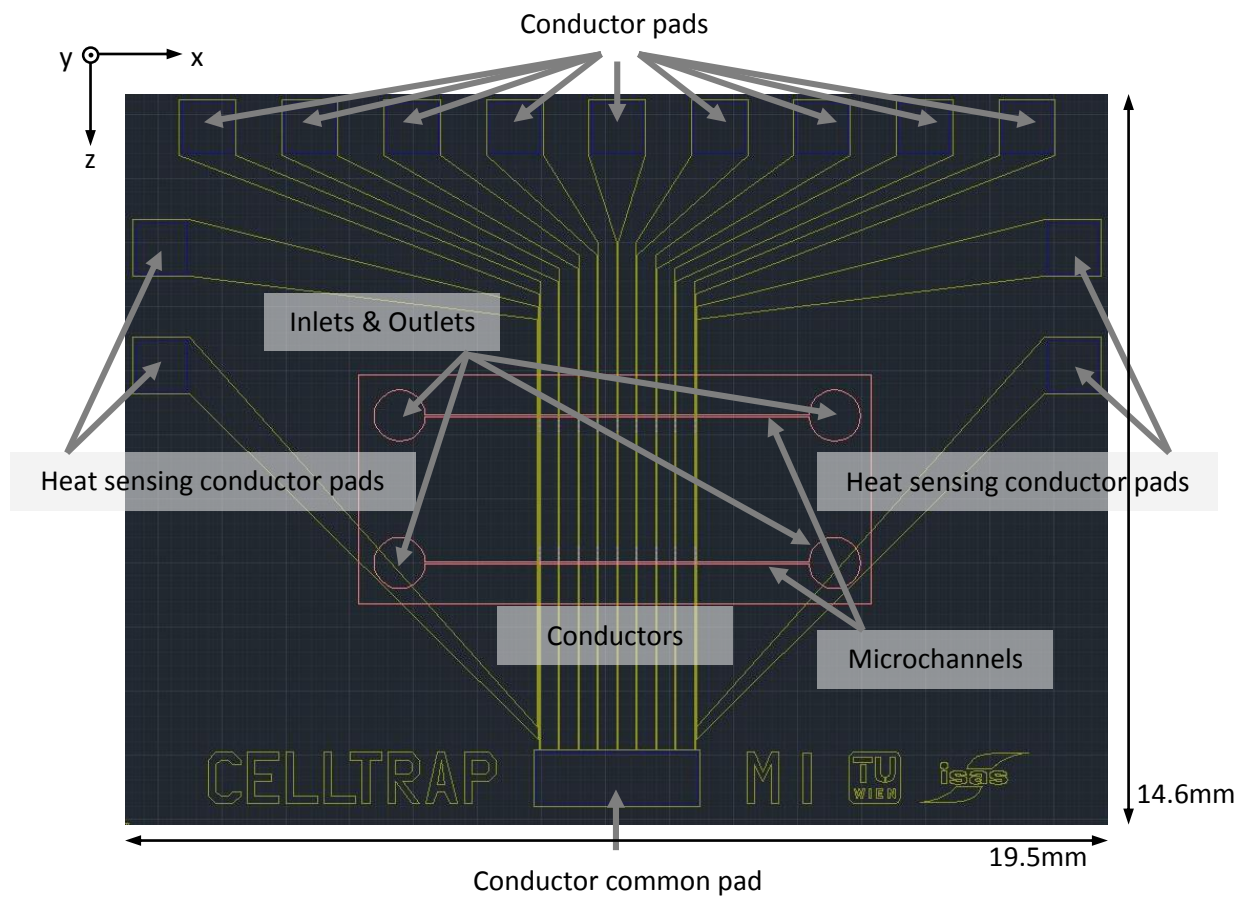


*Figure 36:      Standard chip M1 with conductors, current sensors and fluid channels (AutoCAD)*

*Yellow:            Conductor outlines (and captions)*
*Pink:               Microfluidic outlines*
*Blue:               Passivation outlines for conductor pads*

The chip was mounted on an existing PCB; used in other projects [34]. Therefore the dimension of 19.5 mm x 14.6 mm was predetermined.

### 2.3.3 Trap position and sizes

When a cell moves through the channel there is a possibility to catch it at 9 different positions. One at every conductor (Compare with Fig. 35). Since the goal is to capture single cells it was necessary to make different trap sizes to test how big they have to be to capture a single cell and hold it there. The dimensions of the microtraps increase from the inlet to the outlet. If the trap is too small for a cell to get trapped or the speed of the fluid is too high there is a greater possibility that the same cell will get captured at a later trap which is bigger and therefore the cell has more time to move towards the base of the trap. The sizes used for this work are depicted in Fig. 37.
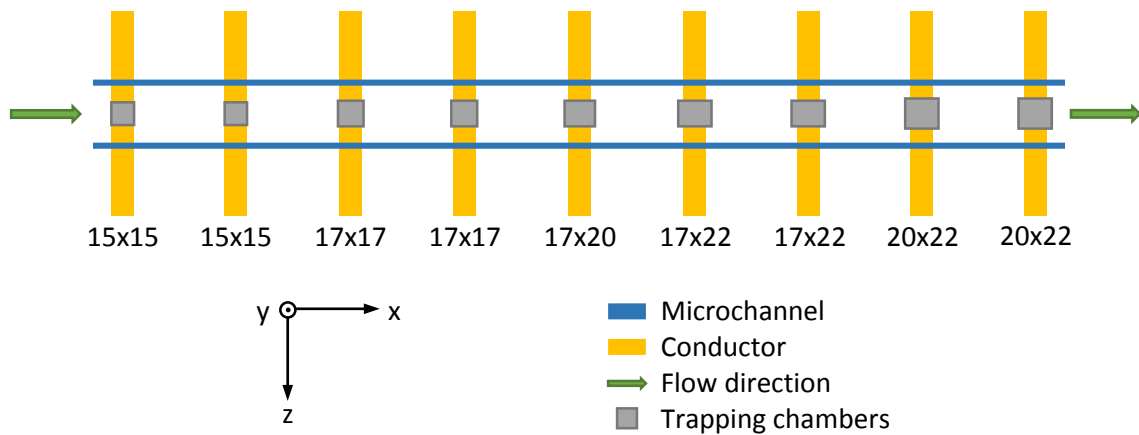


*Figure 37:* *Microtraps positions with dimensions in µm for the single-row design (top view)*
*Proportions between conductors and microtraps are correct, but distance between conductors is about 360µm (about 6 times bigger than depicted)*

As aforementioned there are 3 different chips with different conductor sizes, but it appeared useful to take the same trap size distribution for every chip to make the results comparable. Nevertheless there are two rows of traps on every chip to change the position of the channel, if a component is damaged and/or contaminated. They have a distance of 3 mm from each other (Fig. 36).
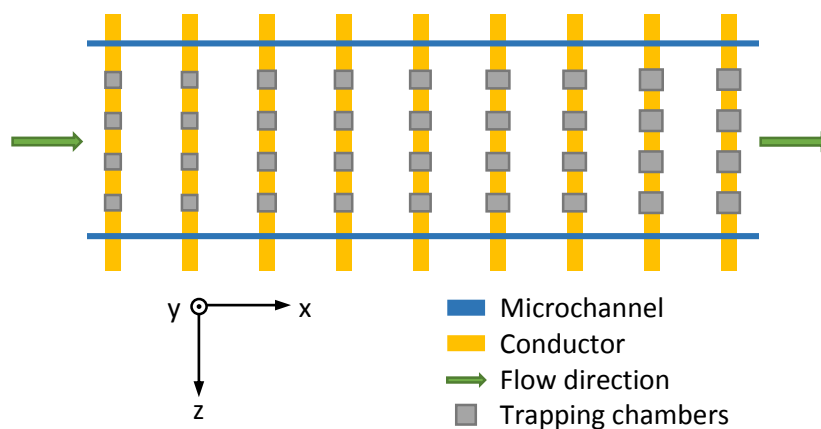


*Figure 38:* *Microtraps positions for the multi-row design (top view)*
*Proportions between conductors and microtraps are correct, but distance between conductors is about 360 µm (about 6 times bigger than depicted) and distance between microtraps in z direction is about 100 µm (about 6 times bigger than depicted)*

The mask for the traps on one side of the wafer is different from the other one. On the left side (and for one half of the chips; 1xM0, 4xM1, 3xM2) there are two separated single-rows of traps on every chip only, like described above. The traps in one channel are shown in Fig. 37.

On the other half there are 4 rows of traps for every channel and therefore 8 rows of traps overall. The positions of the traps are depicted in Fig. 38.
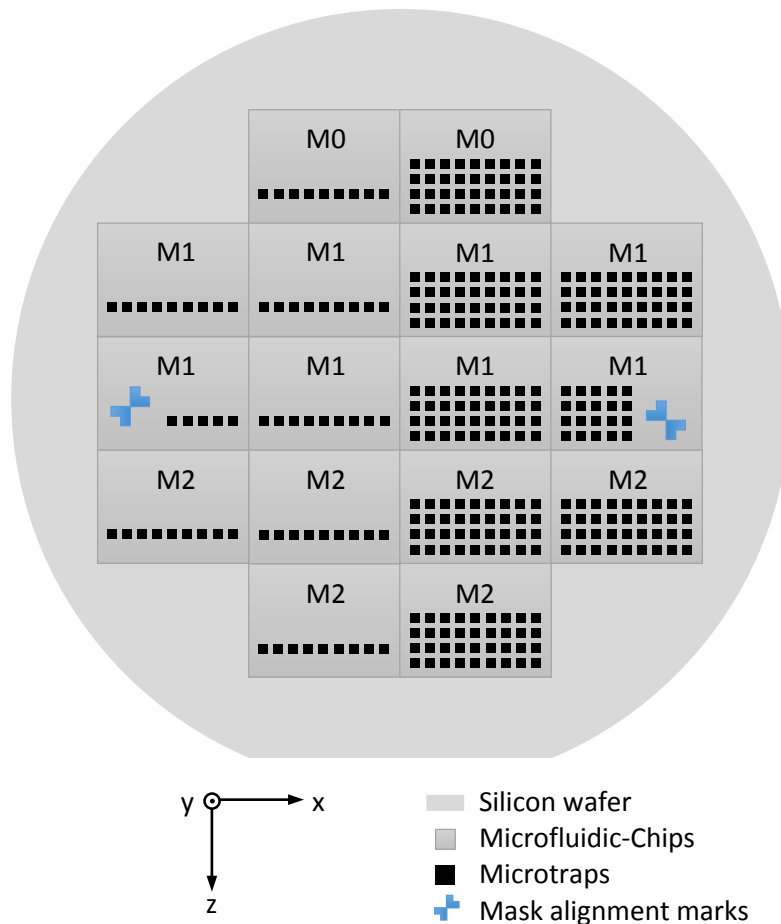


*Figure 39:*     *Complete wafer overview with chip positions and microtraps*
                *Every black square symbolizes a microtrap in one channel. So each chip has the twofold*
                *amount of traps as depicted above*

A complete overview of the type of chips combined with the microtraps on the first Ordyl layer is given in Fig. 39. The AutoCAD file is shown in Appendix 9.4. Note that only one half of the traps is shown, because of limited space in the figure. As previously mentioned there is always a second channel with the same amount of traps on every chip. It can also be observed that two M1 chips have fewer traps, because of the space which is needed for the alignment marks.

The microtraps were also produced with a photolithographic process, applied directly onto the complete wafer before dicing. For that reason it was considered to use a 17 µm thick "Ordyl SY300" (Specifications are given in Appendix 9.3), which can be laminated to the chip and directly processed. Overall 2 new masks were produced. One with the conductors on the chip and one only with the microtraps. All other masks were previously fabricated and ready for use.

# 3 Chip Development and Characterization

In this chapter the procedures and techniques used for fabrication of the cell chip and the preparation of the used cells will be presented, followed by the explanation of the measurement set up, which was used for testing the device and the results which were obtained with it.

## 3.1 Fabrication

This chapter describes the fabrication of the wafer, the microtraps and the microfluidic channel.

### 3.1.1 Wafer fabrication

For the fabrication of the wafer two masks were needed:

1.  Mask with microstructures (conductors and pads)
2.  Mask for passivation layer (open at pads for bonding)

The following steps were carried out in the cleanroom of the institute.

The microconductors were produced with a standard photolithographic process by using a negative resist and were sputtered with gold. The thickness of the microconductors was 1 µm as previously simulated and concluded to be best for the application. After sputtering the desired microconductors, the complete chip was passivated. Only the bonding pads were excluded with the use of the 2nd mask. The complete procedure is shown in Fig. 41.

A picture of the chip with the passivation layer is shown in Fig. 40.
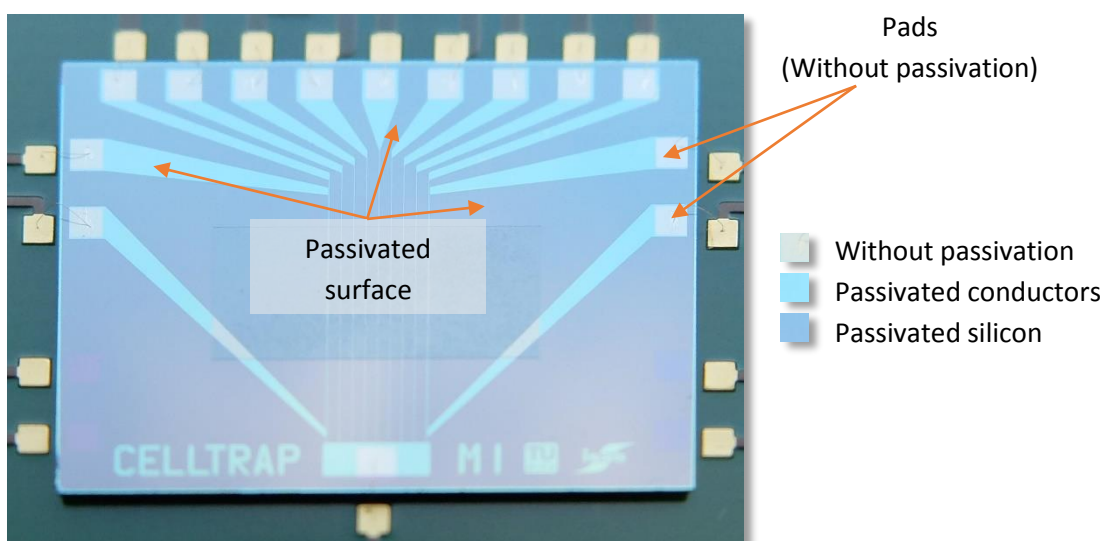


*Figure 40:* *Diced and bonded chip without the microfluidic channel*
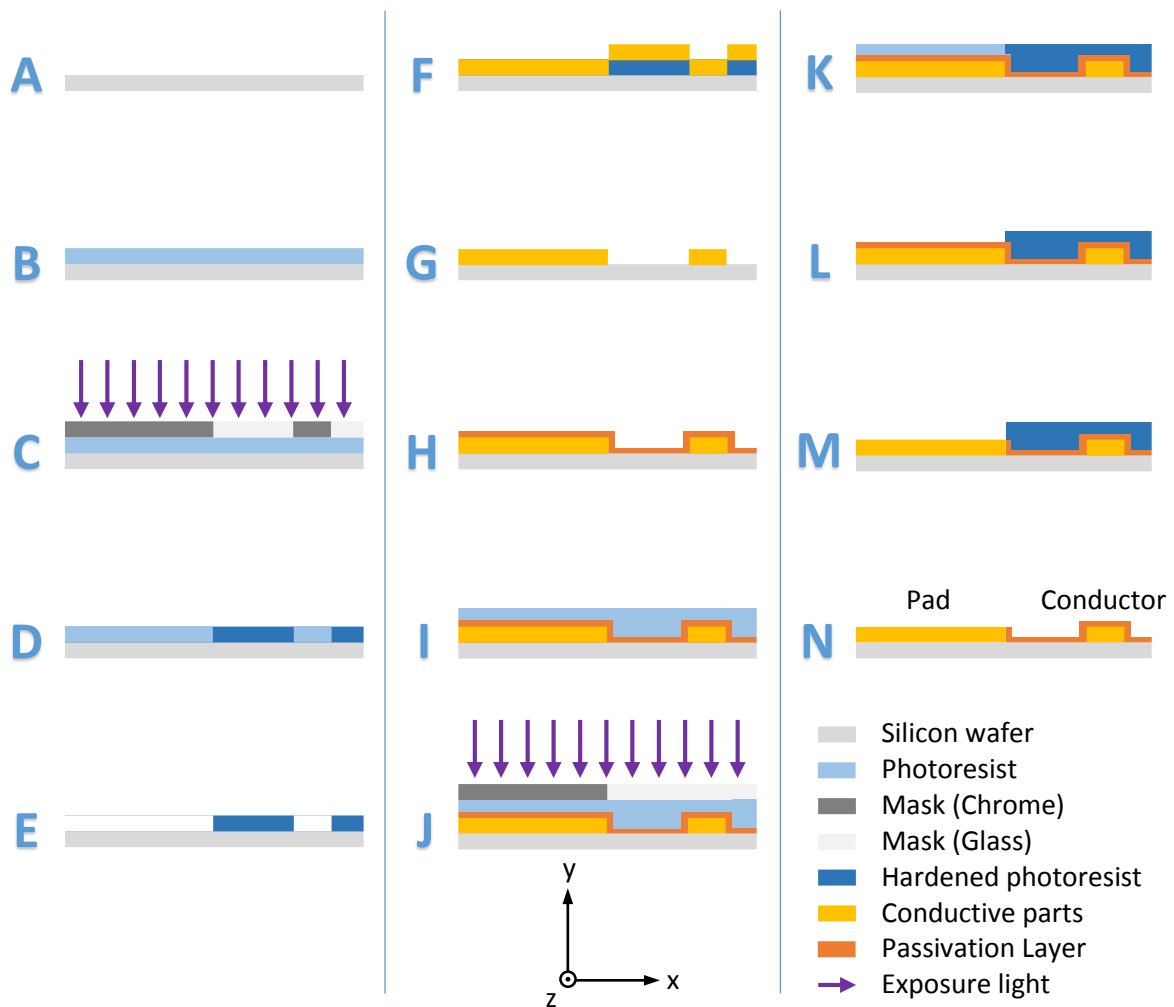
*Figure 41:* Fabrication of the structures (conductor/pad) and passivation

A) Bulk Silicon

B) Spin coating of photo resist and soft baking

C) Exposure with 1st mask (microconductors and pads)

D) Development / Hard Bake

E) Removal of unexposed photoresist

F) Sputtering of conductors and pads

G) Lift off

H) Passivation

I) Spin coating of photo resist and soft baking

J) Exposure with 2nd mask (passivation layer)

K) Development / Hard Bake

L) Removal of unexposed photoresist

M) Plasma etching for removal of unneeded passivation

N) Stripping of photoresist – Ready for microtrap-layer

### 3.1.2 Fabrication of the microtraps

The microtraps were directly positioned on the chip with a layer made out of "Ordyl SY300", which is a negative dry-film photoresist. The manual is given in Appendix 9.3 [35].
Ordyl is available in different thicknesses starting with 17 µm, which was used for the proposed device. It is directly laminated onto the wafer and then patterned with a standard lithographic process. The process can be roughly separated in 3 steps:

1. Lamination
2. Exposure
3. Development

#### 3.1.2.1 Lamination

The lamination was made with a standard laminator, which was preheated to 121 °C. The wafer was placed between an overhead transparency and its paperback (Folex-X472). Afterwards the Ordyl SY300 was cut into about the same size as the wafer and positioned on top of the wafer and fixed with tape on the paperback. Then the complete stack of overhead transparency, wafer and Ordyl was inserted into the laminator. The bottom protective foil of the Ordyl was slowly removed during the movement through the laminator so that the Ordyl binds to the surface of the wafer (Fig. 42).
After lamination the overhead transparency was removed and the wafer with the Ordyl on top was brought to the cleanroom in an UV-secure wafer carrying case (wafer was positioned topside down). Note that the other protective layer on top of the Ordyl was still in place and removed later after exposure.
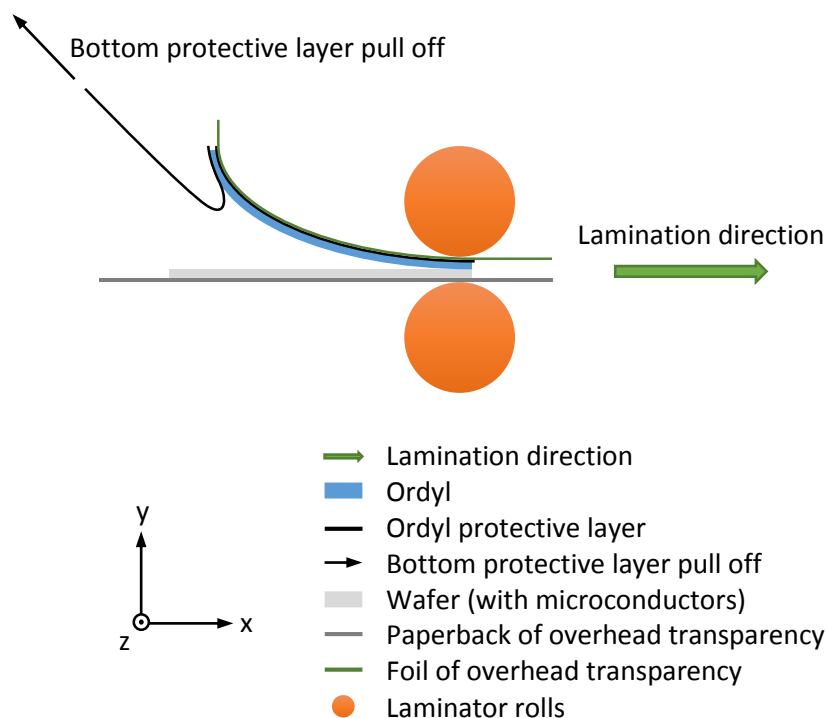


*Figure 42:     Lamination of the Ordyl onto the wafer (secured by overhead transparency)*

### 3.1.2.2 Exposure and development

The wafer (with the already laminated Ordyl) was preheated to 90 °C. Meanwhile the mask for the microtraps was put into the mask aligner. Marks on the wafer were used to align the Ordyl layer with the microconductor layer.
After alignment the wafer with the Ordyl on top was exposed for 20 s to harden the desired structure. Afterwards the top protective layer was pulled off and the wafer was put on the hot plate again for 1 minute at 90 °C to cure the Ordyl.
The last step was the development in an ultrasonic bath filled with Ordyl developer for 60 seconds. It is possible to use different developers, but there is a special developer for Ordyl available. The complete process is given in Fig. 43.A-E.

The processed Ordyl is thinner than the original one. Hence the thickness was reduced from 17µm to about 10 – 12µm, which is enough for the proposed device to hold a single cell which is labeled with a particle.

The final wafer was diced into pieces according to the dimensions depicted in Chapter 2.3.2.
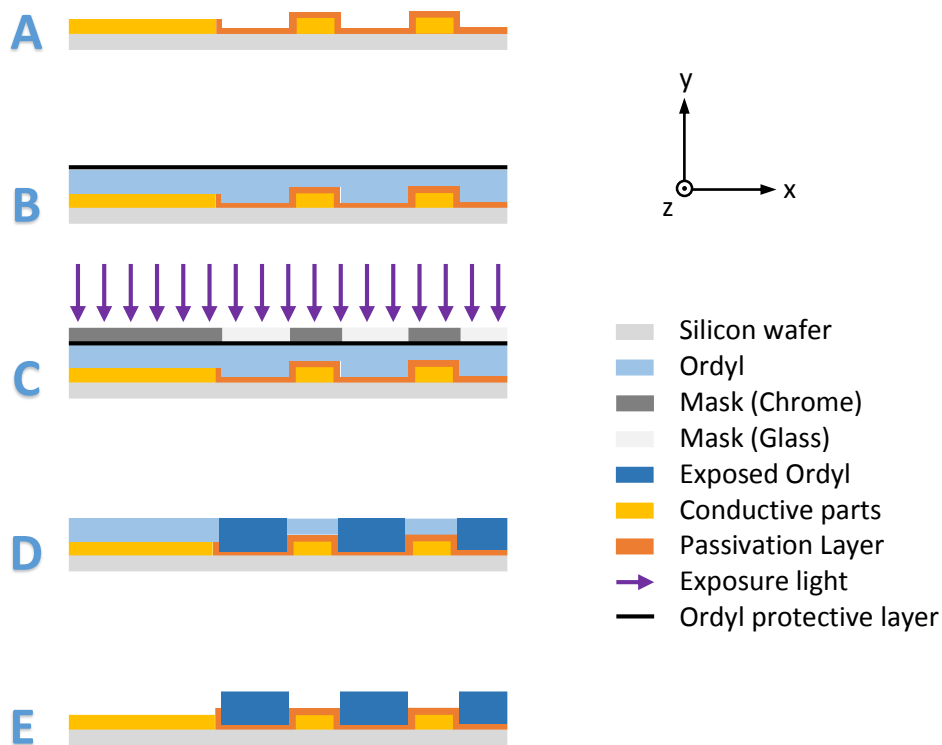


Figure 43:     Ordyl exposure and development using lithographic processes

    A)  Wafer before Ordyl lamination (Fig. 41)
    B)  Wafer laminated with Ordyl
    C)  Exposure with microtrap mask
    D)  Removal of protective layer and post exposure bake at 90 °C for 1 minute
    E)  Wafer after 60 seconds development and cleaning

### 3.1.3 Microfluidic channel fabrication

The microfluidic channel used for the cell trapping device was fabricated out of PDMS (Polydimethylsiloxane). To reduce cost and work load a previously used channel design was used. The channel consist of an inlet, an outlet, a straight part for fluid transportation and a wider trapping/measurement area (Fig. 44). A picture of the channel for comparison is given in Fig. 45.

The channel was fabricated using standard soft lithographic processes, which means that the desired structure was patterned onto a wafer with a photoresist. This wafer was then used as a mold for the PDMS channel. The PDMS is a two component chemical, which was mixed in a ratio of 10:1 with 10 parts base and 1 part curing agent (both liquid). After mixing the liquid was poured over the mold and cured for 1 hour at 70 °C on the hot plate.

In the last step the PDMS was gently pulled off from the mold and cut into pieces, because more than one channel was prepared at the same time to reduce time and costs.

Note that the channel is only at the bottom part of the PDMS. The only parts which are crossing the complete PDMS are the inlet and the outlet.



Inlet     Transportation channel     Trapping / Measurement area     Outlet

y →x

z

■ PDMS (over complete height)
■ PDMS (thinner because of channel)
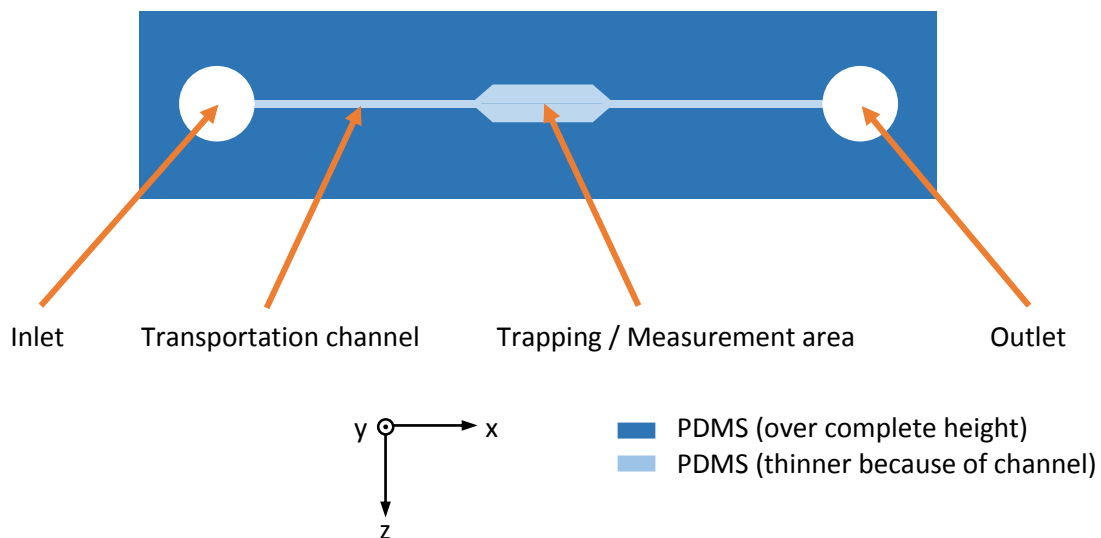
*Figure 44:     Microfluidic channel design used for the measurements of the cell trapping device*



*Figure 45:     PDMS channel with inlet, outlet and a broader trapping channel area in the middle*
*The channel is in the µm range, while the overall PDMS is some mm thick*

## 3.2 Magnetic Labeling of Cells

In this chapter the preparation of the cells, the particles and the binding of particles with cells will be explained.

### 3.2.1 Preparation environment

To achieve high cell-particle binding rates and prevent contamination of the samples and the final products all preparation tasks were performed with gloves. The working area was cleaned with Isopropanol before usage and most tasks were accomplished under a laminar flow hood (Fig. 46).



*Figure 46:     Laminar flow hood used for preparation of cells and particles*

Materials and equipment used:

- 3 Pipettes – Eppendorf Research Plus (0.5 - 10 µl, 10 - 100 µl and 100 - 1000 µl)
- Corresponding pipette tips
- Sterile micro tubes for sample storage (Fig. 47)
- 96 well plate for micro tube holding
- Tweezers
- Garbage sack for solid waste and a tube for liquid waste
- Tube holder
- Permanent ink pen



*Figure 47:     Micro tubes used for sample preparation and storage (cells, particles)*

### 3.2.2 Magnetic particle preparation

Aforementioned "Dynabeads ® - M-450 – Anti-CD3" Particles were used as magnetic particles. They are being delivered in a small bottle with 5 ml content with a density of 400 million particles per milliliter. The buffer consists of "Phosphate buffered saline" (PBS) with 0.1 % "Bovine serum albumin" (BSA) and 0.02 % sodium azide as a preservative. The manual of the particles can be found in Appendix 9.2 [36].

Before usage the beads were washed with buffer of "PBS sterile and BSA". The buffer was prepared by dissolving 5 PBS tablets in 500 ml DI water followed by sterilization in an autoclave (121 °C). Afterwards 44.5 ml PBS sterile and 500 µl "Blocker BSA 10 %" were mixed in a tube to get the needed concentration of 0.1 % BSA.

**Particle preparation protocol:**

- Take a fresh sterile micro tube and label it with "CD3" and "Date"
- Vortex the bottle with the beads for at least 30 to 60 seconds
- First wash:
    - Pipette 100 µl ($40*10^6$ particles) from the bottle into a micro tube
    - Fill up with 900 µl "PBS sterile + BSA"
    - Vortex the micro tube
    - Put tube into magnet to separate buffer and particles for 30 seconds (Fig. 48.A)
    - Discard buffer (Carefully with pipette)
- Second wash:
    - Add 1000 µl "PBS sterile + BSA" to the particles
    - Vortex the micro tube
    - Put tube into magnet to separate buffer and particles for 30 seconds (Fig. 48.A)
    - Discard buffer (Carefully with pipette)
- Third wash:
    - Add 1000 µl "PBS sterile + BSA" to the particles
    - Vortex the micro tube
    - Put tube into magnet to separate buffer and particles for 30 seconds (Fig. 48.A)
    - Discard buffer (Carefully with pipette)
- Add 100 µl "PBS sterile + BSA" (Fig. 48.B)
- Vortex the micro tube
- Put the particles in the micro tube into the fridge for storage (2 - 8 °C)
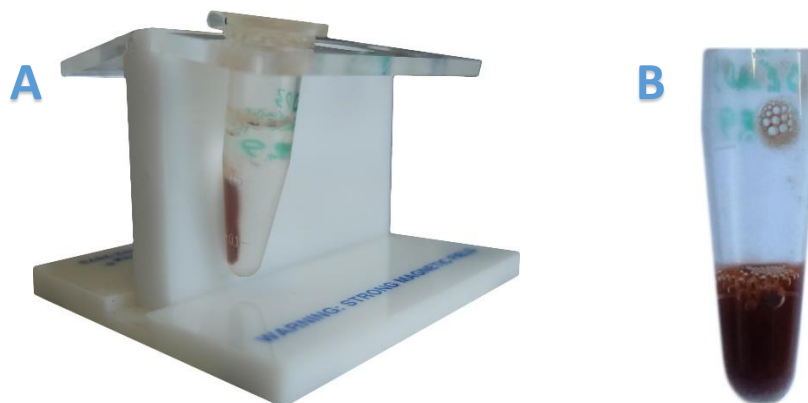


*Figure 48:    A: Separation of particles and buffer with a magnet.    B: Washed particles*

### 3.2.3   Cell preparation

The proposed device was tested with T-Lymphocyte cells, originated from an acute T cell leukemia. The cell line is called "Jurkat cells" and was established from the peripheral blood of a 14 year old boy in 1977 [37, 38].

The cells were provided by "BOKU – University of Natural Resources and Life Sciences, Vienna" [39] and cultured by the "Austrian Institute of Technology" (AIT) [40]. After culturing the cells were filled into tubes holding 1 ml with 1 million cells each (Fig. 49.B) and put onto a rack for storage. The complete rack (Fig. 49.A) was transported in a polystyrene box to maintain the temperature.



*Figure 49:     A: Tray with sample tubes (+ 15 ml medium). B: Tube with 1 ml cell suspension*

The cells were stored at 37 °C and usually they were viable and usable for about 7 days. However best results were obtained in the first three days.

**Cell preparation protocol:**

- Prepare sterile micro tube and label it with "JC" and "Date" (concentration when different)
- Vortex the sample tube with the cell-solution (Fig. 51.A)
- Pipette the complete  1000 µl into the micro tube
- Vortex the micro tube
- Centrifuge the micro tube for 5 minutes with 1.4 * 1000 rpm (Fig. 51.B)
- Remove the original buffer with a pipette (Fig. 50)



Cells are at the bottom after centrifugation and the buffer can be easily discarded
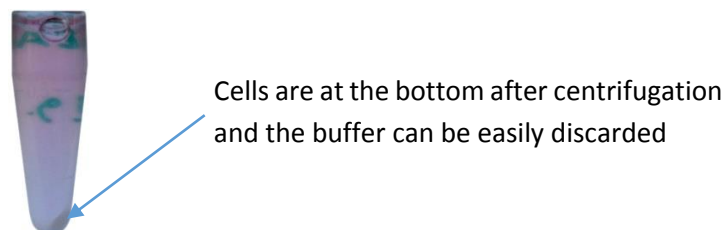
*Figure 50:     After centrifugation the cells are at the bottom and the buffer can be discarded*

- Add 1000 µl "PBS sterile with 0.1 % BSA" into micro tube
- Vortex the micro tube (Fig. 51.A)
- Centrifuge the micro tube for 5 minutes with 1.4 * 1000 rpm (Fig. 51.B)
- Remove the buffer with pipettes
- Add 200 µl "PBS sterile with 0.1 % BSA"
- Vortex the micro tube
- Store cells at 37 °C
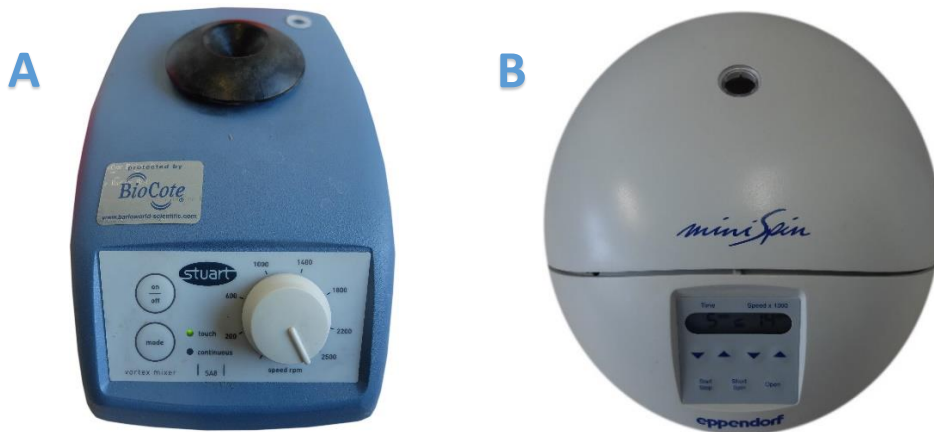


*Figure 51:    A: Vortex Mixer by Stuart          B: Centrifuge – miniSpin by Eppendorf*

### 3.2.4   Cell-Particle coupling

**Cell-Particle binding protocol:**

- Take the previously prepared particles and cells (2 micro tubes)
- Add 2 µl of particles (suspension with 800.000 particles) to the cells (1 million cells)
- Put the micro tube for 20 minutes into the multi rotator (Fig. 52)
- Take the micro tube out of the multi rotator
- Control the binding rate under microscope (put 7 µl onto a microscope slide)
- Store cell-particle couples at 37 °C until usage



*Figure 52:    Grant-bio PTR-60 incubator/mixer used to support cell-particle binding*

## 3.3 Experimental Setup

In this section the measurement set-up and the relevant equipment is presented.

### 3.3.1 Measurement board
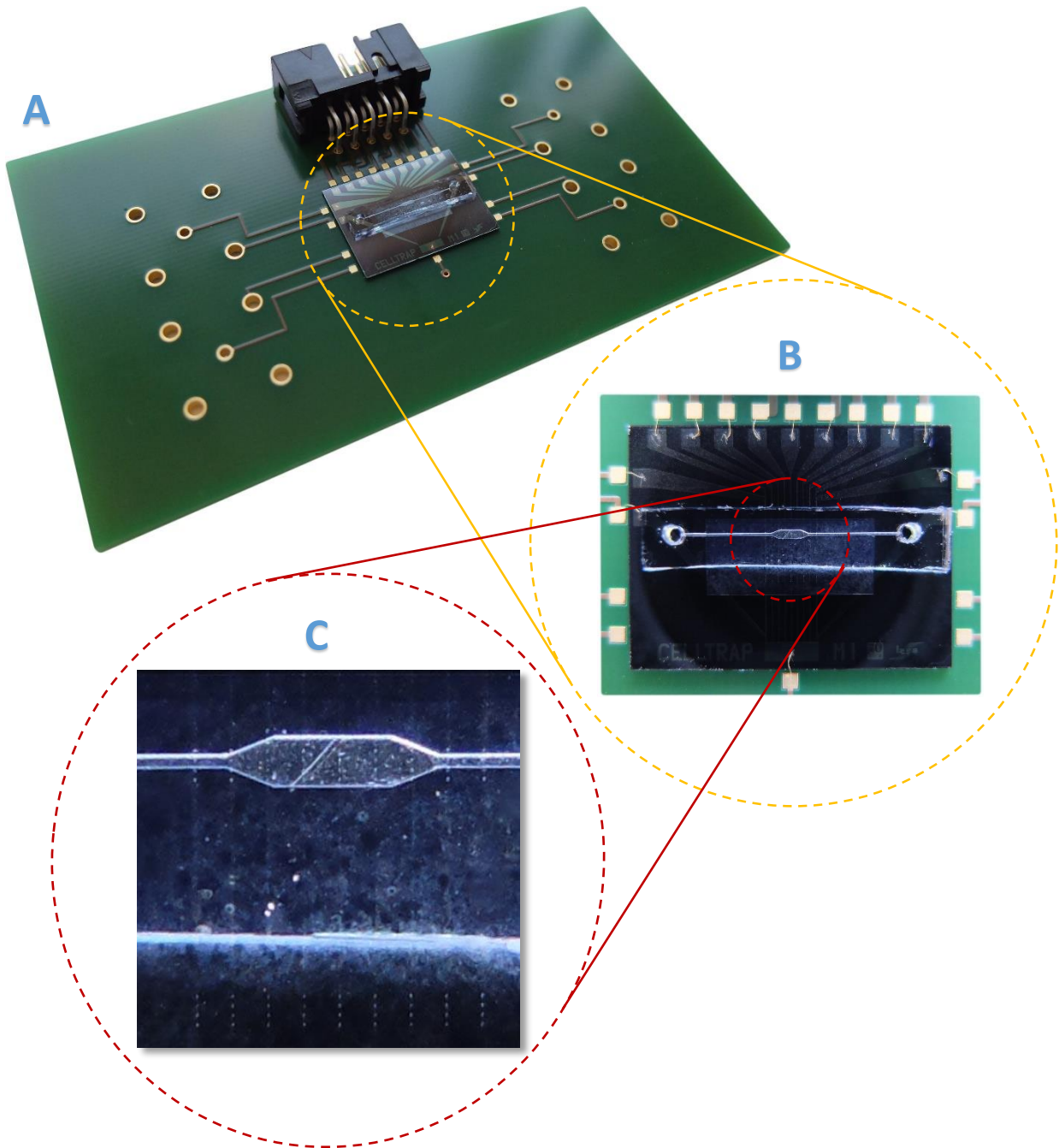


*Figure 53:*     *Fully equipped board with the cell trapping chip "M1" in the middle*

        *A) Complete PCB with chip and PDMS channel on top*
        *B) Only the chip with Ordyl layer and PDMS channel on top of it*
        *C) PDMS channel on Ordyl layer with microtraps visible as small dots – Multi row*
           *design with spare channel visible on bottom and conductors in light grey*

The previously produced chip with the microtraps was bonded to a PCB which has a connector to simplify the setup of the trapping device. Unused holes in the PCB are for optional mounting of coaxial connectors for heat sensing or for connecting magnetic sensors (for particle detection). The fully equipped board is given in Fig. 53, which shows all important structures including channel, microtraps and microconductors.

For comparison a microscope image is given in Fig. 54. The picture is composed of 3 single images combined in digital postproduction to show the complete trapping area in one sharp image.
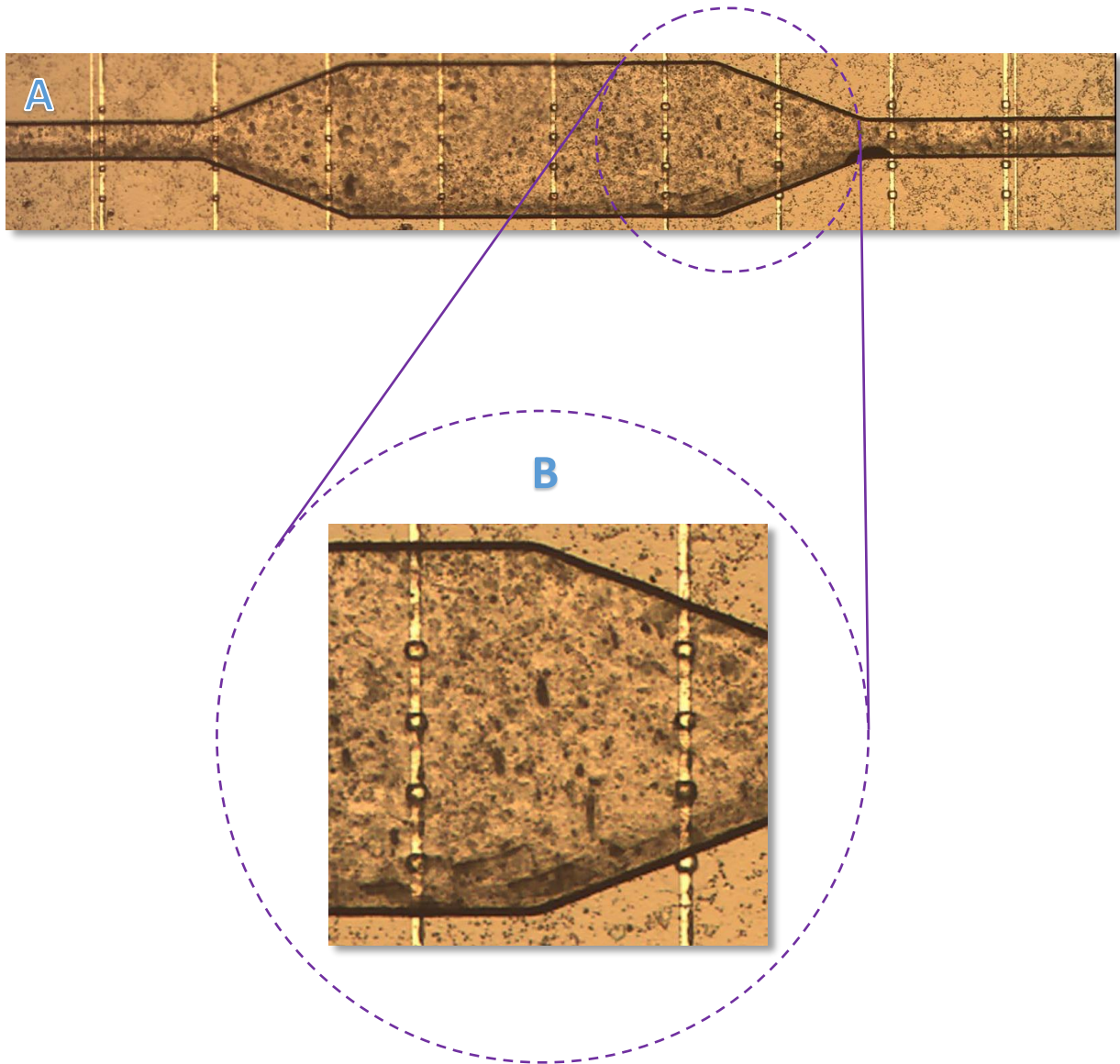


*Figure 54:    Trapping area of the channel with visible microtraps and microconductors*

*A)  Composed image of the complete trapping area (Multi row design)*
*B)  Extract showing the 17x22 µm microtraps at the end of the channel*

## 3.3.2 Lab environment

The measurement board (equipped as given in Chapter 3.3.1 and an additional BNC connector) was placed under a microscope and the multi pin connector on the board was used to attach a cable. This cable was used to supply the microconductors with current. The setup is shown in Fig. 55.
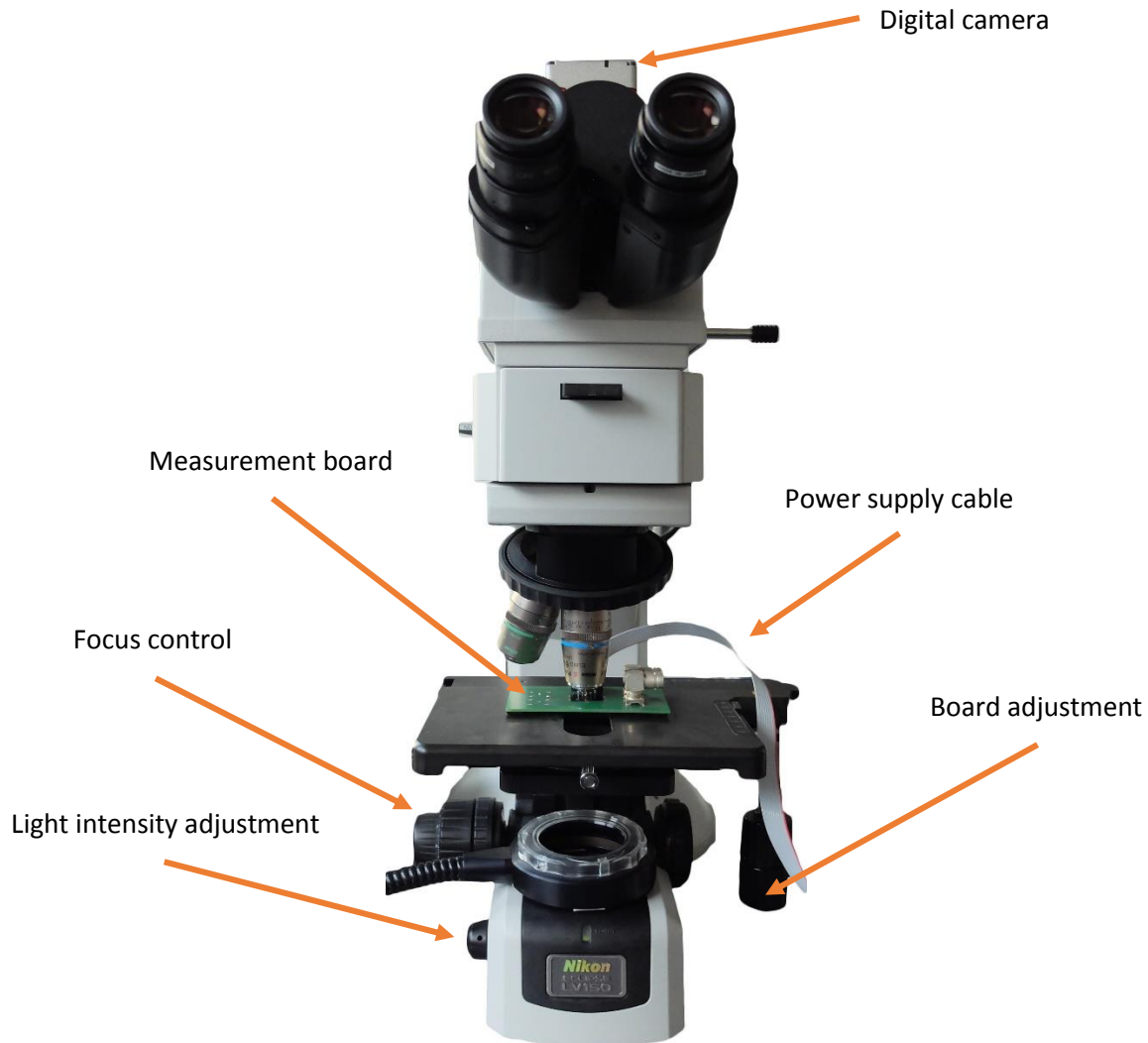


*Figure 55:      Measurement set-up under the microscope with supply cable and digital camera*

Materials and equipment used:

- Microscope:       Nikon - Eclipse LV150
- Lens:                 Nikon S Plan Fluor ELWD 60x/0.70 and standard 10 and 15 fold lenses
- Camera:            Moticam 2500 - 5.0 MP - USB 2.0
- Power Supply:  Agilent E3649A Dual Output DC Power Supply
- Pipette:            Eppendorf Research Plus (0.5 - 10 µl) with tip
- Syringe:            1 ml with needle and attached plastic tube
- Computer:        For camera control and data acquisition (videos/images)
- Tweezers:         Positioning of the syringe tip for filling the channel

The aforementioned power supply cable was connected to a 10-Pin socket connector (mounted on the PCB) to supply and control the microconductors. The current was directly driven from the corresponding port to the common ground pin with help of the DC power supply (which was manually connected). The pin assignment is given in Table 7 and Fig. 56.

| 10-Pin socket number | Microconductor (left to right) |
|---|---|
| 1 | 15x15 |
| 2 | 15x15 |
| 3 | 17x17 |
| 4 | 17x17 |
| 5 | GND |
| 6 | 17x20 |
| 7 | 17x22 |
| 8 | 17x22 |
| 9 | 20x22 |
| 10 | 20x22 |

Table 7:        Socket number and corresponding microconductor/microtrap (trap size in µm)
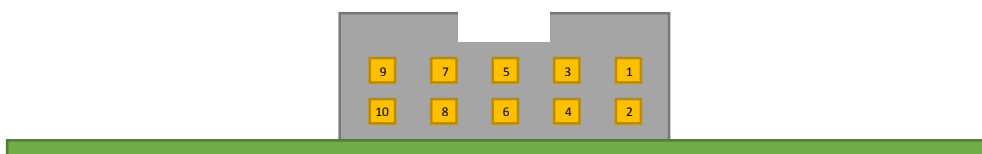


Figure 56:        Socket numbering from the backside of the board (green)

Although the complete system was designed for use with microfluidic pumps, the measurements were carried out with manual injection to minimize set-up time. The cell-particle suspension was pipetted onto the inlet hole and then sucked through the channel with a syringe (Fig. 57). The syringe has a needle tip with a plastic tube on it which is pressed onto the outlet with tweezers to soak in the sample.



Figure 57:        Syringe with needle and plastic tube as tip used for channel filling

When the channel was filled a small sample droplet was put onto the inlet to raise the pressure on this site and generate a flow in the channel.

## 3.4    Measurement

In this chapter the measurements and the results are presented. First a test setup without cells followed by the real setup with a single row and a multi row chip are explained.

### 3.4.1    Testing the microtraps and microconductors

For testing purposes "Dynabeads® M-270 Carboxylic Acid" particles without cells were used. They have a diameter of 2.8 µm and a susceptibility of 1. That means they are smaller in size and the magnetophoretic force is not as strong as for the 4.5 µm particles. The setup and the board were the same as given in Chapter 3.3 but only with a single trapping row (M1 chip). All pictures were made with a 60-fold lens and with microconductor 1 (15x15 µm). The current in the microconductor was 50 mA, because of the reduced weight of the single particles in comparison to cell-particle couples.

The capturing of a particle is given in Fig. 58.
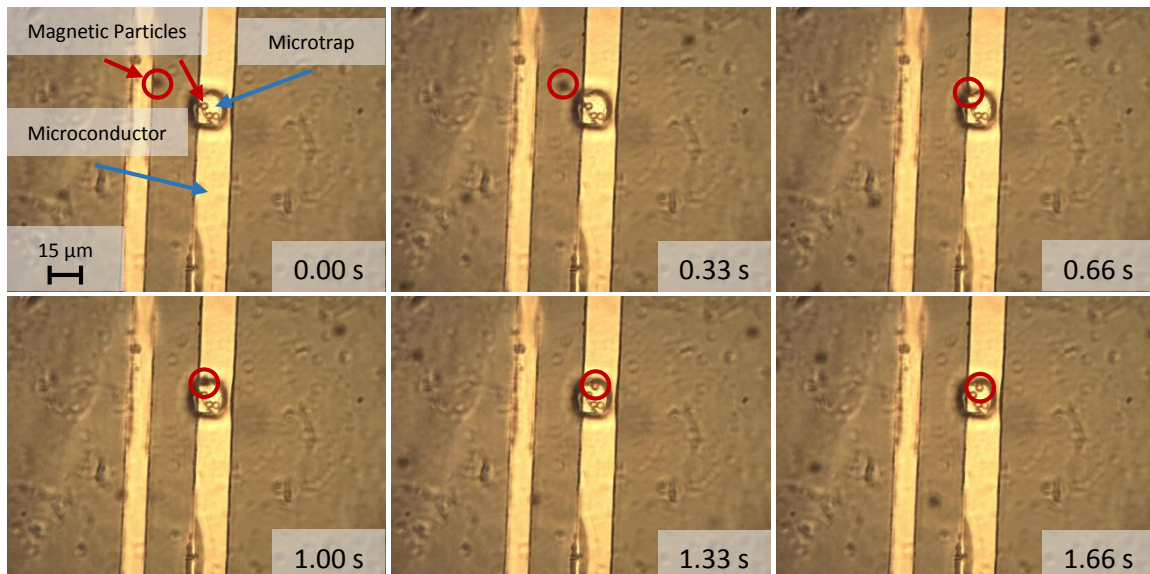


*Figure 58:    Activated microtrap with already captured particles and capture of a new particle*
*Trace of new particle is circled red*

The device was also able to hold particles in the microtrap with disabled microconductors (Fig. 59). Also the fluid flow over a trap is not influenced by the trap itself, which is shown in Fig. 59 where a particle flowing over the trap can be seen. It is not changing its direction.

When the microconductor was activated for a longer time (40 seconds) a lot of particles got captured in the microtrap. This behavior is shown in Fig. 60.
The estimated velocity of the particles was 20 µm/s, which was calculated from the isolated frames.

The tests with the particles showed that the device should be capable of capturing cell-particle couples, which are flowing directly over a microtrap.
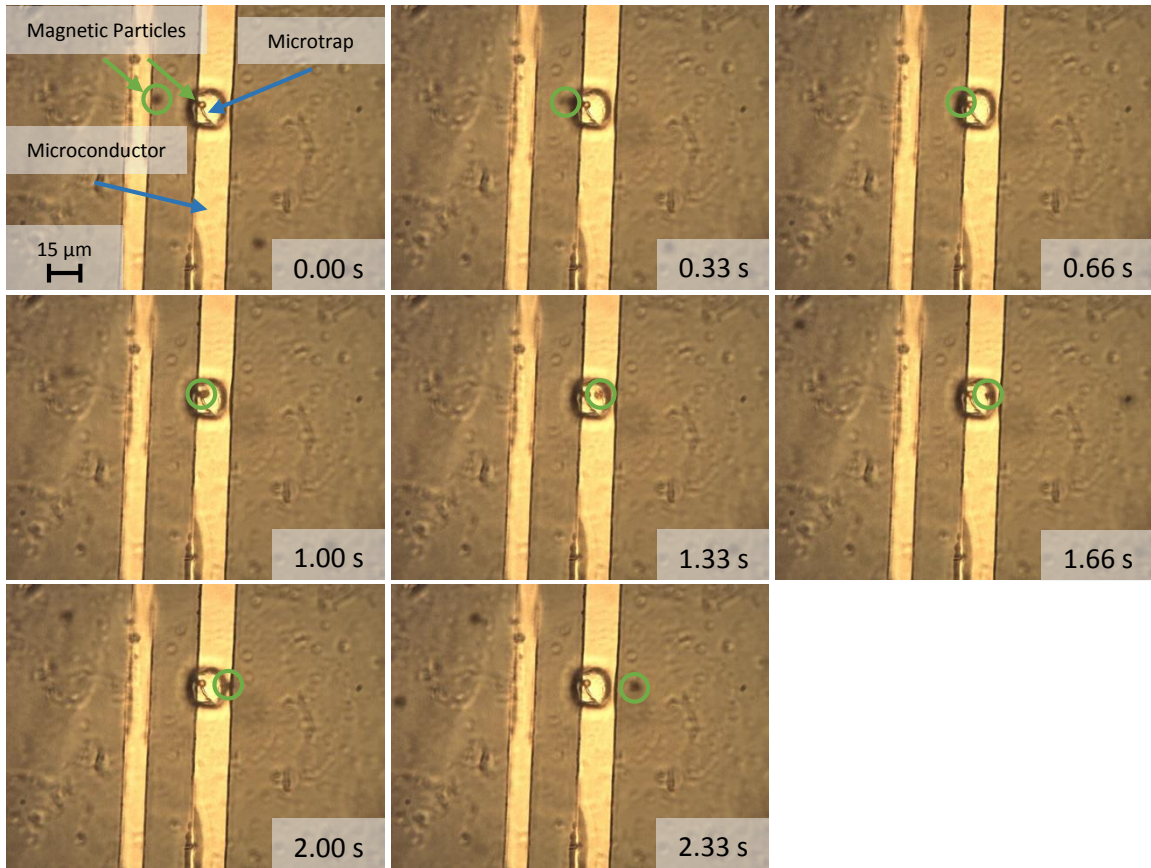
Figure 59:    A Single trapped particle stays in the microtrap after switching off the current
A flowing particle can freely move over the trap (marked red)
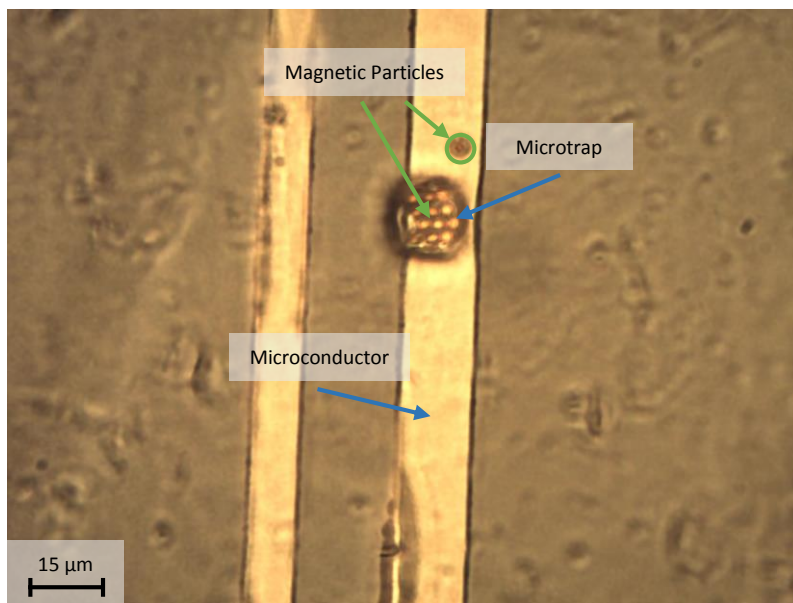


Figure 60:    Microtrap is full with particles after some time (activated microconductor)

### 3.4.2 Cell trapping – Single row chip

The first measurements with cells were made with a single row "M1 chip" and the previously prepared cell-particle couples. That means Jurkat-cells labeled with "Dynabeads® M-450 anti-CD3" particles were used. These MPs have a diameter of 4.5 µm and a susceptibility of 1.6. The setup and board were the same as given in Chapter 3.3 except that a single row Ordyl layer was used. All pictures were made with a 60-fold lens and with microconductor 4 (17x17 µm). The current in the microconductor was 150 mA, which was concluded to fit the given situation, because of the higher velocity of the cells compared to the calculation. Note that the current was only raised by 10 mA, because the Ordyl layer is thinner than in the simulation.

Fig. 61 shows that the microtrap is not influencing cells or even cell-particle couples when the microconductor is switched off. The estimated velocity is about 50 µm/s.
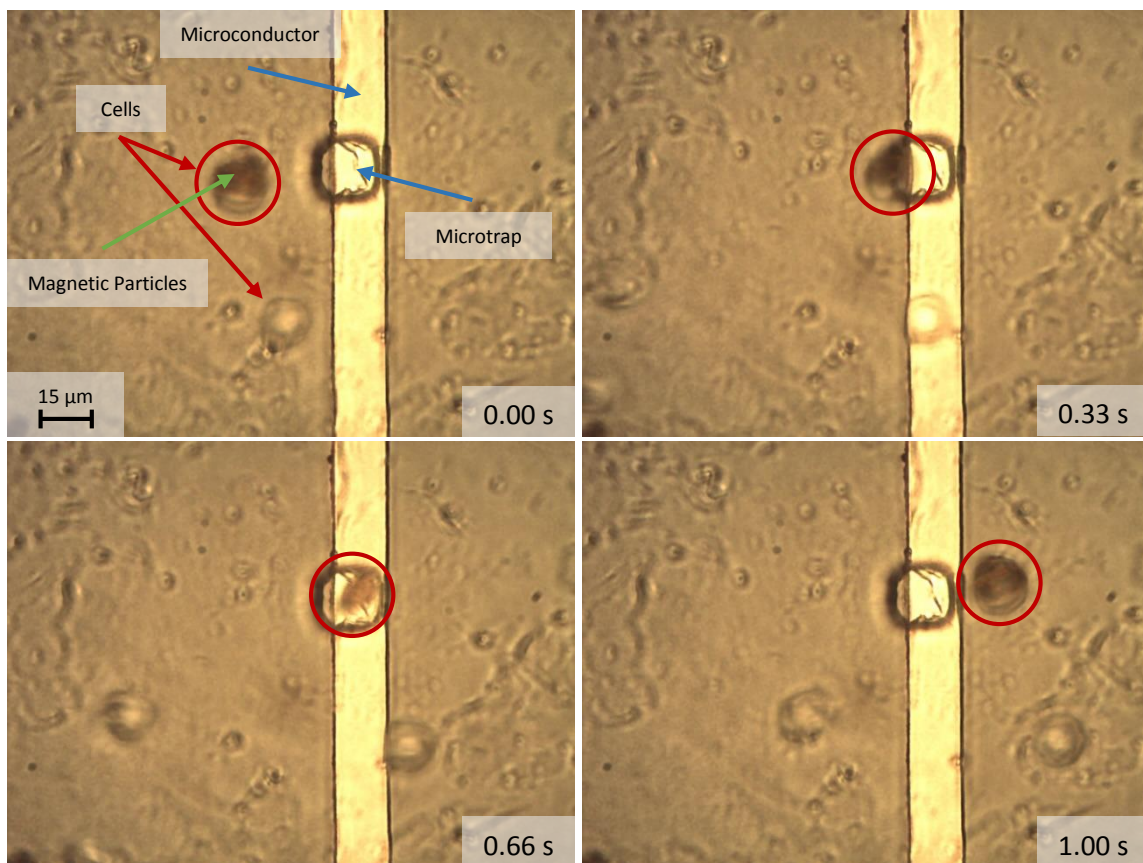


*Figure 61:     A cell-particle couple is moving over the disabled microtrap without interruption*

A complete capture of a cell-particle couple is given in Fig. 62. In this case a Jurkat cell labeled with two MPs is presented. It can be seen in Fig. 62.D that the labeled cell was not immediately trapped. Nevertheless the current density was strong enough to retrack the labeled cell inside the trap (Fig. 62.G - Fig. 62.I). In Fig. 63 the deactivation of the microconductor is shown with the same microtrap and the same cell-particle couples used in Fig. 62. It is clearly shown that the cell remains trapped after the microconductor was switched off. It can also be seen that a couple which adhered on the surface, because of the high field density, is moving again after switching off the current.
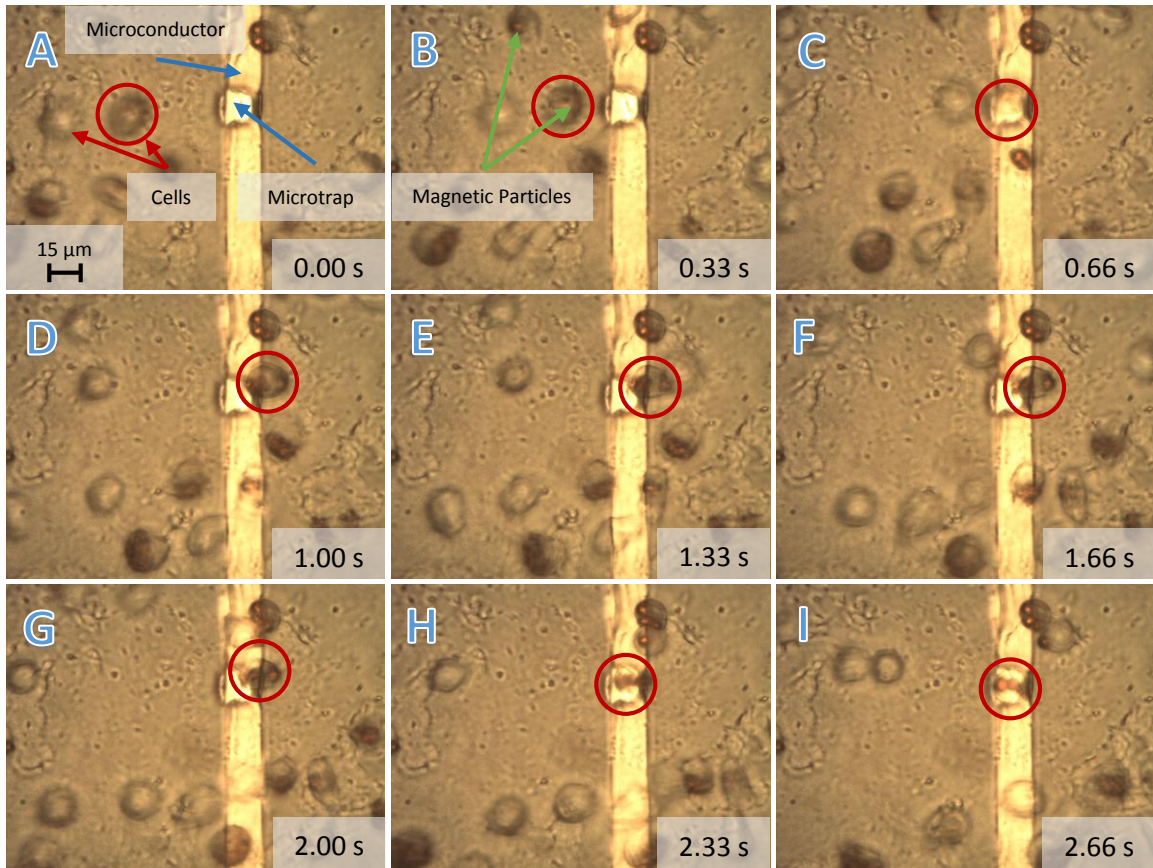
*Figure 62:    A cell-particle couple with two magnetic particles gets captured in a microtrap*
*The couple to be captured is circled red*
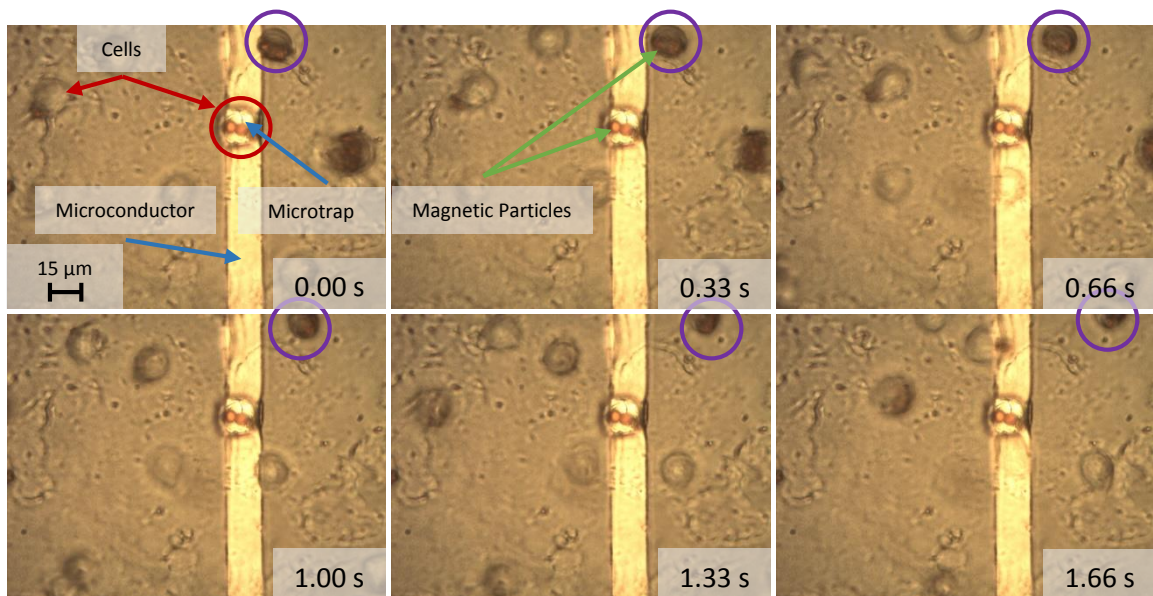


*Figure 63:    Disabling of the microconductor and resting of trapped cell-particle couple*
*The purple circled cell is moving again after turning off the microconductor*
*The red circled cell-particle couple is staying in the trap*

### 3.4.3 Cell trapping – Multi row chip

The second chip tested with cells was a multi row "M1 chip". As in the previous experiments Jurkat-cells labeled with "Dynabeads® M-450 anti-CD3" particles were used. The setup and board were the same as given in Chapter 3.3. Pictures were made with a 60 and a 15-fold lens and with microconductor 4 (17x17 µm). The current in the microconductor was again set to 150 mA.

A capture process without user interaction is shown in Fig. 64. In the video it can be seen that the cell needed 3.6 s from one microconductor to the next one and they have a distance of 360 µm so the estimated velocity of the couples was 100 µm/s.
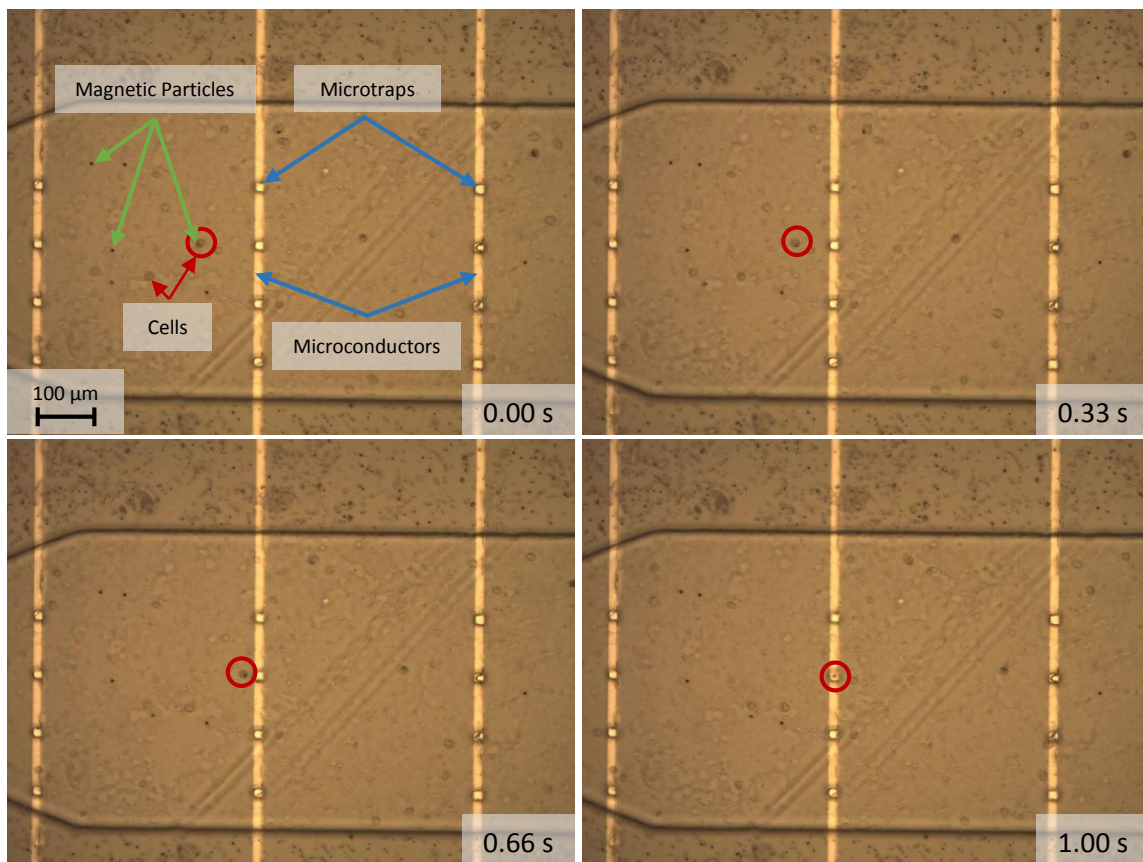


*Figure 64:     Cell capture with the multi row "M1 chip"*
*Labeled cell to be captured is circled red*

Fig. 65 shows the same measurement as Fig. 64 after 1 minute. The complete column of microtraps (with microconductor 4 beneath it), was fully filled with cell-particle couples. Fig. 66 gives a magnification of this filled column.
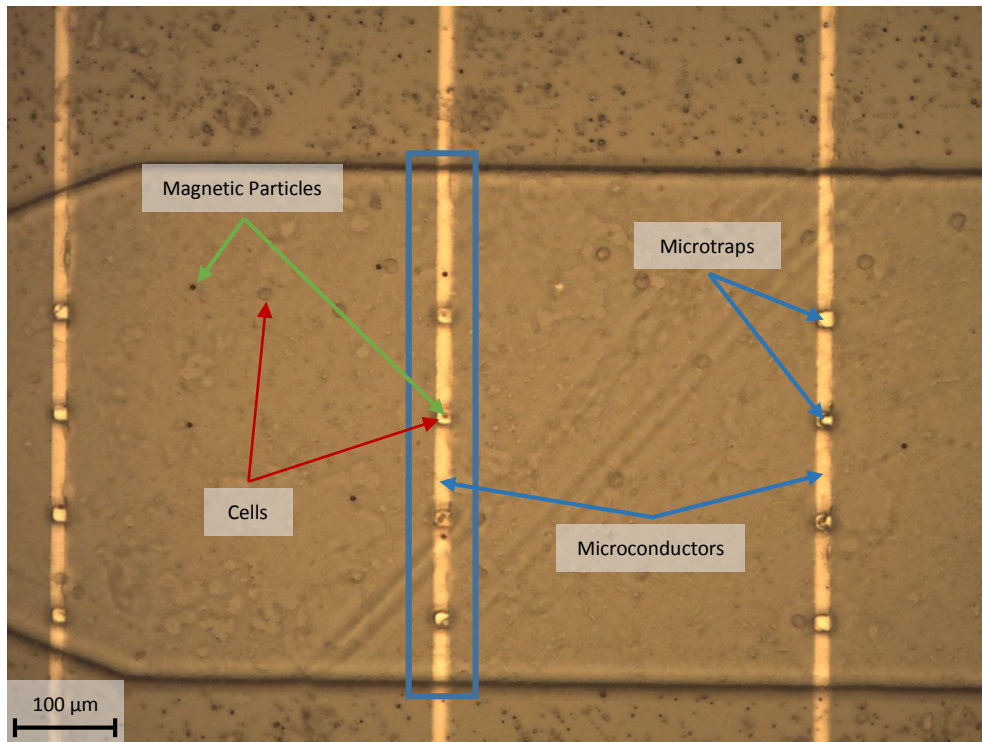
*Figure 65:      Completely filled column after 1 minute without user interaction*
*Every couple which was flowing over (or nearby) the traps was captured*
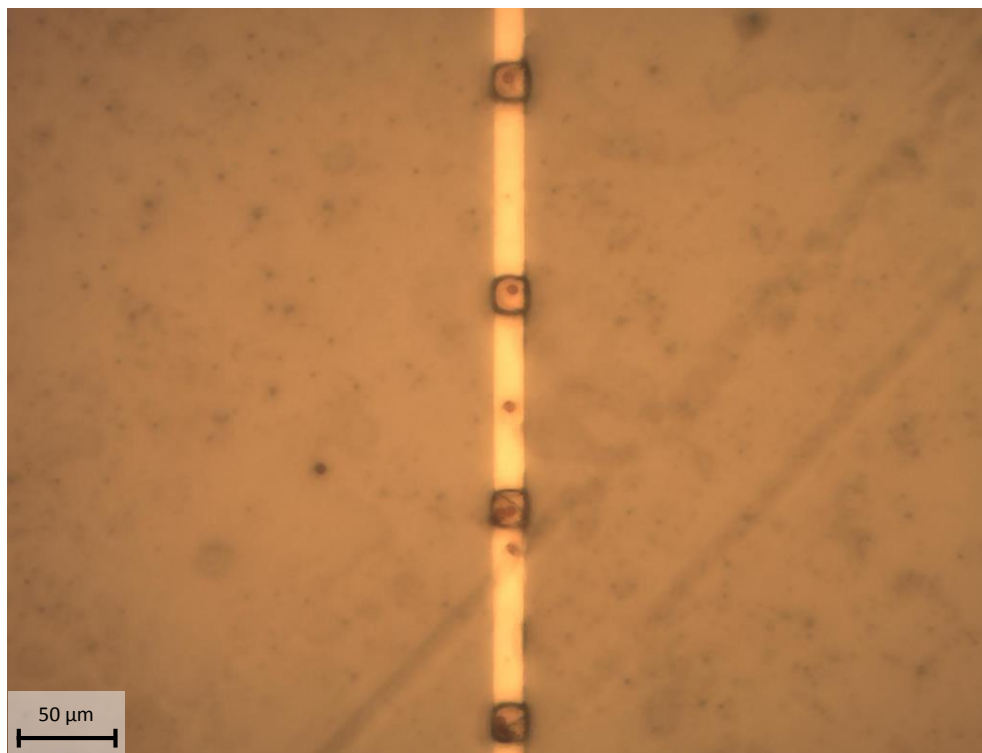


*Figure 66:      Fully filled trapping column with single and double labeled cells*

# 4 Conclusions and Outlook

In this thesis a new cell trapping device for capturing CTCs was presented, using magnetic methods. Cells labeled with superparamagnetic particles are being attracted by microconductors and captured in precisely produced and positioned microtraps.

The simulations/calculations of the flux density and the cell-particle couple capture process that were previously carried out were confirmed by the measurements.

The measurements also showed that the proposed device fulfills every intended purpose. It was possible to capture single and multiple labeled cells in microtraps and hold them there without permanent electric current and magnetic field.
Also the fluid flow over the microtraps is nearly not influenced by the trapped cell-particle couples or by the empty microtraps, which illustrates one of the main benefits of the cell trapping device.
No clustering occurred in the channel even when all traps were filled; a difference to devices tested in other research.

This thesis is part of a three year project, which should be able to capture detect and quantify CTCs in one device in the last stage. The designed chip is ready to be combined with highly sensitive magnetic sensors like GMR and GMI. In future it should be possible to detect single magnetic particles and attached cells (through movement of the particles). This means that with the microtraps it should be possible to lead the CTCs directly to precisely positioned sensors, which are positioned underneath the traps.
The GMR sensor detection was already investigated by other team members [16] and the next essential step would be to combine the trapping and the detection of superparamagnetic particles.

There are many steps still to be taken to the final TAS, but the concept of trapping magnetically tagged cells was successfully proven.

# 5 List of Figures

# 6    List of Equations

# 7    List of Tables

# 7    List of Tables

# 8 Literature

[1] T. R. Ashworth, "A case of cancer in which cells similar to those in the tumors were seen in the blood after death," *Aus. Med. J.,* no. 14, pp. 146-149, 1869.

[2] E. Diamond, G. Y. Lee, N. H. Akhtar, B. J. Kirby, P. Giannakakou, S. T. Tagawa and D. M. Nanus, "Isolation and characterization of circulating tumor cells in prostate cancer," *Frontiers in Oncology,* no. 2, pp. 1-11, 11 October 2012.

[3] R. Shayan, M. G. Achen and S. A. Stacker, "Lymphatic vessels in cancer metastasis: bridging the gaps," *Carcinogenesis,* vol. 27, no. 9, pp. 1729-1738, September 2006.

[4] Y. Dong, A. M. Skelley, K. D. Merdek, K. M. Sprott, C. Jiang, W. E. Pierceall, J. Lin, M. Stocum, W. P. Carney and D. A. Smirnov, "Microfluidics and Circulating Tumor Cells," *The Journal of Molecular Diagnostics,* vol. 15, no. 2, pp. 149-157, March 2013, © Elsevier - Figure used with permission.

[5] W. J. Allard, J. Matera, M. C. Miller, M. Repollet, M. C. Connelly, C. Rao, A. G. J. Tibbe, J. W. Uhr and L. W. M. M. Terstappen, "Tumor Cells Circulate in the Peripheral Blood of All Major Carcinomas but not in Healthy Subjects or Patients With Nonmalignant Diseases," *Clinical Cancer Reasearch,* vol. 10, October 2004.

[6] N. Howlader, A. M. Noone, M. Krapcho, N. Neyman, R. Aminou, W. Waldron, S. Altekruse, C. L. Kosary, J. Ruhl, Z. Tatlovich, H. Cho, A. Mariotto, M. P. Eisner, D. R. Lewis, H. S. Chen, E. J. Feuer, K. A. Cronin and B. K. Edwards, "SEER Cancer Statistics Review," National Cancer Institute, Bethesda, 2011.

[7] G. Vona, A. Sabile, M. Louha, V. Sitruk, S. Romana and K. Schützke, "Isolation by size of epithelial tumor cells: A new method for the immunomorphological and molecular characterization of circulating tumor cells," *American Journal for Pathology,* vol. 156, pp. 57-63, 2000.

[8] R. E. Zigeuner, R. Riesenberg, H. Pohla, A. Hofstetter and R. Oberneder, "Isolation of circulating cancer cells from whole blood by immunomagnetic cell enrichment and unenriched immunocytochemistry," *The Journal of Urology,* vol. 169, pp. 701-705, 2003.

[9] P. Gascoyne, J. Noshari, T. J. Anderson und F. F. Becker, „Isolation of rare cells from cell mixtures by dielectrophoresis," *Electrophoresis,* Nr. 30, pp. 1388-1398, 2009.

[10] M. Alshareef, N. Metrakos, E. Juarez Perez, F. Azer, F. Yang, X. Yang and G. Wang, "Separation of tumor cells with dielectrophoresis-based microfluidic chip," *Biomicrofluidics,* vol. 7, pp. 1-12, 2013.

[11] M. N. Dickson, P. Tsinberg, Z. Tang, F. Z. Bischoff, T. Wilson and E. F. Leonard, "Efficient capture of circulating tumor cells with a novel immunocytochemical microfluidic device," *Biomicrofluidics,* vol. 5, pp. 1-15, 2011.

[12] L. V. Sequist, S. Nagrath, M. Toner, D. A. Haber and T. J. Lynch, "The CTC-Chip: An Exciting New Tool to Detect Circulating Tumor Cells in Lung Cancer Patients," *Journal of Thoracic Oncology,* vol. 4, no. 3, pp. 281-283, March 2009.

[13] U. Dharmasiri, S. K. Njoroge, M. A. Witek, M. G. Adebiyi, J. W. Kamande, M. L. Hupert, F. Barany and S. A. Soper, "High-throughput selection, enumeration, electrokinetic manipulation, and molecular profiling of low-abundance circulating tumor cells using a microfluidic system," *Analytical Chemistry,* no. 83, pp. 2301-2309, 2011.

[14] J. G. Moreno, G. M. Croce, R. Fischer, M. Monne, P. Vihko and S. G. Mulholland, "Detection of hematogenous micrometastasis in patients with prostate cancer," *Cancer Research,* vol. 52, pp. 6110-6112, 1992.

[15] "Cell Search - Circulating Tumor Cell Test," Janssen Diagnostics, [Online]. Available: https://www.cellsearchctc.com/. [Accessed 17th October 2014].

[16] G. Kokkinis, F. Keplinger and I. Giouroudi, "On-chip microfluidic biosensor using superparamagnetic microparticles," *Biomicrofluidics,* vol. 7, 2013.

[17] P. Tabeling, Introduction to Microfluidics, Oxford University Press, 2005.

[18] N.-T. Nguyen and S. T. Wereley, Fundamentals and Applications of Microfluidics, Boston, Mass.: Artech House, 2002.

[19] G. Fasching, Werkstoffe für die Elektrotechnik, 4th ed., Wien: Springer Wien / New York, 1984, pp. 376-452.

[20] D. Jiles, Introduction to Magnetism and Magnetic Materials, Iowa: Springer-Science, 1991.

[21] V. K. Varadan, L. Chen and J. Xie, Nanomedicine: Design and Applications of Magnetic Nanomaterials, Nanosensors and Nanosystems, Chippenham, Wiltshire: Wiley, 2008.

[22] H. Kronmüller und M. Fähnle, „Micromagnetism and the Microstructure of Ferromagnetic Solids," Cambridge University Press, Cambridge, 2003.

[23] D. L. Leslie-Pelecky and R. D. Rieke, "Magnetic Properties of Nanostructured Materials," *Chemical Materials,* no. 8, pp. 1770-1783, 1996.

[24] G. H. Hansen, L. Immerdal, E. Thorsen, L. Niels-Christiansen, N. T. Birth, E. J. F. Demant and M. E. Danielsen, "Lipid Rafts Exist as Stable Cholesterol-independent Microdomains in the Brush Border Membrane of Enterocytes," *The Journal of Biological Chemistry,* no. 276, pp. 32338-32344, June 2001.

[25] S. Hardt and F. Schönfeld, Microfluidic Technologies for Miniaturized Analysis Systems, Springer, 2007.

[26] N. Pamme, "Magnetism and microfluidics," *Lab on a Chip,* pp. 24-38, 2006.

[27] M. A. M. Gijs, F. Lacharme and U. Lehmann, "Microfluidic Applications of Magnetic Particles for Biological Analysis and Catalysis," *Chem. Rev.,* no. 110, pp. 1518-1563, 2010.

[28] A. Prechtl, Vorlesungen über die Grundlagen der Elektrotechnik, vol. 2, Wien New York: Springer Verlag, 1995.

[29] J. C. Olivares-Galván, I. Hernández, P. S. Georgilakis und E. Campero-Littlewood, „Calculation of the Magnetic Field Intensity in a Rectangular Conductor Carrying Current," Boston, 2009.

[30] A. Dangl, "Biosensing based on magnetically induced motion of magnetic microparticles," April 2013.

[31] "Dynabeads Physical Characteristics," Life Technologies Technical Support, 2014.

[32] "Celeromics," [Online]. Available: http://www.celeromics.com/en/Support/cell-lines/jurkat.php. [Accessed 12th August 2014].

[33] C. Fumarola, S. La Monica, R. R. Alfieri, E. Borra and G. G. Guidotti, "Cell size reduction induced by inhibition of the mTOR/S6K-signaling pathway protects Jurkat cells from apoptosis," *Cell Death and Differentiation,* no. 12, pp. 1344-1357, 2005.

[34] M. Jamalieh, "Microfluidic Biosensing using Giant Magnetoresistance Sensors," 2014.

[35] „ELGA Europe - Ordyl SY300," 2014. [Online]. Available: http://www.elgaeurope.it/ENG/Default.aspx?SEZ=3&PAG=9&MOD=CTG&CAT=12&PRD=11. [Zugriff am 21 October 2014].

[36] "Life Technologies - Dynabeads CD3," 2014. [Online]. Available: http://www.lifetechnologies.com/order/catalog/product/11151D. [Accessed 20th October 2014].

[37] U. Schneider, H. U. Schwenk and G. Bornkamm, "Characterization of EBV-genome negative "null" and "T" cell lines derived from children with acute lymphoblastic leukemia and leukemic transformed non-Hodgkin lymphoma.," *International Journal of Cancer,* no. 15, pp. 621-626, May 1977.

[38] "ATCC," 2014. [Online]. Available: http://www.lgcstandards-atcc.org/products/all/TIB-152.aspx?geo_country=at#characteristics. [Accessed 20th October 2014].

[39] "BOKU - University of Natural Resources and Life Sciences," 2014. [Online]. Available: http://www.boku.ac.at/en/. [Accessed 20th October 2014].

[40] "Austrian Institute of Tehcnology," 2014. [Online]. Available: http://www.ait.ac.at/. [Accessed 20th October 2014].

# 9    Appendix

## 9.1    Dynabeads Properties

**Dynabeads physical characteristics**

Dynabeads are uniform, superparamagnetic, porous polystyrene spheres with an even dispersion of magnetic material throughout the bead. The magnetic material within the Dynabeads is a mixture of the two iron oxides maghemite (gamma-$Fe_2O_3$) and magnetite ($Fe_3O_4$), which is encased in the bead matrix by an additional thin polymer shell. This prevents any iron leakage from the beads which could otherwise have a detrimental toxic effects on target cells, while at the same time providing a defined surface area for adsorption or conjugation of various biomolecules.

| Dynabeads type | Diameter (µm) | Monodispersity | | Specific surface area ($m^2$/g DS) | Density (g DS/$cm^3$) |
|---|---|---|---|---|---|
| | | SD (µm) | CV (%) | | |
| MyOne Dynabeads | 1.0 | 0.02 | 2.0 | 8 - 16 | 1.8 |
| M-270 Dynabeads | 2.8 | 0.04 - 0.05 | 1.6 - 1.8 | 2 - 5 | 1.6 |
| M-280 Dynabeads | 2.8 | 0.04 | 1.6 | 4 - 8 | 1.4 |
| M-450 Dynabeads | 4.5 | 0.05 | 1.2 | 1 - 4 | 1.6 |

Table 1 Physical properties of Dynabeads (typical values)
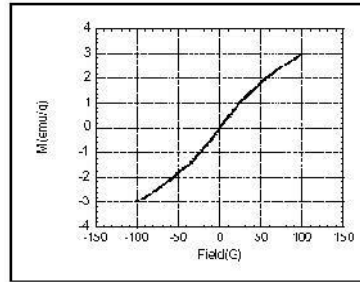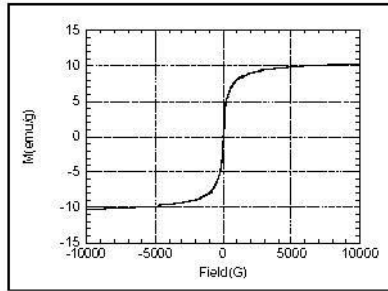
**Magnetic properties of Dynabeads**

Due to the small size of the iron domains of the magnetic material in the matrix, Dynabeads are *superparamagnetic*. This means they will only exhibit magnetic properties when subjected to a magnetic field, and both *remanence* and *coercivity* equals zero. This can be seen from the magnetisation curves for the beads below.
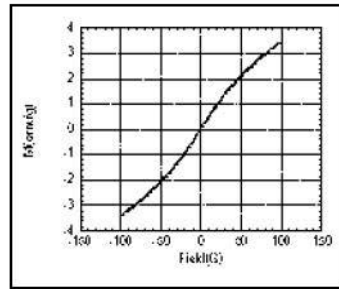
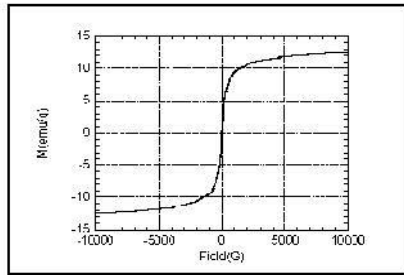**MyOne, 1 micron Dynabeads**
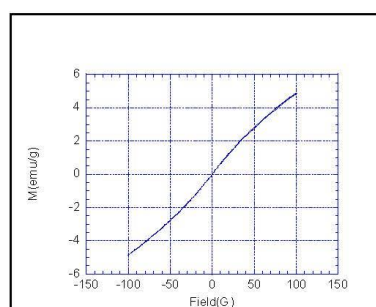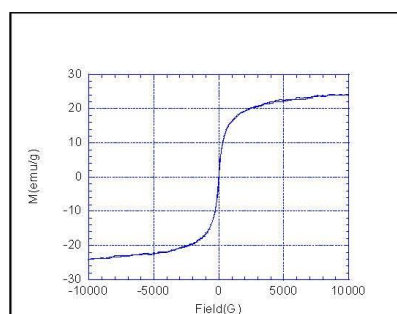
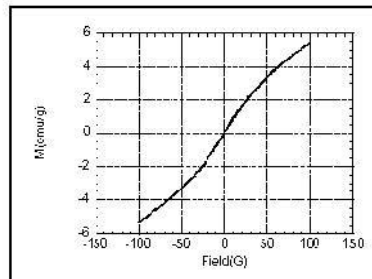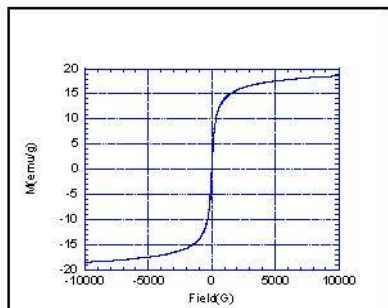M-270 /M-280 Dynabeads (2.8 micron)

M-280 Dynabeads:



M-270 Dynabeads:



M-450 Dynabeads (4.5 micron)

The *magnetic susceptibility* is used by Dynal as a measure of the beads magnetic properties. Magnetic susceptibility is measured by the oscillator method in the linear range of the magnetisation curve, and typical values for the different bead types are listed in table 2.

The magnetic force exerted on a bead – and hence the separation efficiency when exposed to a magnetic field – is dependant on the degree of magnetisation of the bead. The maximum magnetic field that may be generated by the beads is referred to as their *saturation magnetisation* (table 2). Due to the high magnetic content of Dynabeads their saturation magnetisation is high, which enables a quick and efficient separation even in viscous samples. Iron content in the beads are in the range 12% - 26%, depending on the bead type. This is further specified in table 2.

| Dynabeads product | Diam. (µm) | Magnetic Susceptibility[1] (dry substance) | | Saturation Magnetisation[2] (kA/m) | | Iron content (%, w/w dry substance) |
|---|---|---|---|---|---|---|
| | | $m^3/kg$ (mass) | Dimensionless (volume) | $A \cdot m^2/kg$ (mass) | kA/m (volume) | |
| MyOne Dynabeads | 1.0 | $8 \cdot 10^{-4}$ | 1.4 | 24 | 43 | 26 |
| M-270 Dynabeads | 2.8 | $6 \cdot 10^{-4}$ | 1.0 | 13 | 20 | 14 |
| M-280 Dynabeads | 2.8 | $5 \cdot 10^{-4}$ | 0.7 | 10 | 14 | 12 |
| M-450 Dynabeads | 4.5 | $10 \cdot 10^{-4}$ | 1.6 | 19 | 30 | 20 |

Table 2 Magnetic properties of Dynabeads (typical values)

## 9.2 Dynabeads Manual

**invitrogen**
by *life technologies*

## Dynabeads® CD3

**Catalog no. 11151D**

**Store at 2˚C to 8˚C**
**Rev. Date:** March 2012 (Rev. 003)

### Product Contents

| Product contents | Volume |
|---|---|
| Dynabeads® CD3 | 5 mL |

**Product capacity**
Whole blood: 200 mL
MNC: ~2 × 10³ cells

Dynabeads® CD3 contains
4 × 10⁸ beads/mL in phosphate
buffered saline (PBS), pH 7.4,
with 0.1% bovine serum albumin
(BSA) and 0.02% sodium azide as a
preservative.
**Caution:** Sodium azide may react
with lead and copper plumbing to
form highly explosive metal azides.

### Product Description

Isolate or deplete human CD3⁺
T cells directly from whole
blood, buffy coat or MNC with
Dynabeads® CD3. The beads are
mixed with the cell sample in a
tube. The beads bind to the target
cells during a short incubation,
and then the bead-bound cells are
separated by a magnet (fig. 1).

**Depletion** – Discard the bead-
bound cells and use the remaining,
untouched cells for any application.

**Positive isolation** – Discard the
supernatant and use the bead-
bound cells for downstream
molecular applications.

### Downstream Applications

CD3⁻ T cells can be efficiently
depleted from a sample. For rapid
and consistent results in protein or
gene expression analysis, lyse the
CD3⁻ T cells while still attached
to the beads and directly process
for further molecular analysis. For
positive isolation for functional
studies, cell activation/expansion,
or for flow cytometer analysis,
the cells need to be released after
isolation. For this, we recommend
using Dynabeads® FlowComp™
Human CD3 (bead-free cells).
See "Related Products" for T cell
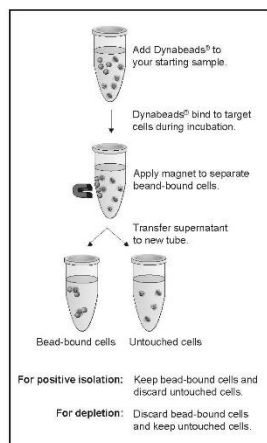activation/expansion product
recommendations.



Figure 1: Overview of method

For research use only. Not for human or animal therapeutic or diagnostic use.

### Required Materials

- Magnet (DynaMag™ portfolio). See www.lifetechnologies.com/magnets for recommendations.
- Mixer allowing tilting and rotation of tubes (e.g. HulaMixer® Sample Mixer).
- Isolation Buffer: Ca²⁺ and Mg²⁺ free PBS supplemented with 0.1% BSA and 2 mM EDTA, pH 7.4.
  **Note:** BSA can be replaced by human serum albumin (HSA) or fetal calf serum (FCS). EDTA can be replaced by sodium citrate.

### General Guidelines

- Visit www.lifetechnologies.com/samplepreparation for recommended sample preparation procedures.
- Use a mixer that provides tilting and rotation of the tubes to ensure that beads do not settle in the tube.
- This product should not be used with the MPC™-1 magnet (Cat. no. 12001D).
- Avoid air bubbles (foaming) during pipetting.
- Carefully follow the recommended pipetting volumes and incubation times.
- Keep all buffers cold.

### Protocol

#### Wash the Beads

See Table 1 for volume recommendations.

1. Resuspend the beads in the vial (i.e. vortex for >30 sec, or tilt and rotate for 5 min).
2. Transfer the desired volume of beads to a tube.
3. Add the same volume of Isolation Buffer, or at least 1 mL, and resuspend.
4. Place the tube in a magnet for 1 min and discard the supernatant.
5. Remove the tube from the magnet and resuspend the washed beads in the same volume of Isolation Buffer as the initial volume of beads (step 2).

#### Prepare Cells

- Cells can be directly isolated from any sample such as whole blood, bone marrow, MNC suspensions or tissue digests. Whole blood and buffy coat need to be washed prior to isolation.
- Prepare MNC to 1 × 10⁷ cells/mL in Isolation Buffer.
- See "General Guidelines" for sample preparation procedures.

#### Wash Whole Blood and Buffy Coat

Wash the blood/buffy coat to remove interfering soluble factors.
**Note:** Buffy coat has 8–10 times higher concentration of leucocytes than whole blood and should be diluted prior to use.

1. Dilute the whole blood/buffy coat in Isolation Buffer 1 (1:2).
2. Centrifuge at 600 × g for 10 min at 2°C to 8°C.
3. Discard the plasma fraction/upper layer.
4. Resuspend whole blood to the original volume in Isolation Buffer and buffy coat 1:1 in Isolation Buffer before adding the beads.

## Deplete or Positively Isolate CD3⁺ T Cells

The protocol is based on 1 mL ($1 \times 10^7$) MNC or 1 mL washed whole blood/ washed and diluted buffy coat as starting sample, but is scalable from $1 \times 10^7 - 5 \times 10^8$ (1–50 mL). When working with lower volumes than 1 mL, use the same volumes as indicated for 1 mL. When working with larger volumes, scale up all volumes accordingly, as shown in Table 1.

1. Transfer 1 mL cells ($1 \times 10^7$) to a tube and add 25 µL pre-washed and re-suspended beads.

2. Incubate for 20 min (positive isolation) or 30 min (depletion) at 2°C to 8°C with gentle tilting and rotation.

3. Place the tube in a magnet for 2 min.

4. For *depletion*; transfer supernatant to a new tube for further use and discard the beads.
   *or*
   For *positive isolation*; while the tube is still in the magnet, carefully remove and discard the supernatant.

5. Remove the tube from the magnet and add 1 mL Isolation Buffer, pipet 2–3 times (or vortex 2–3 sec) and place the tube in a magnet for 2 min. While the tube is still in the magnet, carefully remove and discard the supernatant.

6. Repeat step 5 at least once to wash the bead-bound CD3⁺ T cells. This step is critical to obtain a high purity of isolated cells.

7. Resuspend the cell pellet in preferred cell medium.

Keep the cells on 2°C to 8°C until further use in downstream applications.

Table 1: Volumes for isolation/depletion of human CD3⁺ T cells. This protocol is scalable from $1 \times 10^7$ to $5 \times 10^8$ cells.

| Step | Step description | Small scale (1X) | Large scale (10X) |
|------|------------------|------------------|-------------------|
| | Recommended tube size | 5 mL | 15 mL |
| | Recommended magnet | DynaMag™-5 | DynaMag™-15 |
| 1* | Sample volume (MNC/blood/buffy) | 1 mL | 10 mL |
| 1** | Bead volume | 25 µL | 250 µL |
| 5–6 | For positive isolation only: Wash cells (Isolation Buffer) | 3 × ~1 mL | 3 × ~10 mL |

\* $1 \times 10^7$ MNC/mL.
\*\* If very high cell-depletion efficiency is required, increase the beads volume up to double the recommended amount.

## Description of Materials

Dynabeads® CD3 are uniform, superparamagnetic polystyrene beads (4.5 µm diameter) coated with a primary monoclonal mouse antibody specific for the CD3 membrane antigen, which is predominantly expressed on human T cells.

## Related Products

| Product | Cat. no. |
|---------|----------|
| DynaMag™-5 | 12303D |
| DynaMag™-15 | 12301D |
| DynaMag™-50 | 12302D |
| HulaMixer® Sample Mixer | 15920D |
| Dynabeads® Human T Activator CD3/CD28 | 11161D |
| Dynabeads® FlowComp™ Human CD3 | 11365D |

REF on labels is the symbol for catalog number.

## Limited Use Label License

## Limited Product Warranty

SPEC-05870

## 9.3    Ordyl SY300

# Elga Europe

# ORDYL SY 300

## PRODUCT DATA SHEET
### Edition 02 - 30 January 2014

## PRODUCT DESCRIPTION

Ordyl SY 300 is a solvent type permanent dry film for special MEMS applications.

The Ordyl SY 300 in connection with his auxiliary product line CFC free: Ordyl SY Developer, Ordyl SY Rinse and Stripper 104, offer the following performances:

- Excellent resolution
- Excellent heat resistance
- Excellent chemical resistance
- High stability
- Biocompatibility

Ordyl SY 300 could be used for sealing application, due to the capability to be pressed together with a top plate.
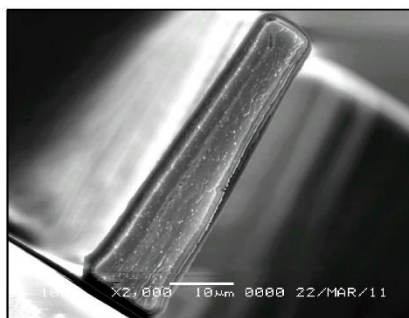
### SY 350
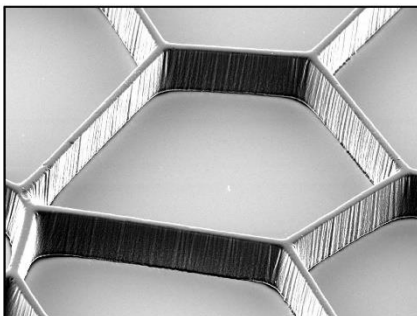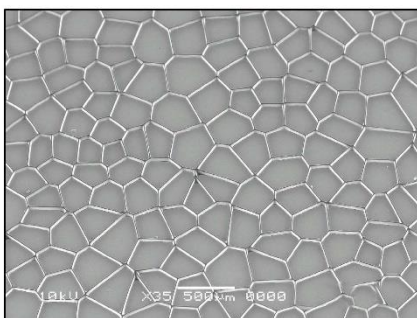


**Main Features:**
- Excellent chemical resistance
- Biocompatibility

**Typical Application:**
- MEMS
- Sealing application

**Available Thickness:**
- 17 µm (0.7 mils), 20 µm (0.8 mils), 30 µm (1.2 mils) and 55 µm (2.2 mils)
- Different thickness available on request





Ordyl SY 300  Ed. 02 30 January 2014
Form EE.P32.AT.01-01                                                   Page 1 of 5

**PROCESS INFORMATION**

Ordyl SY 300 guarantee good adhesion on the following surface:
- Glass
- Silicium
- Kapton
- Mylar

We recommend good surface cleaning in order to obtain optimal performance.

**Lamination**

Panels must be thoroughly dry prior to lamination.

|  | MANUAL LAMINATOR | AUTOMATIC LAMINATOR |
|---|---|---|
| Pre-heat | (OPTIONAL) | (OPTIONAL) |
| Hot roll temperature | 105 – 125°C (221 – 257°F) | 105 – 125°C (221 – 257°F) |
| Lamination roll pressure | 2.5 – 3.5 bar (35 – 50 Psi) | 2.5 – 6.0 bar (35 – 85 Psi) |
| Lamination speed | 1 – 3m/min (3 – 10 feet/min) | 1 – 3m/min (3 – 10 feet/min) |
| Seal temperature | --- | 40-80°C (105-180°F) |
| Seal pressure | --- | 3.0-6.0 bar |
| Seal time | --- | 1-4 sec. |

**Post lamination Hold Time**

We recommend a hold time of at least 15 min, or in any case the minimum hold time necessary to allow panels to cool down to room temperature.

Hold time should not be over 1 week.

**Exposure**

We recommend using UV lamps or laser source with emission peak at 360 – 380nm.

| Energy (mJ/cm$^2$) | 100 | 150 | 200 | 250 | 300 | 350 | 400 |
|---|---|---|---|---|---|---|---|
| SST 21 | 5 | 6 | 7 | 8 | 9 | 9.5 | 10 |
| RST 25 | 4 | 7-8 | 10 | 13 | 16 | 17-18 | 19 |

**Hold Time after exposure**

We recommend a minimum hold time after exposure of at least 15 minutes.

**Developing**

SY 300 could be develop with spray, paddle or dipping method.

Using Ordyl SY Developer in dipping process at room temperature maintain the Break Point between 60% and 80% depend on application.

Use Ordyl SY Rinse to remove scum and clean the surface.

If final rinse with DI water is necessary an intermediate rinse with IPA is suggested.

**Post Bake**

After developing is necessary a post-baking at 150°C for 30 - 60min.

**Stripping**

Ordyl SY 300 could be stripped only before post bake using Stripper 104 at 70-75°C in dipping method.
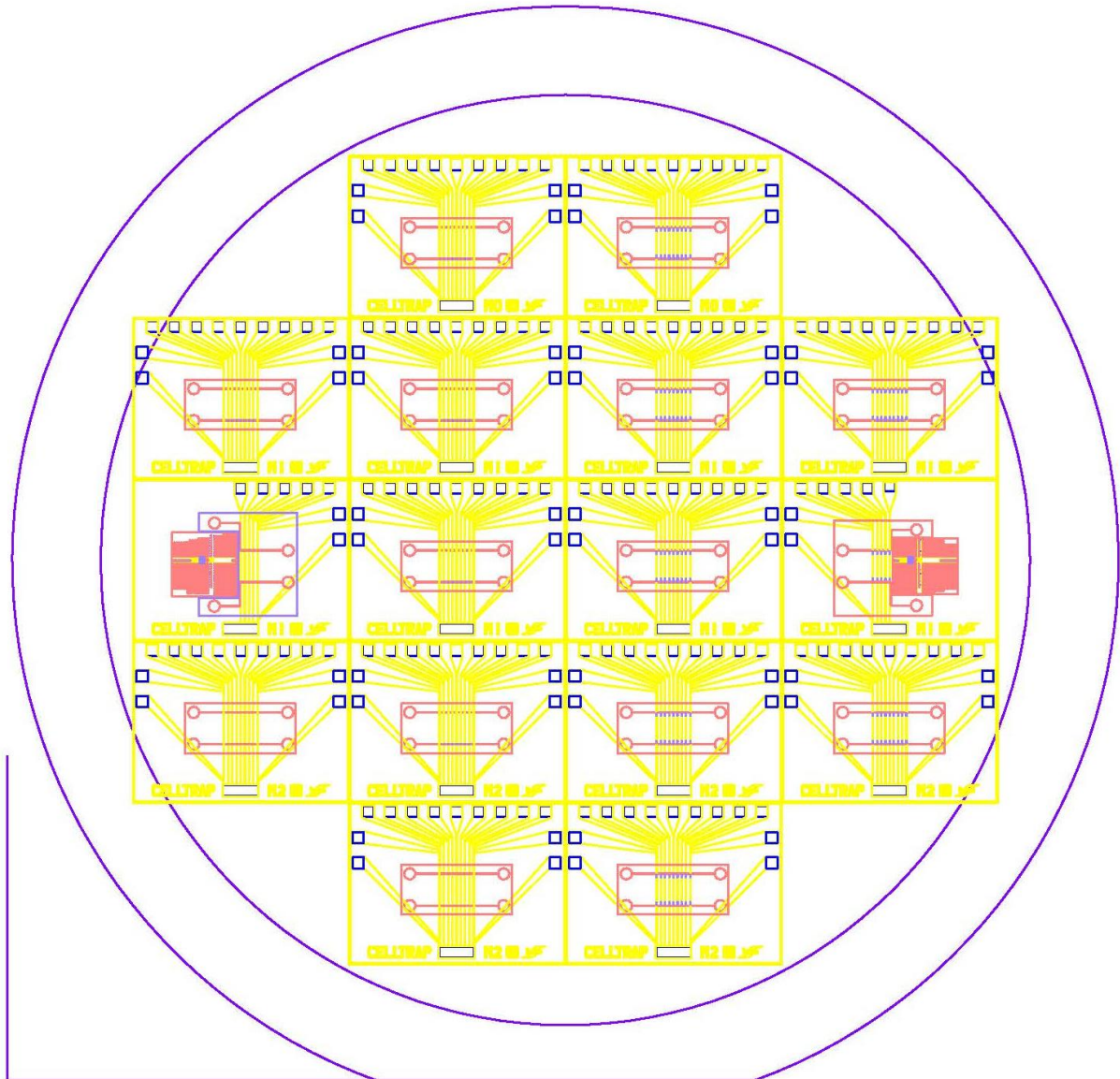
## RESIST PROFILE

For the test we used a 55 µm thickness dry film, laminated on $SiO_2$ wafer.

| EXPOSURE | LINE | SPACE |
|---|---|---|
| $100mJ/cm^2$ | 60 µm | 50 µm |
| $150mJ/cm^2$ | 50 µm | 60 µm |
| $200mJ/cm^2$ | 40 µm | 70 µm |
| $250mJ/cm^2$ | 40 µm | 80 µm |

Exposure Unit ORC HMW201B not collimated.

## 9.4 Mask of the Complete Wafer

## 9.5 Mask of a Single Chip